Majd Lahham, M.Sc

Characterization of a fungal and a yeast flavoprotein

DISSERTATION

zur Erlangung des akademischen Grades

Doktor der Naturwissenschaften

eingereicht an der

Technischen Universität Graz

Betreuer

Betreuer: Univ.-Prof. Mag. rer. nat. Dr. rer. nat. Peter Macheroux

Institut für Biochemie

Technische Universität Graz

Graz, November 2018

EIDESSTATTLICHE ERKLÄRUNG

Ich erkläre an Eides statt, dass ich die vorliegende Arbeit selbstständig verfasst, andere als die angegebenen Quellen/Hilfsmittel nicht benutzt, und die den benutzten Quellen wörtlich und inhaltlich entnommenen Stellen als solche kenntlich gemacht habe. Das in TUGRAZonline hochgeladene Textdokument ist mit der vorliegenden Dissertation identisch.

19.9.2018
Datum

Majd Lahha
Unterschrift

Contents

Acknowledgements

شكر و تقدير

بعد شكر الله

سورية...أنت بداية كل شيء، وعلة كل شيء،...

أود أن أشكر كل من ساعدني ووقف بجانبي في كل مراحل حياتي:

أبي و أمي الغاليين... لكم مني كل تقدير ومحبة لما قدمتموه من تضحية وجهد فأنتم قدوتي ومصدر فخر لي...

أخوتي نادر ونضال... أنتم رفاق دربي وستبقون كذلك ..

زوجتي وصديقتي الحبيبة... تضحيتك وحنانك كانت وستبقى منارة لعائلتنا الصغيرة ..

ابني الحبيب سبيرو وابنتي الأميرة كريستينا ماريا... أنتم مصدر كل فرح في حياتي...

رب أخوات لم تلدهم أمي... هنادي وريم...

جوزيف وجون وورد وتيم...الجيل الجديد في عائلتي الذي سوف يزهر نجاحا...

نوال وريم وسراد ورامي...أنتم عائلتي الثانية التي بها أفتخر....

إلى كل أصدقائي الذين عشت معهم لحظات لا تنسى....

إلى كل أساتذتي الذين بذلوا كل جهد لأصل إلى هذا النجاح...

إلى كل الذين ساعدوني ووقفوا بجانبي ولم تسعفني هذه الصفحات القليلة لذكرهم...

و أخيراً إلى روح كل شهيد ضحى بنفسه فداءً... **لسورية. . .**

Abstract

Oxidative cyclization of N-methyl-dopa by a fungal flavoenzyme of the amine oxidase family

Flavin-dependent enzymes catalyze many oxidations, including formation of ring structures in natural products. The gene cluster for biosynthesis of fumisoquins, secondary metabolites structurally related to isoquinolines, in the filamentous fungus *Aspergillus fumigates* harbors a gene that encodes a flavoprotein of the amine oxidase family, termed *fsqB* ("fumisoquin biosynthesis gene B"). This enzyme catalyzes an oxidative ring closure reaction that leads to the formation of isoquinoline products. This reaction is reminiscent of the oxidative cyclization reported for berberine bridge enzyme and tetrahydrocannabinol synthase. Despite these similarities, amine oxidases and berberine bridge enzyme-like enzymes possess distinct structural properties, prompting us to investigate the structure-function relationships of FsqB. In this thesis, I report the recombinant production and purification of FsqB, elucidation of its crystal structure, and kinetic analysis employing five putative substrates. The crystal structure at 2.6 Å resolution revealed that FsqB is a member of the amine oxidase family with a covalently bound FAD cofactor. *N*-methyl-dopa was the best substrate for FsqB and was completely converted to the cyclic isoquinoline product. The absence of the *meta*-hydroxyl group, as *e.g.* in L-*N*-methyltyrosine, resulted in a 25-fold lower rate of reduction and the formation of the demethylated product L-tyrosine, instead of a cyclic product. Surprisingly, FsqB did not accept the D-stereoisomer of *N*-methyltyrosine, in contrast to *N*-methyl-dopa, for which both stereoisomers were oxidized with similar rates. On the basis of the crystal structure and docking calculations, I postulate a substrate-dependent population of distinct binding modes that rationalizes the stereospecific oxidation in the FsqB active site.

***The characterization of the wild type of electron transferring flavoprotein from*
Saccharomyces cerevisiae**

Electron transferring flavoproteins (ETFs) are a group of FAD-dependent proteins typically operating in the mitochondrial matrix of eukaryotic organisms. The main function of these proteins is to accept electrons from client dehydrogenases and the subsequent transfer of electrons to the respiratory chain for ATP production. The mechanism of these proteins is still under investigation. Recently, it was reported that the FAD cofactor in human ETF (hETF) is subject to oxidation at the 8α-methyl group leading to the formation of 8-formyl-FAD. In present thesis, the ETF from the yeast *Saccharomyces cerevisiae* (yETF) was recombinantly produced and purified in order to investigate if 8-formyl-FAD is formed in this basic unicellular eukaryotic organism. The protein was successfully purified in sufficient amounts. However, formation of 8-formyl-FAD was not observed at any of the tested pH conditions. Furthermore, anoxic photoreduction of yETF showed a different reduction pattern in comparison with hETF. The homology model of yETF showed a high degree of structural similarity to its human counterpart with the exception of βTyr-16 in hETF, which appeared to be a phenylalanine in yETF. Since this tyrosine residue plays a crucial role in the formation of 8-formyl-FAD in hETF, the replacement of this residue by a phenylalanine in the yeast protein rationalizes, at least in part, the finding that the 8α-methyl group is not oxidized to the 8-formyl group in yETF. Further investigations will be necessary to fully understand the differences of these two electron transferring flavoproteins.

Zusammenfassung

Oxidativer Ringschluss von N-Methyldopa durch ein Flavoenzym der Aminoxidase-Familie

Flavoenzyme sind bekannt dafür in der Natur viele Oxidationsreaktionen zu ermöglichen. Dazu zählen auch Ringschlussreaktionen in komplexen Verbindungen wie etwa pflanzlichen Sekundärmetaboliten. Im Gencluster der Fumisoquin-Biosynthese des filamentösen Pilzes *Aspergillus fumigatus* findet sich *fsqB* („fumisoquin biosynthesis gene B)*, das ein Flavoprotein der Aminoxidase Familie kodiert und mutmaßlich die Bildung von Isoquinolinen in oxidativen Ringschlussreaktionen katalysiert. Bis jetzt waren derartige Reaktionen nur von Enzymen Berberine Bridge Enzym Familie (wie BBE oder Tetrahydrocannabinolsynthase) bekannt, die sich jedoch strukturell sehr stark von den Aminoxidasen unterscheiden. Diese Tatsache veranlasste mich dazu die Struktur und Funktion von FsqB genauer zu beleuchten. Die Kristallstruktur von FsqB zeigte, dass das Protein mit einem kovalent gebundenen FAD-Kofaktor zur Aminoxidase Familie zu zählen ist. In kinetischen Experimenten mit fünf unterschiedlichen Substratanaloga erwies sich *N*-Methyldopa als bestes Substrat für FsqB: *N*-Methyldopa wurde vollständig zum zyklischen Isoquinolinprodukt umgesetzt. Das Fehlen der *meta*-Hydroxylgruppe, wie etwa in L-*N*-Methyltyrosin, führte zu einer 25-mal langsameren Reduktionsrate und zur Bildung des demethylierten Produktes L-Tyrosin anstelle des zyklischen Endproduktes. Überraschenderweise wurde im Gegensatz zu *N*-Methyldopa, wo beide Stereoisomere mit ähnlichen Raten umgesetzt wurden, das D-Stereoisomer von *N*-Methyltyrosin nicht als Substrat von FsqB akzeptiert. Aufgrund der vorliegenden Kristallstruktur und verschiedener Dockingexperimente postuliere ich daher, dass verschiedene Substrate unterschiedlich im Aktivzentrum von FsqB gebunden werden und dadurch unterschiedliche stereospezifische Oxidationen ermöglicht werden.

Charakterisierung des Elektronentransferierenden Flavoproteins (ETF) der Hefe
Saccharomyces cerevisiae

Elektronentransferierende Flavoproteine (ETFs) sind eine Gruppe von FAD-abhängigen Proteinen, die in der mitochondrialen Matrix von Dehydrogenasen Elektronen aufnehmen und diese an die Atmungskette weiterleiten. Der Mechanismus von ETFs ist immer noch Gegenstand vieler Untersuchungen. Erst kürzlich wurde berichtet, dass der FAD Kofaktor des menschlichen ETF (hETF) oxidiert wird und dabei die 8α-Methylgruppe zum 8-Formyl-FAD umgewandelt wird. Im Rahmen meiner Arbeit wurde das Elektronentransferierende Flavoprotein der Hefe *Saccharomyces cerevisiae* (yETF) heterolog hergestellt und gereinigt, um zu untersuchen, ob 8-Formyl FAD auch in einfachen eukaryontischen Zellen gebildet wird. yETF konnte in ausreichenden Mengen hergestellt und gereinigt werden. Das 8-Formyl-FAD konnte jedoch bei keiner der getesteten Bedingungen (pH –Werte zwischen pH 7 bis pH 8.5) nachgewiesen werden. Photoreduktionsexperimente zeigten Unterschiede in dem Reduktionsverhalten zwischen hETF und yETF. Ein Homologiemodell zeigte eine hohe Ähnlichkeit zwischen yETF und hETF mit einem entscheidenden Unterschied im Tyrosin-Rest (βTyr-16), welches im humanen Protein eine entscheidende Rolle bei der Bildung des 8-Formyl-Produktes spielt. Im yETF befindet sich anstelle des Tyrosinrestes ein Phenylalanin und daher kann davon ausgegangen werden, dass dieser Aminosäureaustausch für die beobachteten Unterschied verantwortlich ist. Weitere Untersuchungen sind allerdings notwendig um diese Unterschiede auf molekularer Ebene zu verstehen.

Section I

Oxidative cyclization of *N*-methyl-dopa by a fungal flavoenzyme of the amine oxidase family

Chapter 1: Introduction

Flavoenzymes and the family of amine oxidase

Flavoproteins constitute a versatile group of enzymes playing major roles in the catalysis of different redox reactions (1). These enzymes employ either flavin adenine dinucleotide (FAD) or flavin mono nucleotide (FMN) as cofactor (2). These two cofactors are derived from riboflavin (vitamin B2) and comprise a redox-active isoalloxazine ring. Flavoproteins are broadly spread in all domains of life including fungi, where they are mostly found in the saprotrophs (3). Most of these enzymes are oxidases or dehydrogenasse that are used by the fungus in diverse biosynthetic pathways leading to the production of secondary metabolites such as alkaloids (3, 4). Flavin-dependent enzymes catalyze a broad range of oxidations including reactions that entail the formation of rings in natural product biosynthesis, such as tetrahydrocannabinol and isoquinoline alkaloids (5). Thus far, oxidative cyclisation reactions appeared to be confined to flavoenzymes belonging to the vanillyl oxidase family, such as tetrahydrocannabinol synthase (THCS) and berberine bridge enzyme (BBE) (6, 7). An oxidase isolated from *Aspergillus fumigatus* was found in the biosynthesis of the isoquinoline alkaloid fumisoquin and belonging to amine oxidase family. This enzyme named FsqB has a similar function to berberine bridge enzyme (BBE) isolated from *Eschscholzia californica* (8). Both FsqB and BBE are involved in the biosynthesis of isoquinoline alkaloids (8, 9). Flavin-dependent amine oxidases have a well-defined structural topology that diverges substantially from the vanillyl oxidase family. On the other hand, covalent linkage of the FAD cofactor to the protein backbone was reported for both the amine oxidases (*e.g.* sarcosine oxidase, MSOX and *N*-methyltryptophan oxidase, MTOX) and the family of berberine bridge enzyme-like enzymes (*e.g.* berberine bridge enzyme and tetrahydrocannabinol synthase). The suggested mechanism of FsqB is similar to BBE. In both enzymes a hydride is abstracted from the substrate to reduce FAD subsequently. A proton is abstracted from the phenol moiety in a concerted or stepped wise manner enabling the nucleophilic attack on the iminum intermediate leading to the formation of the cyclized product (6, 10, 11). FsqB is structurally similar to sarcosine oxidase (accession number EAL85695), a member of the D-Amino acid oxidase family, that is well known to operate by a hydride transfer mechanism from methyl group of the substrate to the FAD (11). It is suggested that FsqB shows the P-hydroxybenzoate hydroxylase (PHBH) fold which is common for D-amino acid oxidases (DAAOs) (12). This fold contains generally two domains; FAD binding domain consisting of β-sheets sandwiched by α-helices and catalytic domain consisting of eight β-sheets that form the cavity, where the FAD-isoalloxazine ring is embedded. These sheets are also surrounded by long α-helices (12–14).

The family of D-amino acid oxidases (DAAO)

The first D-amino acid oxidase (DAAO), which is classified as a subgroup of the dehydrogenase-oxidase class of flavoproteins, was discovered in pig kidney (15) in 1935. Warburg O. and Christian W. identified FAD as cofactor in this enzyme in 1938 (16). Since then, this enzyme family turned to be interesting for further investigationsand new members of the enzyme family were characterized like glycine oxidase. These enzymes have the same proposed mechanism as the pig kidney DAAO, although they have different biological function that vary from metabolic utilization in yeast to neromodulator in humans. It has been proved by steady state kinetics and presteady state kinetic studies that in the reductive half reaction, a hydride equivalent [scheme 1] is transferred from the substrate to the flavin to yield the reduced cofactor and the oxidized substrate bound to the reduced enzyme. The active site of DAAOs has a loop which changes its conformation upon binding of the substrate. This switch increases the hydrophobicity of the active site and improves the efficiency of hydride transfer (17–21). In detail, the enzyme dehydrogenates the amino acid to the corresponding imino acid by forming the reduced flavin. Then, the imino acid hydrolysis non-enzymatically to α-keto acid and ammonia (19).
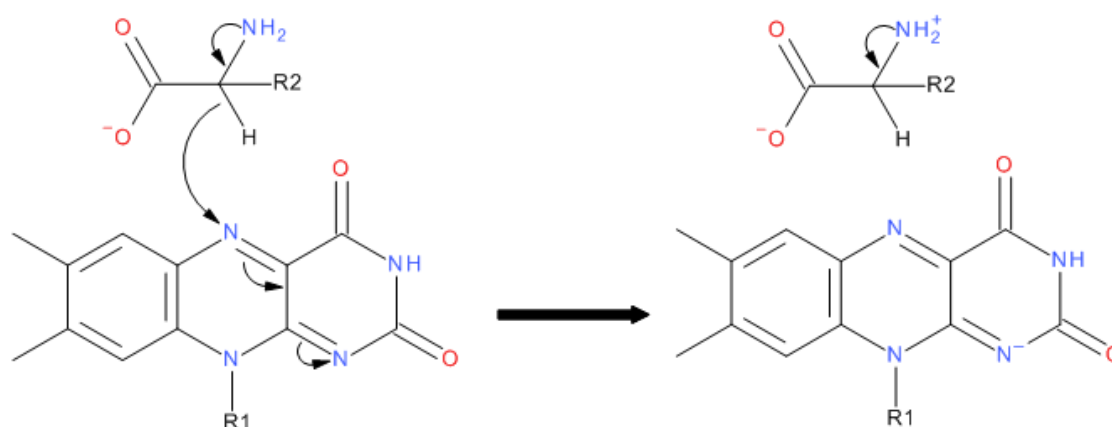
Scheme 1. Hydride transfer mechanism of DAAO (19)

After product dissociation from the enzyme, the reduced flavin reacts subsequently with oxygen to regenerate the oxidized enzyme. Alternatively, oxygen can react with the reduced enzyme before the product dissociates and then followed by product dissociation from the oxidized enzyme (11) [scheme 2].
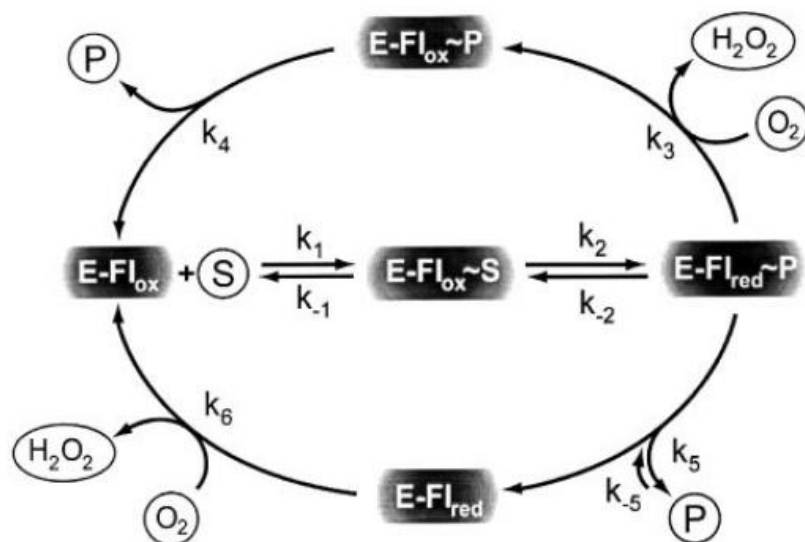
Scheme 2. Kinetic mechanisms proposed for the catalytic cycle of DAAO. The upper part represents a sequential mechanism and the lower one shows a ping-pong mechanism (19)

DAAO enzymes have a conservative three dimensional structure among all species from representatives in microorganisms to mammals (22–24). This structure was named PHBH fold [P-hydroxy benzoate hydroxylase] (12, 25). This fold contains generally two domains; The FAD binding domain consisting of β-sheets sandwiched by α-helices and the catalytic domain consisting of eight β-sheets that form the cavity, where the FAD-isoalloxazine ring is embedded. These sheets are also surrounded by long α-helices. In all DAAO enzymes, the FAD binding domain contains the Rossman fold βαβ, motif which is known as the dinucleotide binding motif. The isoalloxazine ring of flavin is located at the interface of two domains with its *re*-face facing the inner part of the substrate binding cavity. It is noteworthy to mention that all DAAO enzymes are covalently bound to FAD through a histidyl or cysteinyl bond on the 8α position of FAD (23, 12–14). It is proved that covalent attachment of the flavin to the enzyme enhances the oxidative power of flavin (26). The N1_C2=O locus of the flavin is in contact with a positively charged N-terminus of α-helix (<3.5Å). The positive charge of this location can stabilize the anionic form of the reduced FAD and increases the redox potential of the flavin (12, 27). DAAOs stabilize the anionic semiquinone form of the cofactor. However, this flavin semiquinone does not prove that catalysis involves radical species (11). The reaction catalyzed by DAAO follows a sequential kinetic mechanism in which the rate-limiting step is represented by the product release from the reoxidized enzyme (28). DAAOs show a higher catalytic efficiency for hydrophobic substrates, such as D-

phenylalanine, D-tryptophan, D-proline, and D-tyrosine, and catalyze the oxidation of (29). For the activation of the substrate, the enzyme stabilizes the deprotonated form of the amino group on the substrate and facilitates the formation of the imino product (27). To protect the substrate from the solvent, a mobile loop in DAAO plays the role of a gate to close and open the active site and protect the substrate (27).
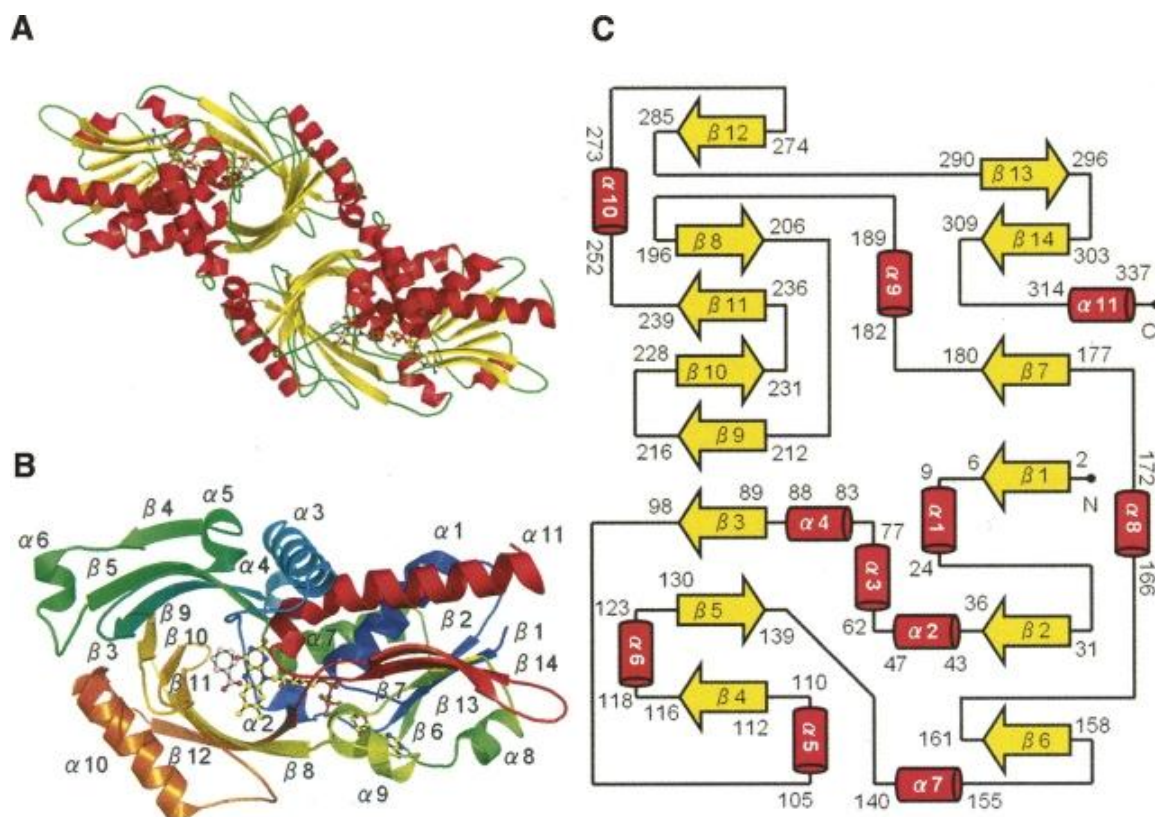
Figure 1. Overall structure of the hDAAO holoenzyme in complex with benzoate. FAD and benzoate are shown as ball-and-stick representations in *A* and *B*. **(A)** The DAAO homodimer colored by secondary structure (helix in red, sheet in yellow, loop in green). **(B)** The DAAO subunit colored spectrum in rainbow from the N terminus (blue) to the C terminus (red). Secondary structure elements are labelled. **(C)** Topology of the DAAO subunit (helix in red, sheet in yellow)(29).

Sarcosine oxidase family

In this family, which is considered as a part of DAAOs, the substrates are *N*-methylated amino acids like sarcosine (*N*-methyl-glycine) and *N*-methyl-tryptophan. The reaction differs from that of DAAOs in that the bond between the amino nitrogen and the methyl group is oxidized instead of the bond between the amino nitrogen and the α-carbon and the formed product is the demethylated substrate with the corresponding aldehyde (11)[scheme 3].

This family does not contain only sarcosine (*N*-methyl-glycine) oxidase, but also *N, N*-dimethyl-glycine oxidase, N-methyl-tryptophan oxidase (MTOX), an archaeal proline

dehydrogenase, heterotetrameric sarcosine oxidase (TSOX), pipecolate oxidase (OIPOX), sarcosine dehydrogenase (SDH) and NikD. These enzymes catalyze similar reactions and have similar structures (30–35).
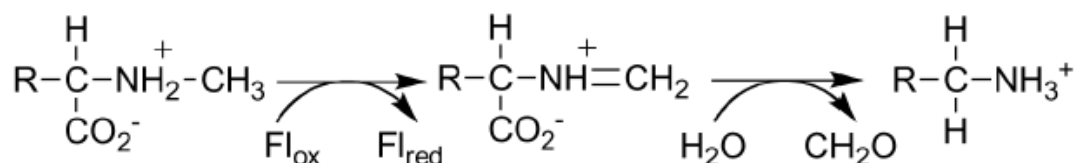
Scheme 3. Oxidation of N-methyl amino acids (D-isomers) catalyzed by sarcosine oxidase family (11).

The bacterial sarcosine oxidase (SOX) enzymes are induced in various microorganisms, when grown on sarcosine as the sole source of carbon and energy. These bacterial enzymes can be divided into three subclasses: the monomeric (MSOX), the heterodimeric (DSOX), and the heterotetrameric (TSOX) enzymes (36).

Structural studies show that the sarcosine substrate binds in the opposite orientation to that in DAAO, providing an explanation for the altered substrate specificity (11). The FAD in these enzymes is covalently attached to the protein through the bond between a cysteine residue and the methyl group at 8α position of the flavin (37). The mutation of this cysteine residue to alanine leads to the apoenzyme.

Four mechanisms were proposed for the sarcosine oxidase family. In all these four reaction mechanisms, two electrons and one proton are transferred from the substrate to the flavin (38). These four mechanisms can be summarized as following [scheme 4].

MSOX suggested mechanisms

a) Single electron transfer mechanism (SET)

First, a single electron is moved from the nitrogen of the substrate to the flavin, to generate a radical pair. Next, a single proton transfers from the amine radical cation in the sarcosine anion to the flavin anion radical; this is followed by the transfer of another electron, resulting in the formation of the corresponding imine product and 1,5-dihydroflavin in sequence. In the other route, after the initial one-electron transfer, a hydrogen radical, that is, a hydrogen atom, moves from the sarcosine radical to the flavin radical, yielding the imine product (38).

b) Polar mechanism

The substrate acts as nucleophile and attacks the C(4a) atom of the flavin ring resulting in the formation of a flavin–substrate adduct, wherein the lone-pair electrons of the N atom of the substrate are transferred to the flavin, which acts as electron sink. This is followed by the loss

of a proton from the methyl group of the substrate. Then the adduct collapses to form the oxidized substrate and reduced flavin (11, 38, 39). Classical studies on sarcosine oxidase family showed that this mechanism is not preferable since no redox intermediate was observed and there is no base in the active site to abstract the proton from the substrate (38, 40, 41). On the other side, this mechanism was strongly suggested for the mono amino oxidase (MAO) family (42–44).

c) Hydride transfer mechanism

A hydride (H^-) ion is directly transferred from the methyl group of the substrate to the flavin N(5) atom (38). The soaking of sarcosine oxidase crystals with inhibitors showed that the methyl group of sarcosine is located above the N(5) of the flavin and the nitrogen of sarcosine is above C(4a) of the flavin and this position is suitable for hydride transfer mechanism (45). The favorable thermodynamics for hydride transfer and the absence of evidence for semiquinone in the reductive half reaction, suggest that hydride transfer is the most likely mechanism for sarcosine oxidase family (11).

d) Carbanion mechanism

A proton from the methyl group of the substrate is abstracted by a base. Then, a transient intermediate forms a covalent bond between the carbanion and the flavin N(5) atom. This reaction was suggested based on stopped-flow spectroscopy studies of heterotetrameric sarcosine oxidase (TSOX) (35).
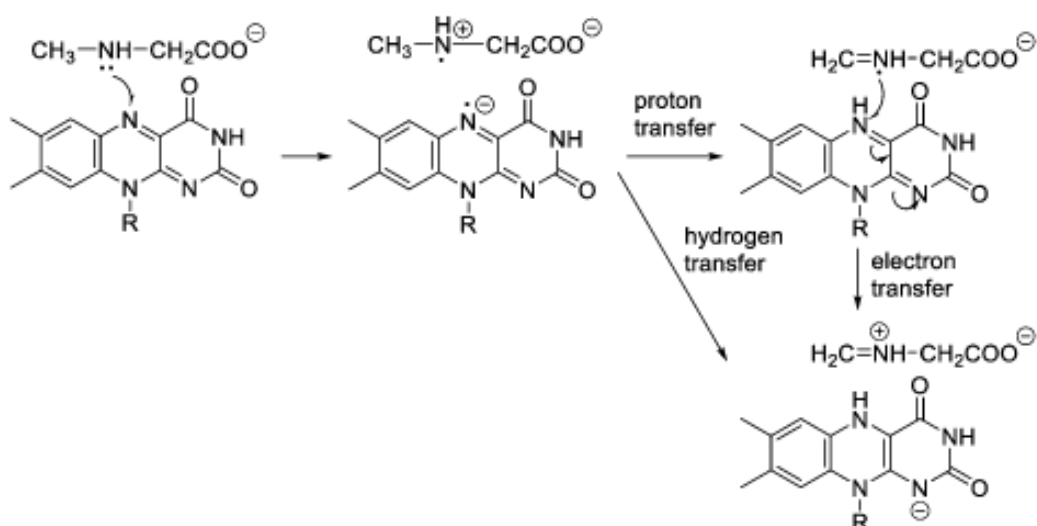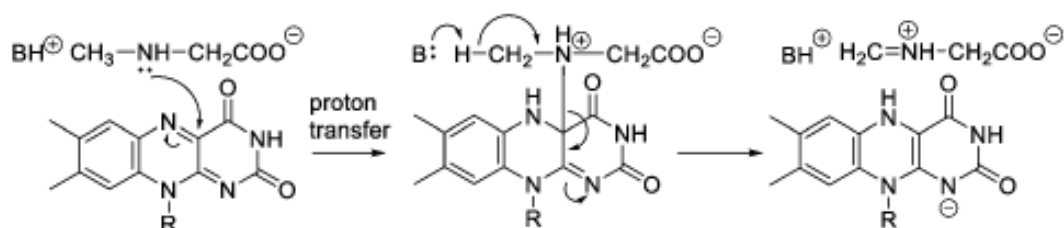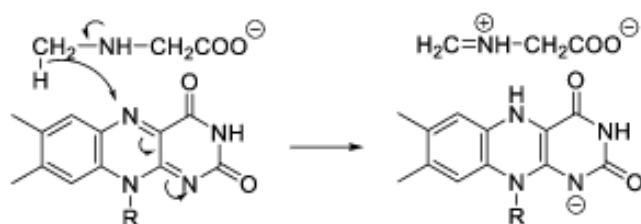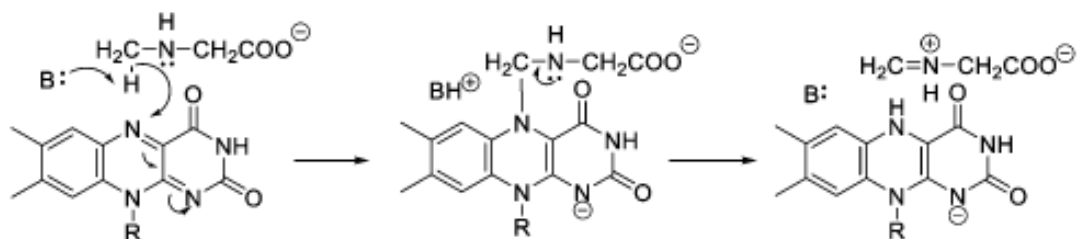
Scheme 4. The four proposed reaction mechanisms for sarcosine oxidase family (38).

Abe et. *al*. (2017) found that a hydride transfer mechanism is the most feasible one for the sarcosine oxidase enzyme based on energy barrier calculations. Based on the HOMO (highest occupied molecule orbital) distribution in the transition state and the changes in the atomic charge density during the reaction, the investigated MSOX reaction is suggested to involve the HACET mechanism (Hydrogen atom coupled electron transfer). In this mechanism, two

electrons are transferred completely to the flavin ring via the transfer of a hydrogen and orbital overlapping between sarcosine and the flavin (38).

For MSOX re-oxidation, Lys 265 is responsible for a positive charge of the pocket above the *si*-face. Lys 265 provides an organized binding site for a superoxide anion. Mutation in Lys 265 causes a loss in the positive charge that results in great reduction of re-oxidation. Moreover, the same mutation disrupts the water relay system near the falvin N(5) atom that probably causes ionization of the protonated sarcosine intermediate (46). Wagner et al. (2000) showed that reoxidation proceed via a modified ping pong mechanism. In this mechanism, the oxygen reacts with the reduced form of the enzyme-product prior to dissociation of the imino acid product (45).

Stopped-flow studies on dimethyl glycine oxidase [DMGO] showed the existence of the imine product as intermediate since the flavin reduction is triphasic. The first observed phase is flavin reduction. The second phase is iminium release from the active site. And the third slow phase is as yet unknown (34).

The protein fold of the sarcosine oxidase family is named PHBH and is the same as for DAAOs(47). FAD is covalently bound to the enzyme and it has an extended conformation and it is almost isolated from bulk solvent (33). Interestingly, a butterfly bending of the flavin is observed. This type of bending modulates substantially the reduction potential of the flavin to favor reduction by the substrate (48). Trickey et. *al*. [1999] showed that the enzyme has an α-helix, named as αF4, which helps to stabilize the electrophilic character of the flavin ring and the anionic forms of the hydroquinone and semiquinone (33).

Concerning the mechanism of MSOX, the carboxylate group of the substrate forms a hydrogen bond with the amino group of Lys 348 and the guanidinium side chain of Arg52 (33). Whereas, the position of Lys 348 is not changed, the binding with Arg 52 causes the movement of this residue into the active site and the displacement of two water molecules in the active site (40). It should be noticed that the three residues: His225, Tyr259, and Gly270 are very conservative residues. His225 forms a hydrogen bond to Tyr259, which is located close to the N(5) of the flavin. The position of this His–Tyr pair allows glycine to occupy position 270 (30).The His–Tyr dyad facilitates ionization of the sarcosine cation to allow a nucleophilic attack at the flavin C(4a) position (34). Arg49 is located below the flavin ring on the *si*-face and its side chain forms a Van der Waals contact with the ring. The flavin O(2) of MSOX forms a hydrogen bond with the Lys348 side chain. The ribityl hydroxyl O(2) is linked to the side chain of Arg49 (33). The N(5) atom of the flavin forms two hydrogen bonds with two water molecules. The first water molecule is located on the *re*-face and the second

one is located on the *si*-face. This type of bonds between N(5) and water seems to be a part of a proton relay system (PRS). The PRS involves Thr48, Lys265 and four water molecules. Water molecule 1 is hydrogen bonded to the flavin N(5), the carbonyl oxygen of Thr48 and the ε-amino group of Lys265 (Figure 1a). The other three water molecules are accessible to bulk solvent(33). Moreover, Trickey et. *al* found that Arg52 and the loop region from Gly56 to Glu60 play the role of a switch for the active site, in which the loop is flexible in the absence of the substrate. Once Arg52 coordinates to the substrate, the loop is locked into a fixed conformation (33). Different studies showed that the anionic substrate is the active form that can be catalyzed by MSOX (40, 49, 50). It is noteworthy to mention that MSOX does not have an acidic residue in the region surrounding the flavin ring. It is believed that the positive residues in the pocket and an α helix dipole, which starts at Phe347, might cause a positive shift in the flavin redox potential (33).

Covalent flavinylation

The covalent bond between the flavin and the apoenzyme of MSOX occurs via initial flavin tautomerization to give an electrophilic iminoquinone methide. The ε-amino group of Lys348 in MSOX is 2.8 Å away from the C(2) carbonyl oxygen of the isoalloxazine ring. The positive end of a helix dipole (αF4) also points toward the same carbonyl oxygen. Both are ideally positioned to facilitate the development of a negative charge at the N(1)–C(2) = O(2) locus during tautomerization. In a second step, the nucleophilic addition of Cys315 thiolate to the flavin iminoquinone methide generates the (8a– S-cysteinyl)-1,5-dihydroFAD anion. A base is needed to act as a proton acceptor from the 8a-methyl group of FAD during tautomerization and possibly to generate the reactive thiolate form of Cys315 (Scheme 5) (33).
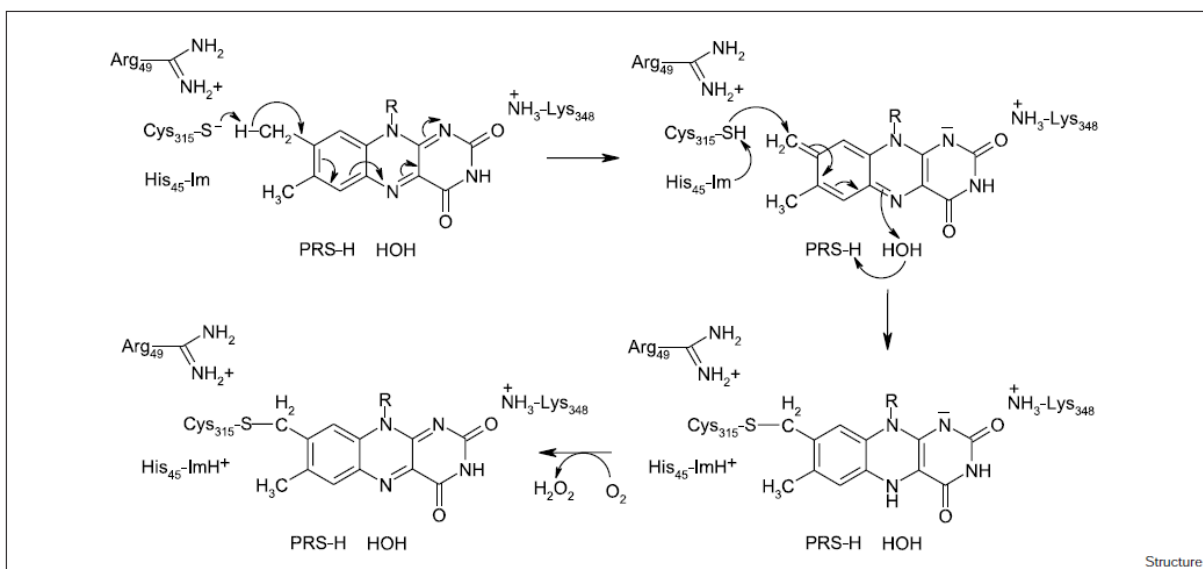
Scheme 5. Proposed mechanism for covalent flavinylation in MSOX (33).
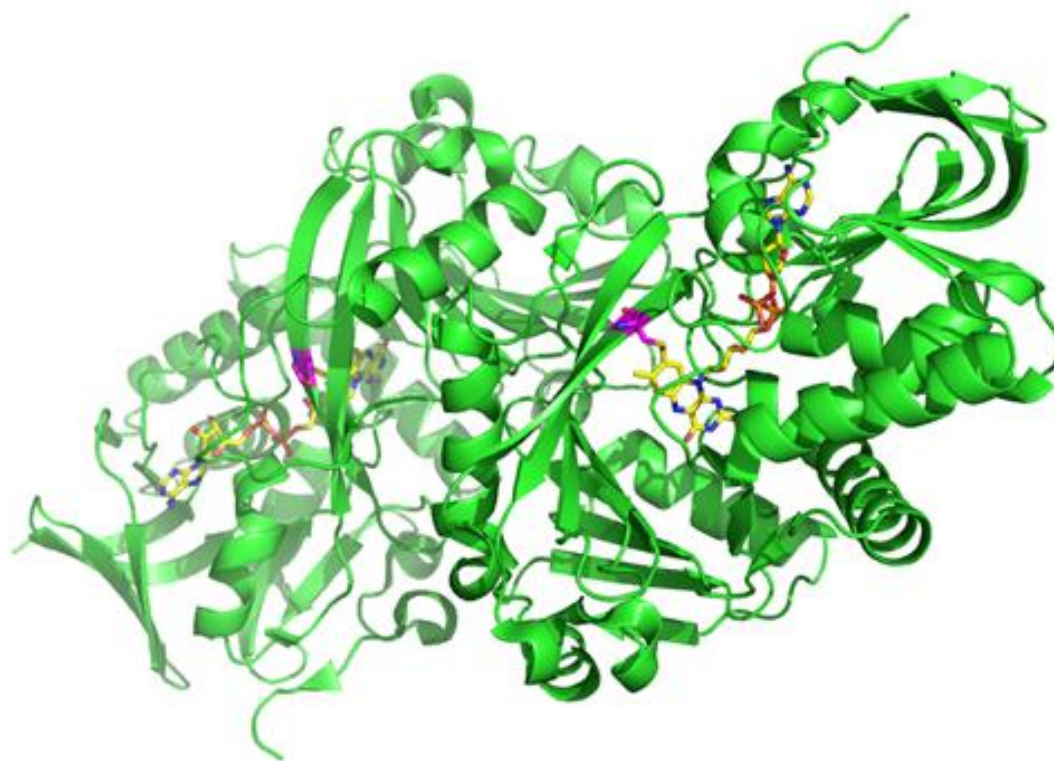
Figure 2. Cartoon representation of MSOX from Bacillus sp. showing the dimeric form of the enzyme and covalent attachment of the flavin to the enzyme by a cystein residue. The protein is shown in green; Flavin is shown in yellow and the cystein residue that binds the flavin is in magenta. The pdb code for this structure is 2GB0 (33).

The second important member of the sarcosine oxidase family is N-methyl-tryptophan oxidase (MTOX). This enzyme catalyzes the oxidation of N-methyl-tryptophan as substrate and to a lesser extent sarcosine is accepted (37). MTOX catalyzes the oxidation of the L-

stereoisomer of the substrate(51). In both MSOX and MTOX, the anionic form of the substrate forms a charge transfer complex with the oxidized form of flavin, which serves as charge acceptor (52–54). Moreover, this complex is stabilized by the pairs of (MSOX/MTOX: R49/R48-K265/K259 and R52/R51-K348/K341 on the *si* and *re* face of flavin, respectively)(54, 55). In MTOX, amine oxidation leads to a reduction of the flavin through two-electron transfer. The flavin, then, is reoxidized by molecular oxygen and produces hydrogen peroxide through a modified ping-pong mechanism (56). According to the quantum mechanics study of Karasulu and Thiel (2015), the proton relay system in MSOX was not observed in MTOX. A proton shuttle was not observed in any of the NVT ensembles with *N*-methyl-tryptophan (NMT), except for the special case of Non-ZwNMT (Nonzwitterionic form) with both K259 and K341 residues in un-protonated state. Interestingly, Karasulu and Thiel (2015) also reported that the active form of the NMT substrate is the anionic form and it is achieved only in one case: when Lys259 is protonated and Lys341 is unprotonated. Whereas, it is proved that there is a water molecule on the *re*-face of flavin in MSOX, which plays a role in the proton relay system, no water molecules were found in MTOX (57). Talking about the redox potential of flavin, in MTOX, no butterfly effect was observed like in TMADH (48), however, it was shown that the flavin is not planar (57).

Finally, the QM/MM studies for the mechanism of MTOX shows that this enzyme follows the hydride transfer mechanism. The following docking figure shows the substrate pose in the MTOX pocket (57).
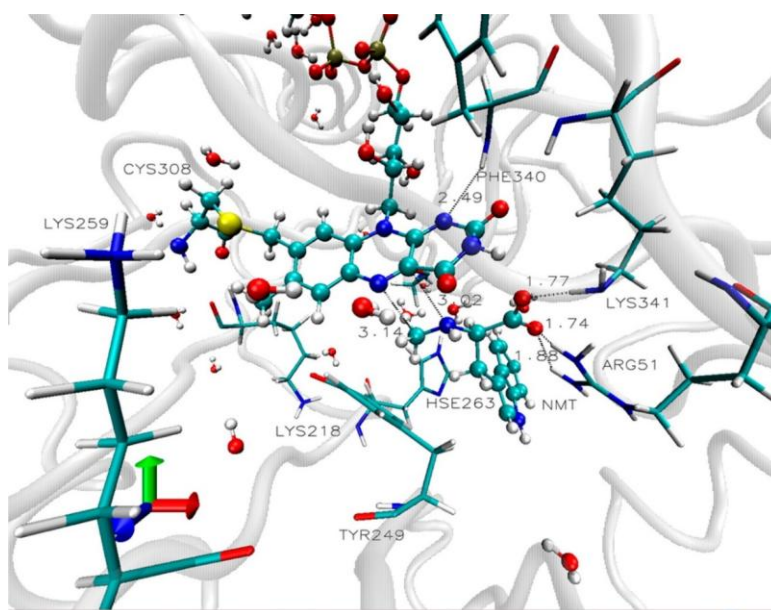
Figure 3. Typical snapshot from the NVT ensemble for AnNMT (K259, protonated; K341, deprotonated). Depicted are FAD and NMT (ball and stick), important MTOX residues (stick), and the MTOX structure (cartoon).

FsqB, a new enzyme member in the family of sarcosine oxidase

In 2016, Baccile et. *al*. reported a new enzyme from *Apergillus fumigates* -named FsqB- which catalyzes the same reaction as berberine bridge enzyme (BBE) and oxidizes the methylamine of a product involved in the biosynthesis pathway of an isoquinoline alkaloid named fumisoquine [scheme 6]. This enzyme is part of a cluster that is synthesized by a nonribosomal peptide synthesis like gene (NRPS) (8).
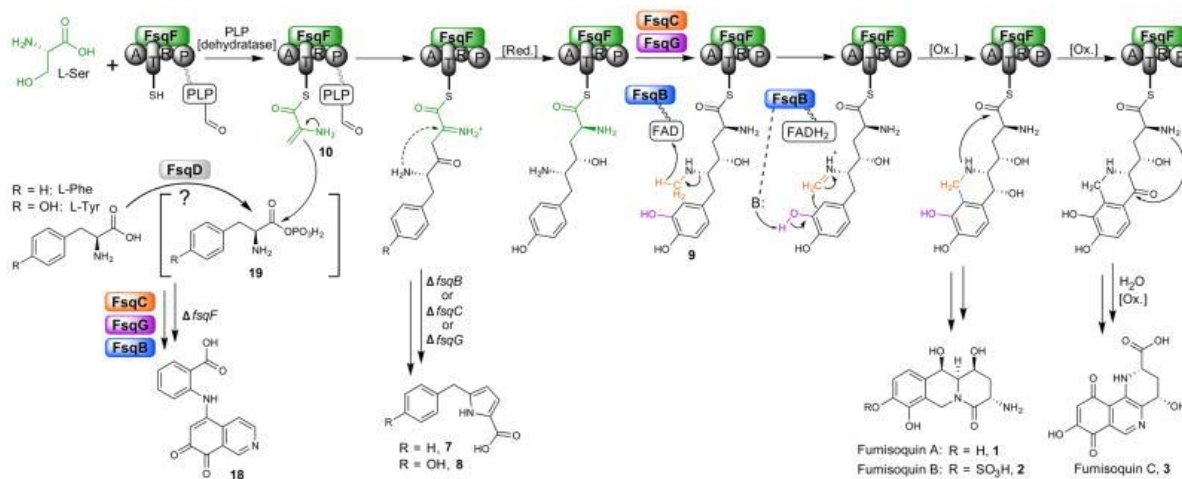
Scheme 6. The biosynthetic pathway of isoquinoline alkaloid fumisquin in *Apergillus fumigates*. The Fsq cluster catalyze the biosynthesis of this alkaloid and FsqB enzyme oxidizes the methyl amine functional group and leads to a ring closure reaction (8).

The genes coding for FsqB cluster consist of seven genes represented as following:
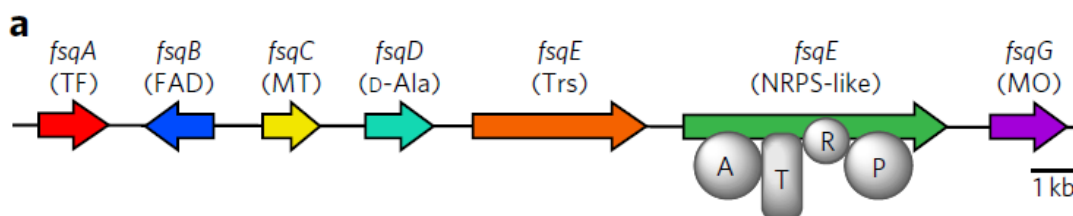
Scheme 7. fsq gene cluster. fsqA is a TF transcription factor; fsqB is FAD-binding domain protein; fsqC is MT, N-methyltransferase; fsqD is ATP-grasp enzyme (D-alanine ligase); fsqE is Trs, transporter; fsqF possesses an adenylation (A); thiolation (T); short-chain dehydrogenase/reductase (R) domain; and a pyridoxal phosphate (P) binding domain; and fsqG is a phenol 2-monooxygenase (MO).

FsqB is a flavoenzyme, which is covalently attached to FAD through Cys414 residue (8). The enzyme accession number is EAL85695 and contains a sarcosine oxidase region. The non-natural substrate for this enzyme is *N*-methyl-dopa as shown in scheme 8.

14
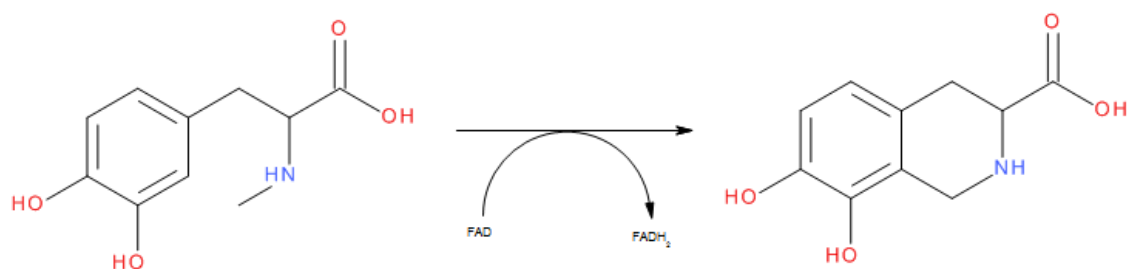
Scheme 8. Reaction catalyzed by FsqB. The *N*-methyl-dopa gets oxidized by the enzyme and a C-C bond is formed between the carbon of imine species and the adjacent carbon of the phenol ring.

Since FsqB oxidizes the methyl amine bond of the substrate, the formed intermediate is a imine species or what so called Schiff base. Baccile et. *al* (2016) proved this hypothesis through capturing this intermediate with dimedone (scheme 10). Later on, and similar to the suggested mechanism of berberine bridge enzyme (BBE), it was suggested that in FsqBthere is an amino acid that plays the role of a base and abstracts the proton from the hydroxyl group (meta position) on the benzene ring and thus leads to a ring closure as shown in scheme 6 (8).

Interstingly, the cyclized product was not observed when *N*-methyl- tyrosine or reticuline, the substate of BBE, were incubated with FsqB. Moreover, it was observed that FsqB tends to be regioselctive as shown in the following scheme (scheme 9) (8):
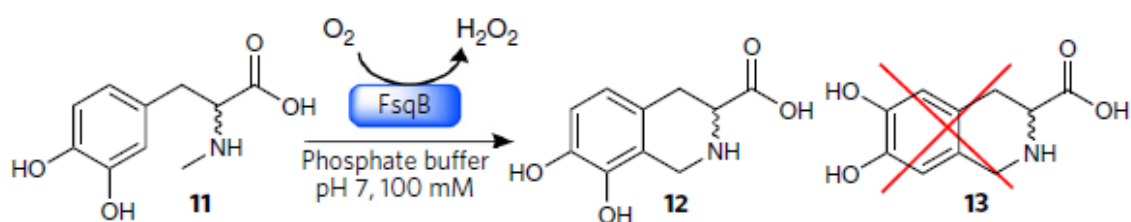
Scheme 9. Oxidation of *N*-methyl-dopa with FsqB shows that the reaction is regioselective.
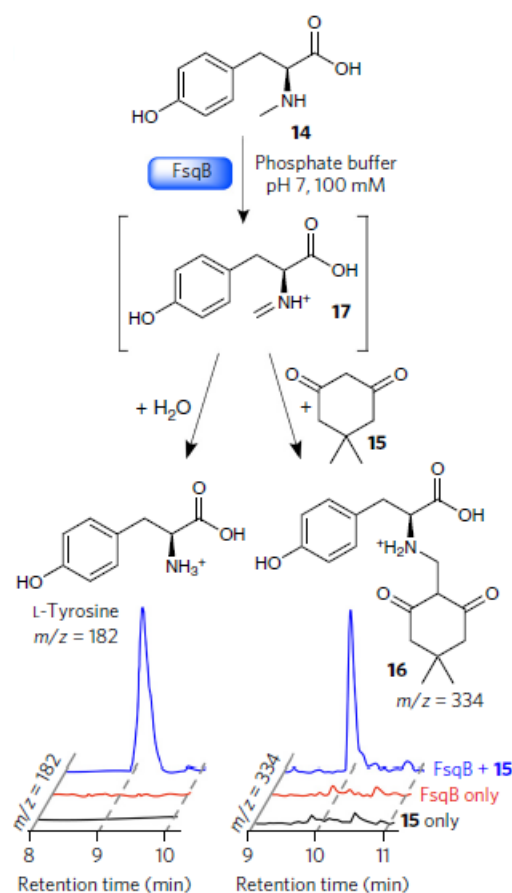
Scheme 10. Reaction of L-*N*-methyl-tyrosine oxidized by FsqB and the intermediate captured by dimedone (8).

The family of Berberine bridge enzyme like enzymes

Berberine bridge enzyme (BBE) is considered the key stone in the biosynthesis pathway of the isoquinoline alkaloid berberine. BBE catalyzes the oxidative cyclization of the *N*-methyl moiety of (S)-reticuline into the berberine bridge carbon, C-8, of (S)-scoulerine. (scheme 11) (1, 10).
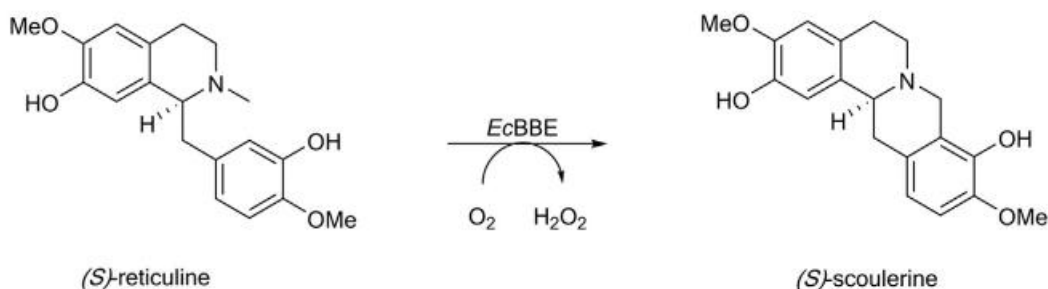
Scheme 11. Reaction catalyzed by BBE during isoquinoline biosynthesis in plants.

BBE exhibits typical flavoprotein oxidase properties as proved by the occurrence of an anionic semiquinone species (9). The reaction of BBE involves the oxidation of N-methyl functional group to the corresponding iminium species with subsequent cyclization to (*S*)-scoulerine (9). It is hypothesized that the electrons are passend to the flavin molecule either in a single two electron reduction step or in two one electron steps (10).

Two reaction mechanisms were proposed for this enzyme. The first one is a step-wise mechanism; a hydride equivalent is transferred from the substrate to the flavin, forming a methylene iminium ion intermediate; subsequently, an active-site base, Glu417, deprotonates a substrate phenol, making the adjacent carbon more nucleophilic and allowing its attack on the *N*-methylene group, yielding the cyclized product (58). The second mechanism is a concerted one; deprotonation of the phenol occurs during the concomitant attack on the *N*-methyl group by C2′ and the transfer of a hydride to the flavin (scheme 12) (6).
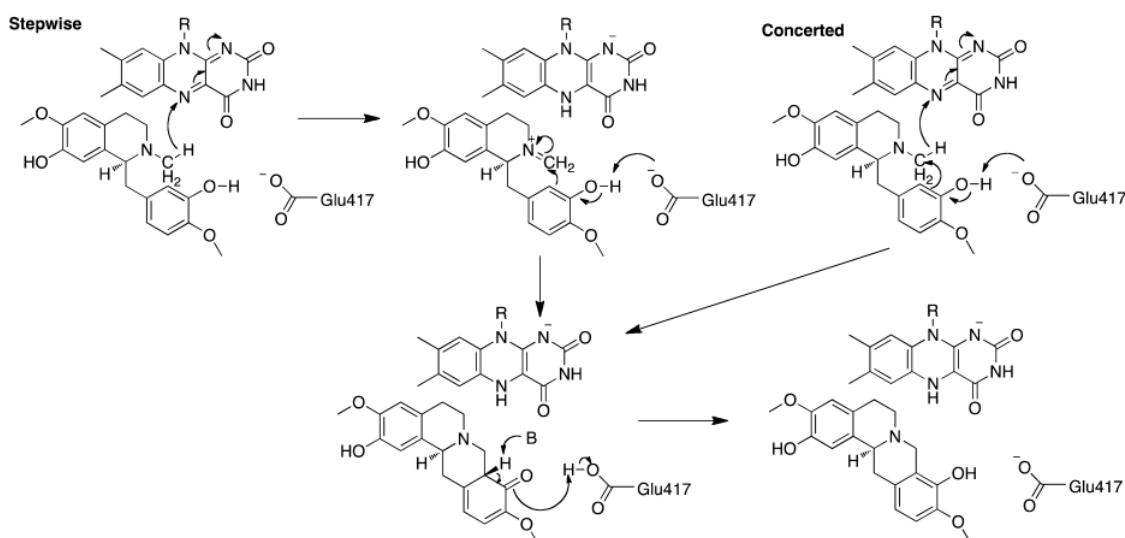
Scheme 12. Proposed mechanisms for BBE. The scheme shows the concerted and step-wise mechanisms (58).

One interesting hallmark of the family of BBE-like proteins was found during the in depth characterization of BBE and glucooligosaccharide oxidase (GOOX) from *Acremonium strictum*: a bicovalently attached FAD cofactor. The characteristic 6-S-cysteinyl-, 8a-N1-histidyl-FAD linkage is only found in the BBE-subfamily of the FAD-linked oxidases and has been shown to increase the redox potential of the cofactor by more than 300 mV compared to free flavin. The family of BBE-like enzymes forms a relatively large subgroup featuring a characteristic C-terminal structural element following the substrate binding region. BBE-like enzymes form a subgroup of the superfamily of FAD linked oxidases (SCOPe d.58.32) that is structurally characterized by a typical fold observed initially for vanillyl-alcohol oxidase (VAO). Therefore, the structural architecture has been described initially as the VAO-fold and

all members of this superfamily share a common architecture that can be divided into a FAD binding domain and a substrate binding domain, which is also referred to as the cap domain (Figure 4) (5) .
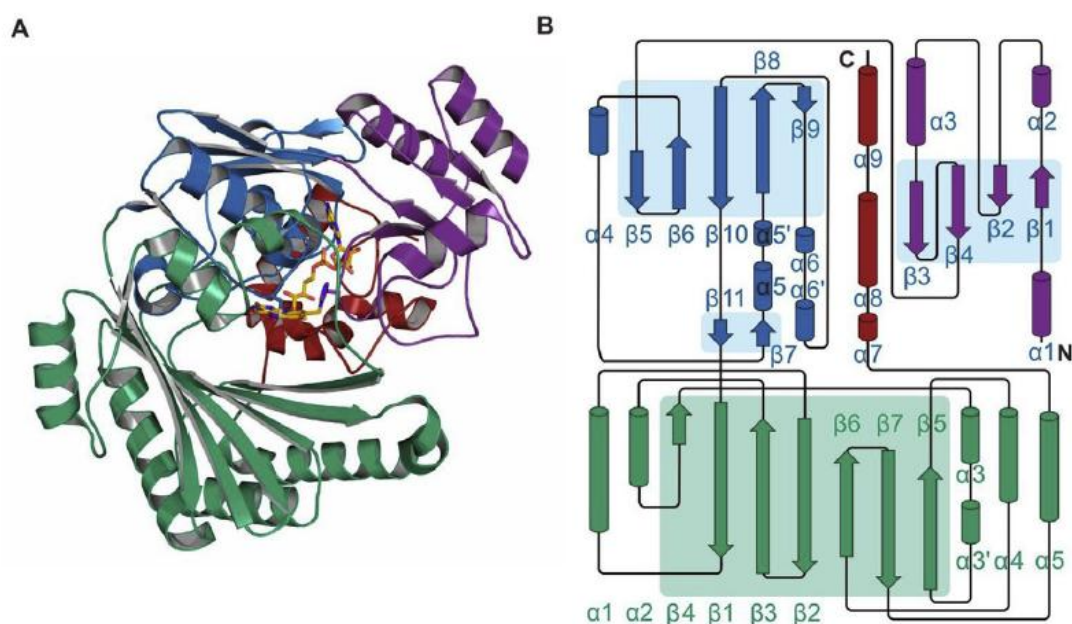
Figure 4. Overview of structural properties of the BBE-like family. A: The overall structure of a representative member (EcBBE; pdb 3D2J) is shown in cartoon representation. Individual sub-domains of the upper flavin-binding module are coloured in purple, blue and red. The FAD cofactor (shown as orange stick model) is bound in an extended conformation with the ribityl chain and the adenyl moiety sandwiched between all three subdomains. The isoalloxazine ring projects towards the active site that is formed by residues from the substrate binding module (green) and the initial part of the BBE-like specific C-terminus. B: Topology plot of the structure shown in panel A. Secondary structure elements are numbered consecutively for α-helices and β-strands in the flavin- and substrate-binding modules and are labelled in green and blue, respectively(5).

Isoquinoline alkaloids

Alkaloids, in general, are bicyclic, tricyclic, and tetracyclic derivatives of Nitrogen-containing low-molecular weight compounds. Alkaloids are widely distributed in species belonging to different families. They are found to have antimicrobial activity against fungal or bacterial phytopathogens and they were used historically as poisons and active agents in traditional medicine (59–61).

Benzylisoquinoline alkaloids are a large group of alkaloids, which are derived from tyrosine by a series of decarboxylation, intramolecular coupling, reduction, methylation, hydroxylation, and further modification reactions. And they share the benzylisoquinoline

heterocycle as common structural feature. Berberine and fumisoquin are good examples of this class of alkaloids (Figure 5) (62, 63).

Fumisoquin A: R = H
Fumisoquin B: R = SO$_3$H
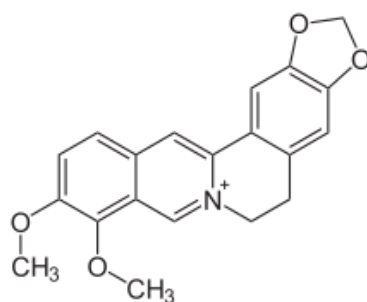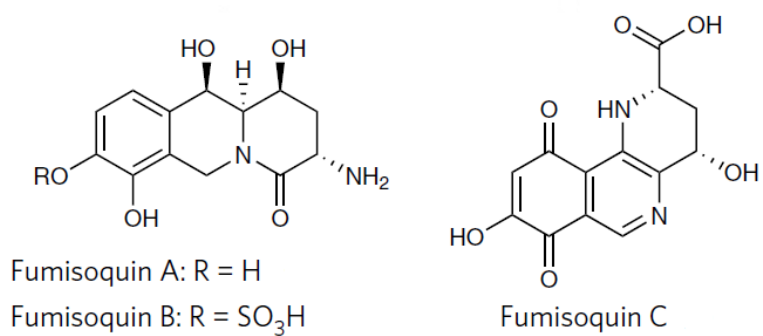
Fumisoquin C

Berberine

Figure 5. Structure of two different alkaloids, fumisoquin and berberine.

References

1. Wallner, S., Dully, C., Daniel, B., and Macheroux, P. (2012) *Berberine bridge enzyme and the family of bicovalent flavoenzymes*, 10.1515/9783110268911.1

2. Zafred, D., Steiner, B., Teufelberger, A. R., Hromic, A., Karplus, P. A., Schofield, C. J., Wallner, S., and Macheroux, P. (2015) Rationally engineered flavin-dependent oxidase reveals steric control of dioxygen reduction. *FEBS J.* **282**, 3060–3074

3. MacHeroux, P., Kappes, B., and Ealick, S. E. (2011) Flavogenomics - A genomic and structural view of flavin-dependent proteins. *FEBS J.* **278**, 2625–2634

4. Coyle, C. M., and Panaccione, D. G. (2005) An ergot alkaloid biosynthesis gene and clustered hypothetical genes from Aspergillus fumigatus. *Appl. Environ. Microbiol.* **71**, 3112–3118

5. Daniel, B., Konrad, B., Toplak, M., Lahham, M., Messenlehner, J., Winkler, A., and Macheroux, P. (2017) The family of berberine bridge enzyme-like enzymes: A treasure-trove of oxidative reactions. *Arch. Biochem. Biophys.* **632**, 88–103

6. Winkler, A., Łyskowski, A., Riedl, S., Puhl, M., Kutchan, T. M., Macheroux, P., and Gruber, K. (2008) A concerted mechanism for berberine bridge enzyme. *Nat. Chem. Biol.* **4**, 739–741

7. Shoyama, Y., Tamada, T., Kurihara, K., Takeuchi, A., Taura, F., Arai, S., Blaber, M., Shoyama, Y., Morimoto, S., and Kuroki, R. (2012) Structure and function of Δ1-tetrahydrocannabinolic acid (THCA) synthase, the enzyme controlling the psychoactivity of Cannabis sativa. *J. Mol. Biol.* **423**, 96–105

8. Baccile, J. A., Spraker, J. E., Le, H. H., Brandenburger, E., Gomez, C., Bok, J. W., MacHeleidt, J., Brakhage, A. A., Hoffmeister, D., Keller, N. P., and Schroeder, F. C. (2016) Plant-like biosynthesis of isoquinoline alkaloids in Aspergillus fumigatus. *Nat. Chem. Biol.* **12**, 419–424

9. Winkler, A., Hartner, F., Kutchan, T. M., Glieder, A., and Macheroux, P. (2006) Biochemical evidence that berberine bridge enzyme belongs to a novel family of flavoproteins containing a bi-covalently attached FAD cofactor. *J. Biol. Chem.* **281**, 21276–21285

10. Kutchan, T. M., and Dirtrich, H. (1995) Characterization and mechanism of the berberine bridge enzyme, a covalently flavinylated oxidase of benzophenanthridine alkaloid biosynthesis in plants. *J. Biol. Chem.* **270**, 24475–24481

11. Fitzpatrick, P. F. (2010) Oxidation of amines by flavoproteins. *Arch. Biochem. Biophys.* **493**, 13–25

12. MATTEVI, A., VANONI, M. A., TODONE, F., RIZZI, M., and ALEX TEPLYAKOV ALESSANDRO CODA, M. B. B. C. (1996) Crystal structure of D -amino acid oxidase : A case of active site mirror-image convergent evolution with flavocytochrome b 2. *Proc. Natl. Acad. Sci. USA*. **93**, 7496–7501

13. Rigoldi, F., Spero, L., Dalle Vedove, A., Redaelli, A., Parisini, E., and Gautieri, A. (2016) Molecular dynamics simulations provide insights into the substrate specificity

of FAOX family members. *Mol. BioSyst.* **12**, 2622–2633

14. Collard, F., Zhang, J., Nemet, I., Qanungo, K. R., Monnier, V. M., and Yee, V. C. (2008) Crystal structure of the deglycating enzyme fructosamine oxidase (Amadoriase II). *J. Biol. Chem.* **283**, 27007–27016

15. Krebs, H. A. (1935) Metabolism of amino-acids. *Biochem. J.* **29**, 1951–1969

16. Warburg, O., and Christian, W. (1938) Isolierung der prosthetischen gruppe der d-aminosiureoxydase. *Biochem. Z.* **298**, 150–168

17. Settembre, E. C., Dorrestein, P. C., Park, J. H., Augustine, A. M., Begley, T. P., and Ealick, S. E. (2003) Structural and mechanistic studies on thiO, a glycine oxidase essential for thiamin biosynthesis in Bacillus subtilis. *Biochemistry*. **42**, 2971–2981

18. Job, V., Marcone, G. L., Pilone, M. S., and Pollegioni, L. (2002) Glycine oxidase from Bacillus subtilis. Characterization of a new flavoprotein. *J. Biol. Chem.* **277**, 6985–6993

19. Pilone, M. S. (2000) D-Amino acid oxidase: new findings. *Cell. Mol. Life Sci.* **57**, 1732–1747

20. Molla, G., Sacchi, S., Bernasconi, M., Pilone, M. S., Fukui, K., and Pollegioni, L. (2006) Characterization of human d-amino acid oxidase. *FEBS Lett.* **580**, 2358–2364

21. Murtas, G., Sacchi, S., Valentino, M., and Pollegioni, L. (2017) Biochemical Properties of Human D-Amino Acid Oxidase. *Front. Mol. Biosci.* 10.3389/fmolb.2017.00088

22. Pollegioni, L., Diederichs, K., Molla, G., Umhau, S., Welte, W., Ghisla, S., and Pilone, M. S. (2002) Yeast D-amino acid oxidase: structural basis of its catalytic properties. *J Mol Biol*. **324**, 535–546

23. Pollegioni, L., Piubelli, L., Sacchi, S., Pilone, M. S., and Molla, G. (2007) Physiological functions of D-amino acid oxidases: From yeast to humans. *Cell. Mol. Life Sci.* **64**, 1373–1394

24. Pollegioni, L., Sacchi, S., Caldinelli, L., Boselli, A., Pilone, M. S., Piubelli, L., and Molla, G. (2007) Engineering the properties of D-amino acid oxidases by a rational and a directed evolution approach. *Curr. Protein Pept. Sci.* **8**, 600–18

25. Mizutani, H., Miyahara, I., Hirotsu, K., Nishina, Y., Shiga, K., Setoyama, C., and Miura, R. (1996) Three-dimensional structure of porcine kidney D-amino acid oxidase at 3.0 Å resolution. *J. Biochem.* **120**, 14–17

26. Fraaijet, M. W., Van Den Heuvel, R. H. H., Van Berkel, W. J. H., and Mattevi, A. (1999) Covalent flavinylation is essential for efficient redox catalysis in vanillyl-alcohol oxidase. *J. Biol. Chem.* **274**, 35514–35520

27. Fraaije, M. W., and Mattevi, A. (2000) Flavoenzymes: Diverse catalysts with recurrent features. *Trends Biochem. Sci.* **25**, 126–132

28. Sacchi, S., Caldinelli, L., Cappelletti, P., Pollegioni, L., and Molla, G. (2012) Structure-function relationships in human D-amino acid oxidase. *Amino Acids*. **43**, 1833–1850

29. Kawazoe, T., Tsuge, H., Imagawa, T., Aki, K., Kuramitsu, S., and Fukui, K. (2007)

Structural basis of d-DOPA oxidation by d-amino acid oxidase: Alternative pathway for dopamine biosynthesis. *Biochem. Biophys. Res. Commun.* **355**, 385–391

30. Leys, D., Basran, J., and Scrutton, N. S. (2003) Channelling and formation of "active" formaldehyde in dimethylglycine oxidase. *EMBO J.* **22**, 4038–4048

31. Carrell, C. J., Bruckner, R. C., Venci, D., Zhao, G., Jorns, M. S., and Mathews, F. S. (2007) NikD, an Unusual Amino Acid Oxidase Essential for Nikkomycin Biosynthesis: Structures of Closed and Open Forms at 1.15 and 1.90 Å Resolution. *Structure*. **15**, 928–941

32. Tsuge, H., Kawakami, R., Sakuraba, H., Ago, H., Miyano, M., Aki, K., Katunuma, N., and Ohshima, T. (2005) Crystal structure of a novel FAD-, FMN-, and ATP-containing L-proline dehydrogenase complex from Pyrococcus horikoshii. *J. Biol. Chem.* **280**, 31045–31049

33. Trickey, P., Wagner, M. A., Jorns, M. S., and Mathews, F. S. (1999) Monomeric sarcosine oxidase: Structure of a covalently flavinylated amine oxidizing enzyme. *Structure*. **7**, 331–345

34. Basran, J., Bhanji, N., Basran, A., Nietlispach, D., Mistry, S., Meskys, R., and Scrutton, N. S. (2002) Mechanistic aspects of the covalent flavoprotein dimethylglycine oxidase of Arthrobacter globiformis studied by stopped-flow spectrophotometry. *Biochemistry*. **41**, 4733–4743

35. Harris, R. J., Meskys, R., Sutcliffe, M. J., and Scrutton, N. S. (2000) Kinetic studies of the mechanism of carbon-hydrogen bond breakage by the heterotetrameric sarcosine oxidase of Arthrobacter sp. 1-IN. *Biochemistry*. **39**, 1189–1198

36. Suzuki, K., Sagai, H., Imamura, S., and Sugiyama, M. (1994) Cloning, sequencing, and overexpression in Escherichia coli of a sarcosine oxidase-encoding gene linked to the Bacillus creatinase gene. *J. Ferment. Bioeng.* **77**, 231–234

37. Wagner, M. A., Khanna, P., and Jorns, M. S. (1999) Structure of the flavocoenzyme of two homologous amine oxidases: Monomeric sarcosine oxidase and N-methyltryptophan oxidase. *Biochemistry*. **38**, 5588–5595

38. Abe, Y., Shoji, M., Nishiya, Y., Aiba, H., Kishimoto, T., and Kitaura, K. (2017) The reaction mechanism of sarcosine oxidase elucidated using FMO and QM/MM methods. *Phys. Chem. Chem. Phys.* **19**, 9811–9822

39. Brown, L. E., and Hamilton, G. A. (1970) Some Model Reactions and a General Mechanism for Flavoenzyme-Catalyzed Dehydrogenations. *J. Am. Chem. Soc.* **92**, 7225–7227

40. Zhao, G., and Jorns, M. S. (2006) Spectral and kinetic characterization of the Michaelis charge transfer complex in monomeric sarcosine oxidase. *Biochemistry*. **45**, 5985–5992

41. Binda, C., Mattevi, A., and Edmondson, D. E. (2002) Structure-function relationships in flavoenzyme-dependent amine oxidations: A comparison of polyamine oxidase and monoamine oxidase. *J. Biol. Chem.* **277**, 23973–23976

42. Abad, E., Zenn, R. K., and Kästner, J. (2013) Reaction mechanism of monoamine oxidase from QM/MM calculations. *J. Phys. Chem. B*. **117**, 14238–14246

43. Silverman, R. B., and Zelechonok, Y. (1992) Evidence for a Hydrogen Atom Transfer Mechanism or a Proton/Fast Electron Transfer Mechanism for Monoamine Oxidase. *J. Org. Chem.* **57**, 6373–6374

44. Miller, J. R., and Edmondson, D. E. (1999) Structure-activity relationships in the oxidation of para-substituted benzylamine analogues by recombinant human liver monoamine oxidase A. *Biochemistry.* **38**, 13670–13683

45. Wagner, M. A., and Jorns, M. S. (2000) Monomeric sarcosine oxidase: 2. Kinetic studies with sarcosine, alternate substrates, and a substrate analogue. *Biochemistry.* **39**, 8825–8829

46. Jorns, M. S., Chen, Z. W., and Mathews, F. S. (2010) Structural characterization of mutations at the oxygen activation site in monomeric sarcosine oxidase. *Biochemistry.* **49**, 3631–3639

47. Scrutton, N. S. (2004) Chemical aspects of amine oxidation by flavoprotein enzymes. *Nat. Prod. Rep.* **21**, 722

48. Trickey, P., Basran, J., Lian, L. Y., Chen, Z. W., Barton, J. D., Sutcliffe, M. J., Scrutton, N. S., and Mathews, F. S. (2000) Structural and biochemical characterization of recombinant wild type and a C30A mutant of Trimethylamine dehydrogenase from Methylophilus methylotrophus (sp. W3A1). *Biochemistry.* **39**, 7678–7688

49. Zhao, G., and Jorns, M. S. (2002) Monomeric sarcosine oxidase: Evidence for an ionizable group in the E·S complex. *Biochemistry.* **41**, 9747–9750

50. Zhao, G., and Jorns, M. S. (2005) Ionization of zwitterionic amine substrates bound to monomeric sarcosine oxidase. *Biochemistry.* **44**, 16866–16874

51. Ilari, A., Bonamore, A., Franceschini, S., Fiorillo, A., Boffi, A., and Colotti, G. (2008) The X-ray structure of N-methyltryptophan oxidase reveals the structural determinants of substrate specificity. *Proteins Struct. Funct. Genet.* **71**, 2065–2075

52. Bruckner, R. C., Winans, J., and Jorns, M. S. (2011) Pleiotropic impact of a single lysine mutation on biosynthesis of and catalysis by N-methyltryptophan oxidase. *Biochemistry.* **50**, 4949–4962

53. Ralph, E. C., and Fitzpatrick, P. F. (2005) pH and kinetic isotope effects on sarcosine oxidation by N-methyltryptophan oxidase. *Biochemistry.* **44**, 3074–3081

54. Wagner, M. A., Trickey, P., Che, Z. W., Mathews, F. S., and Jorns, M. S. (2000) Monomeric sarcosine oxidase: 1. Flavin reactivity and active site binding determinants. *Biochemistry.* **39**, 8813–8824

55. Hassan-Abdallah, A., Zhao, G., and Jorns, M. S. (2006) Role of the covalent flavin linkage in monomeric sarcosine oxidase. *Biochemistry.* **45**, 9454–9462

56. Khanna, P., and Jorns, M. S. (2001) Characterization of the FAD-containing N-methyltryptophan oxidase from Escherichia coli. *Biochemistry.* **40**, 1441–1450

57. Karasulu, B., and Thiel, W. (2015) Amine oxidation mediated by N-methyltryptophan oxidase: Computational insights into the mechanism, role of active-site residues, and covalent flavin binding. *ACS Catal.* **5**, 1227–1239

58.	Gaweska, H. M., Roberts, K. M., and Fitzpatrick, P. F. (2012) Isotope effects suggest a stepwise mechanism for berberine bridge enzyme. *Biochemistry*. **51**, 7342–7347

59.	Petterson, D. S. (2000) The Use of Lupins in Feeding Systems - Review -. *Asian-Australasian J. Anim. Sci.* **13**, 861–882

60.	Kutchan, T. M. (1995) Alkaloid biosynthesis - The basis for metabolic engineering of medicinal plants. *Plant Cell*. **7**, 1059–1070

61.	Pérez-Laínez, D., García-Mateos, R., San Miguel-Chávez, R., Soto-Hernández, M., Rodríguez-Pérez, E., and Kite, G. (2008) Bactericidal and fungicidal activities of Calia secundiflora (Ort.) Yakovlev. *Zeitschrift fur Naturforsch. - Sect. C J. Biosci.* **63**, 653–657

62.	Facchini, P. J. (2001) Alkaloid biosynthesis in plants: Biochemistry, cell biology, molecular regulation, and metabolic engineering applications. *Annu. Rev. Plant Physiol. Plant Mol. Biol.* **52**, 29–66

63.	Liscombe, D. K., and Facchini, P. J. (2008) Evolutionary and cellular webs in benzylisoquinoline alkaloid biosynthesis. *Curr. Opin. Biotechnol.* **19**, 173–180

Chapter 2: Aim of the study

The oxidation of *N*-methyl groups by members of the flavin-dependent amine oxidases results in the formation of an imine, which subsequently hydrolyses to the free amino group and formaldehyde. Thus the reaction reported for FsqB diverges from the canonical reaction scheme, because the imine is not hydrolysed but subject to nucleophilic attack by the catechol moiety of the substrate. In this sense, the reaction catalysed by FsqB is analogous to those by BBE and THCS (1). This analogy in the outcome of the reactions, i.e. oxidative cyclisation of the substrate, prompted us to ask whether FsqB also shares the mechanism of action with the enzymes of the berberine bridge enzyme-like enzyme family. Thus, we initiated the biochemical and structural characterization of the enzyme to pave the way for a more detailed understanding of FsqB. Here, we report the crystallographic structure of FsqB and kinetic parameters of the wild-type enzyme using a set of five putative substrate analogs. Based on the crystallographic structure, we have generated six protein variants to further analys the role of amino acid residues in the active site of the enzyme.

References

1. Baccile, J. A., Spraker, J. E., Le, H. H., Brandenburger, E., Gomez, C., Bok, J. W., MacHeleidt, J., Brakhage, A. A., Hoffmeister, D., Keller, N. P., and Schroeder, F. C. (2016) Plant-like biosynthesis of isoquinoline alkaloids in Aspergillus fumigatus. *Nat. Chem. Biol.* **12**, 419–424

Chapter 3: Material & Methods

Chemicals

The gene encoding FsqB was synthesized by Invitrogen Life Technologies (Carlsbad, CA, USA). Restriction enzymes, ligases, and Phusion DNA polymerase were from Thermo Fisher Scientific (Waltham, MA, USA). Pre-packed nickel sepharose fast flow columns were from GE Healthcare (Little Chalfont, UK). Solvents, media components and buffer salts were from Carl Roth GmbH (Karlsruhe, Germany). Enzyme substrates, redox dyes used for the determination of redox potentials, and salt free purified oligonucleotides for site directed mutagenesis were from Sigma-Aldrich (St. Louis, MO, USA). *N*-methyl-dopa, and *N*-methyl-meta-tyrosine were synthesized by Prof. Dr. Wofgang Kroutil and Dr. Michael Fuchs according to the protocol listed in the supplementary section. All raw materials were purchased from Sigma Aldrich, Acros Organics or Alfa Aesar and used as received. Solvents were obtained from Roth.

Molecular cloning

On ordering, the gene sequence of FsqB (Afu6g03440) (listed below) was codon optimized for expression in E. coli and an octa-histidine-tag was added to the C-terminus. Additionally, the gene was flanked with an *NdeI* and a *NotI* restriction site at the 5' and 3'-end, respectively (figure 1).
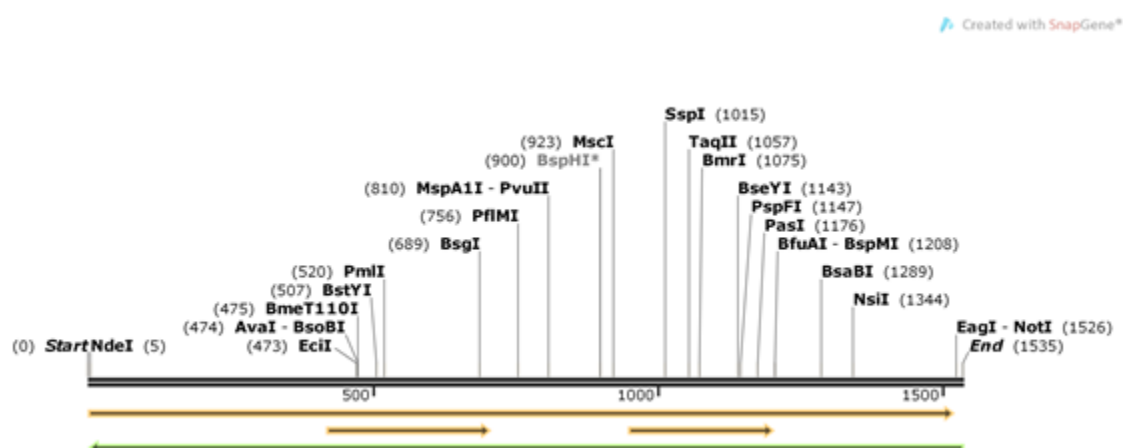
Figure 1. FsqB gene sequence and gene map with restriction sites. Restriction enzymes NdeI & NotI were used to transform the gene start end from blunt to sticky ends. The processed gene was ligated then with pET21a plasmid.

The DNA string was cloned into a shuttle vector (pJET) and transformed into *E. coli* Top 10 cells (Stratagene) for strain preservation and plasmid propagation. After digestion with NdeI and NotI the gene was cloned into the *E. coli* expression vector pET21a (figure2), conferring ampicillin resistance.

Correct insertion of the gene sequence was verified by sequencing, before transforming the plasmid into *E. coli* BL21 Star (Stratagene) cells for expression.
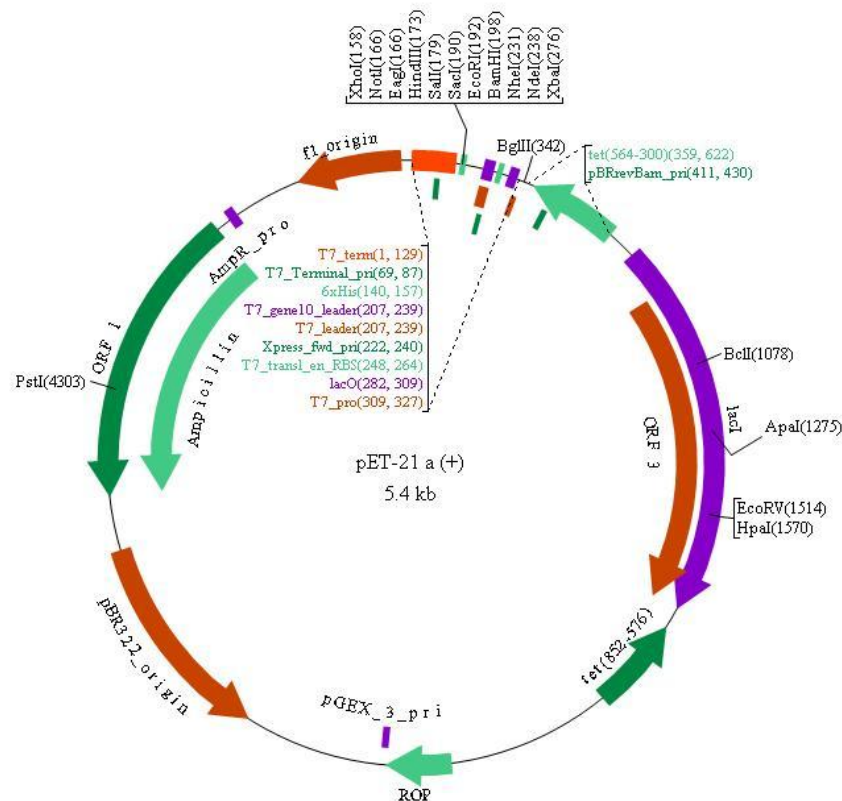
Figure 2. The map of pET21a vector showing the restriction sites with the Ampicillin resistance gene. The map was taken from biovisualtech.com.

Protein expression and purification

Protein production and purification was adapted from Bacille *et al.*(1). FsqB was expressed in shake flasks in an HT Multitron Standard shaking system (Infors AG, Basel, Switzerland). Main cultures were inoculated to an optical density at 600 nm (OD_{600}) of about 0.1, by adding an overnight culture to fresh LB medium containing 100 µg/ml ampicillin, and incubated at 37 °C and 140 rpm until an optical density of 0.7 was reached. Then, production of FsqB was induced by adding 300 µM IPTG, before incubating the cultures at 18 °C for 15 h to maximize the protein yield. The cells were harvested by centrifugation at 5,000 *g* for 15 minutes and stored at -20 °C until further use. Protein purification was carried out under low light conditions at 4 °C. To purify the enzyme, the pellet was suspended in lysis buffer (100 mM phosphate/NaOH, 150 mM sodium chloride, 10 mM imidazole pH 7.6 containing 1 mM PMSF and 0.1 mg/ml lysozyme) and sonicated using a Labsonic U sonication probe (B. Braun Biotech, Berlin, Germany) for 10 min. The lysate was centrifuged at 38500 *g* for 60 min and

the supernatant was filtered through a filter paper. The clear supernatant was loaded onto a Ni-NTA sepharose fast flow column (GE Healthcare) prewashed with lysis buffer without PMSF and lysozyme. The column was washed with 10 column volumes of washing buffer (100 mM phosphate/NaOH 150 mM NaCl,30 mM imidazole pH 7.6), before FsqB was eluted with elution buffer (100 mM phosphate/NaOH, 150 mM NaCl,150 mM imidazole pH 7.6). The eluted protein was dialyzed against 100 mM phosphate/NaOH, 150 mM NaCl pH 7.6 (storage buffer) overnight. Then, the protein was concentrated in an Amicon Ultra-15 centrifugal filter with a 30-kDa cut-off (Merck-Millipore, Darmstadt, Germany). For protein crystallization FsqB was further purified by size exclusion chromatography using a Superdex 200 prep grade XK 16/60 column (GE Healthcare), equilibrated with storage buffer and attached to an ÄKTA FPLC system (GE Healthcare) at 4 °C. Protein purity was monitored by SDS-PAGE with 12.5% separation gel (FsqB molecular mass is 55 kDa).

UV-Vis absorption spectroscopy and calculation of the extinction coefficient

A Specord 210 spectrophotometer (Analytik Jena, Jena, Germany) was used for UV-Vis absorption spectroscopy. Concentrations of purified enzyme samples were determined according to the absorption of bound FAD at 450 nm. The molar extinction coefficient for FsqB was determined as described in reference (2).

Protein thermal stability

The thermal stability of FsqB was assessed by recording the change in fluorescence due to the release of the FAD cofactor as an intrinsic probe to monitor protein stability and folding in a ThermoFAD assay (3). The measurements were carried out in triplicate with an FX Connect real-time PCR system (Bio-Rad) in a 25 μL mixture of 100 mM phosphate/NaOH, pH 7.6 containing 150 mM NaCl, and 3 mg/ml protein. The starting temperature was 20 °C for 5 minutes, then it was increased at a rate of 0.5 °C/min to 95 °C. The CFX Manager 3.0 software was used to determine the melting temperatures for wild type FsqB and the variants generated by site-directed mutagenesis. Furthermore, ThermoFAD was used to assess the impact of substrates and substrate analogs on the melting point of FsqB.

Circular dichroism spectroscopy

Circular dichroism (CD) measurements were performed with a Jasco J715 (JASCO Inst., Gross-Umstadt, Germany) spectropolarimeter using a 0.01 cm water-jacket cylindrical cell. The far-UV spectra were recorded at 20 °C from 190 to 260 nm as an average of three scans. A protein concentration of 0.2 mg/ml was used for all measurements.

Product identification

The products generated from the conversion of substrates by FsqB were analyzed by HPLC-MS. For HPLC-MS analysis, 5 mM of the potential substrate were incubated with 5 μM FsqB in 1 ml of 10 mM phosphate/NaOH buffer, pH 7.6 for 1 hour at 25 °C with shaking at 600 rpm. Then the reactions were quenched with 200 μl of 0.2 M guanidine hydrochloride and the samples were spun down at 10,000 g for 10 min to remove denatured protein. The supernatant was then analyzed by HPLC-MS. Low resolution mass spectra were recorded with an Agilent Technologies 6120 Quadrupole LC/MS detector in combination with an Agilent Technologies 1260 Infinity HPLC system, equipped with a Kinetex 2.6 μ C-18 100A column (50 x 4.6 mm, 2.6 micron). Water/acetonitrile (+0.1 vol-% of formic acid) was used as eluent. HPLC-UV analysis was carried out with a Shimadzu HPLC system [DGU-20A (degasser), LC-20A (pump), SIL-20A (autosampler), CTO-20AC (column oven), SPD-M20A (detector), CBM-20AC (controller)] with water/acetonitrile (+0.1 vol-% of trifluoroacetic acid) as eluent using a Phenomenex Luna 5 μ C18 100A column. High resolution mass spectra were recorded on a Agilent 6230 TOF LC/MS (APCI, positive mode). Optical rotation values were measured on a Perkin Elmer Polarimeter 341. Flash chromatography was performed using Merck silica gel 60 (mesh size 40-63 μm). Petroleum ether had a boiling range of 60-95 °C. NMR-spectra were recorded with a Bruker NMR unit at 300 (1H) and 75 (13C) MHz, shifts are given in ppm and coupling constants (J) are given in Hz.

Crystallization and crystal structure determination

Screening for crystallization conditions was performed with an Oryx8 robot (Douglas Instruments, Berkshire, U.K.) using the following commercially available screens: JCSG+ MD1-37, Morpheus Screen MD 1-46 (Molecular Dimensions, Suffolk, U.K.) and Index HT HR2-144 (Hampton Research, Aliso Viejo, U.S.A.). Trials were set up in 96-well Swissci

plates (Molecular Dimensions, Suffolk, U.K.) using the sitting drop vapor-diffusion method. Drops of 1 μL were pipetted with a 1:1 ratio of protein (concentrations of 10, 20 and 30 mg/ml in 100 mM phosphate/NaOH pH 7.8 and 150 mM NaCl) and screening solution. The crystallization plates were incubated at 289 K.

Initial crystals of FsqB were obtained within 2 weeks in a crystallization condition containing 0.26 M ammonium sulfate and 0.2 M lithium sulfate in 0.1 M Tris/HCl, pH 8.5. Most of the crystals showed anisotropic diffraction to only 3.5-4 Å resolution. The best native crystal diffracted to 2.6 Å and this dataset was used for structure solution. Crystals were also soaked with different potential substrates of FsqB by adding a 0.125 mM solution of the respective compound directly to the crystallization drop using a cryo-loop. The soaked crystals were flash-cooled after different soaking times (15 sec to 5 min) without the use of an additional cryoprotectant.

Crystals were screened and diffraction data were collected at 100 K at the synchrotron sources Elettra (Trieste, Italy; beamline XRDI), ESRF (Grenoble, France; beamlines ID23-1, ID23-2, ID30A-3, ID30B) and PETRA III (Hamburg, Germany; beamlines P11 and P14). The data were processed and scaled using the XDS program package (4). The structure was solved by a combination of molecular replacement using the program Phaser (5), extensive manual rebuilding in Coot (6) and refinement using the PHENIX software suite (7). Molecular replacement was performed using the structure of fructosamine oxidase from *Aspergillus fumigatus* (PDB-entry: 3DJE) (8) as search template. A randomly chosen set of 5% of the reflections was not used in the refinement, but was set aside for R_{free} calculations (9). The stereochemistry and geometry of the resulting model were analyzed using the program Molprobity (10). Data collection and processing statistics are summarized in Table 3. Atomic coordinates and structure factors have been deposited in the Protein Data Bank as entry 6GG2. Visualization of structures (Figures 3-8) was done using the program PyMOL (11).

Site-directed mutagenesis

The pET21a-FsqB wild type construct was used as a template in the polymerase chain reaction based mutagenesis. Primers were designed in order to introduce the desired mutations in the codons pertaining to the targeted amino acids (12). The validity of the generated variants was confirmed by sequencing. Table shows the sequence of primers used to generate the variants.

Table 1: list of primers used for site directed mutagenesis

Mutated residues	Direction	Primers
Asp 60 to Ala	Forward	CAAATGCAGCTACCAGCCGTGTTATTCGTCGTGATTATCC
	Reverse	CAAATGCAGCTACCAGCCGTGTTATTCGTCGTGATTATCC
Arg 63 to Met	Forward	CAGATACCAGCATGGTTATTCGTCGTGATTATC
	Reverse	GACGAATAACCATGCTGGTATCTGCATTTG
Arg 66 to Met	Forward	CCAGCCGTGTTATTATGCGTGATTATCCGCATG
	Reverse	ATAACACGGCTGGTATCTGCATTTGCTGCTG
Tyr 69 to Phe	Forward	CGTGTTATTCGTCGTGATTTCCCGCATGGTCCG
	Reverse	CACGACGAATAACACGGCTGGTATCTGCATTTGCTG
Tyr 121 to Phe	Forward	CCGTGAATTTCATCAAAAAAGCCTATGCCATTAGCTGCGAACTG
	Reverse	GCTTTTTTGATGAAATTCACGGTTTCCAGTGCTTTCGGAGG
Tyr 266 to Phe	Forward	GCCTTCATCCAGCTGACCAAAGAAGAAGCAGACGAAC
	Reverse	CAGCTGGATGAAGGCAACAAATTCGCTATACACATCACACAG
Lys 304 to Ala	Forward	GTCTGGCTTTTGGCCACTTTAGCTATAGCGGTATTGTTGATGTTCTG
	Reverse	GTGGCCAAAAGCCAGACAATTATCATGATCCGGACCAACTG
Tyr 416 to Phe	Forward	GTTGGTTCAACGATACACCGGCACTGGATTTTGTTGTTGATTATCATC
	Reverse	CGGTGTATCGTTGAACCAACATTTACGAACACGGGTAAACGG
Asp 444 to Ala	Forward	GCGACCGGTGGTTGTGCACATGCATTCAAATTCTG
	Reverse	CACCGGTCGCAACAAACAGGGTTTTGCCATAGC
Lys 448 to Ala	Forward	GCATTCGCTTTTCTGCCGATTATTGGTGAAAAAACCCTGGC
	Reverse	GGCAGAAAAGCGAATGCATGATCACAACCACCGGTC

Molecular docking

The natural substrate (truncated to the methyl-thioester, see Figure 7) was docked into the active site using the program ADFR (13). Protein and ligand structures were prepared using the program Maestro from the Schrödinger package (11). 52 independent docking runs employing the genetic-algorithm (GA) optimizer implemented in ADFR were executed with a maximum number of 2.5 million energy evaluations. During these simulations the side chains of the following residues were treated as flexible: V64, L100, I284, V286, F293 and V295. The resulting docking poses were clustered using a maximum root-mean-squares-deviation (rmsd) of 2 Å. The lowest-energy docking pose from each cluster was then visually analyzed with respect to the distance of the *N*-methyl group to the N(5) of the flavin as well as regarding the conformation assumed to be necessary for promoting ring closure. Selected complex structures were further optimized using the program Prime from the Schrödinger package (11). In these calculations, all amino acid residues within 10 Å of the bound ligand were allowed to move and an implicit solvent model was employed.

We have also performed docking simulations with *N*-methyl-tyrosine and the two stereoisomers of *N*-methyl-dopa using the Autodock Vina Plugin (14) of the Yasara structure suite (version 17.3.30, Yasara Biosciences (15)). Docking was performed with the receptor kept rigid, while the ligand was flexible, and with a docking cell lining the cavity of the active site of FsqB. For each ligand 250 independent docking runs were performed and the resulting poses were clustered with an RMSD cut-off of 1 Å. Docking poses representing the lowest energy clusters were inspected visually.

Determination of pH optimum and steady-state kinetics

To evaluate the catalytic activity and the pH-optimum of FsqB, the oxygen consumption in the presence of various concentrations of *N*-methyl-dopa was recorded in triplicate. The measurements were performed utilizing a retractable needle-type oxygen sensor (Type OXR50-UHS) (Pyro Science GmbH, Aachen,

Germany (16)). The pH optimum was determined by monitoring the enzymatic conversion of *N*-methyl-dopa (2 mM) as a substrate for FsqB in different buffer systems with different adequate pH (table 2)

Table 2: buffer systems used for pH optimum experiment with their adequate pH range

Buffer system	pH range
0.1 M citrate/NaOH	4.0 to 5.5
0.1 M Hepes/NaOH	6.0 to 7.0
0.1 M Tris/HCl	7.0 to 8.0
0.1 M borate/HCl	8.0 to 9.0

Kinetic assays were performed in 100 mM Tris/HCl, 150 mM NaCl buffer, pH 7.6, saturated with ambient air at 25 °C with enzyme concentrations of 10 µM in an air-tight cell. Experiments were started by the addition of FsqB to the sample cell containing 0-5 mM *N*-methyl-dopa. The oxygen consumption was monitored for 1 min and the initial velocity was determined in the linear part of the measurement (typically 12 sec).

Pre-steady-state kinetics and determination of k_{ox}

Presteady-state reaction kinetics were measured anaerobically with a Hi-Tech stopped flow instrument (SF-61DX2; TgK Scientific Limited, Bradford-on-Avon, UK) in a glove box (Belle Technology, Weymouth, UK) at 25 °C. The reductive rates of enzyme-bound FAD were determined using a final concentration of 25 µM FsqB in 100 mM phosphate/NaOH buffer, 150 mM NaCl pH 7.6. Enzyme was mixed with various concentrations of substrates (0 to 10 mM) or *N*-methyl-tyrosine (0–5 mM) dissolved in 100 mM phosphate buffer, 150 mM NaCl pH 7.6, and spectral changes were detected with a Kineta-ScanT diode array detector (MG-6560; TgK Scientific Limited) and subsequently analyzed at 460 nm. Flavin reduction was monitored at each substrate concentration in triplicate and the observed rate constants (k_{obs}) for

different substrate concentrations were calculated using an exponential fitting function in the KINETIC STUDIO software (TgK Scientific Limited). By plotting these observed rate constants as a function of the respective substrate concentrations, the reductive rates (k_{red}) as well as dissociation constants (K_D) could be determined employing ORIGIN 8.6 (OriginLab Corp.). The oxidative rates (k_{ox}) were determined three times at a final oxygen concentration of 135 μM, by mixing substrate-reduced FsqB with air saturated buffer (100 mM phophsate/NaOH, 150 mM NaCl, pH 7.6). By dividing the observed rate constants by the amount of oxygen dissolved in the buffer (final conc: 135 μM), bimolecular rate constants (k_{ox}) could be obtained.

Anaerobic photoreduction and reoxidation

Photoreduction of FsqB was done according to the procedure reported by Massey and Hemmerich (17). About 40 μM of FsqB in 100 mM phosphate/NaOH, pH 7.6, 1 mM EDTA, 1 μM 5-deaza-FMN and 2 μM methyl viologen were rendered anaerobic by 2-h incubation in an anoxic, nitrogen-filled glove box (Belle Technology). The anoxic samples were transferred to quartz cuvettes and sealed. Photoirradiation was carried out with a 10 W LED flood light (Luminea, Buggingen, Germany), while cooling the cuvette to 15 °C. Spectra were recorded between 300 and 800 nm until no further changes were observed. For reoxidation of the enzyme, the cuvettes were opened to expose the sample to air and again absorption spectra were recorded between 300 and 800 nm until no further changes were observed.

Determination of redox potential

The redox potential of the enzyme-bound FAD was measured by the dye-equilibration method using the xanthine/xanthine oxidase system as described by Massey (18). The concentrations of enzyme and redox dye were chosen in a way that their absorption maxima were in the same range. The reactions were performed with a Hi-Tech stopped flow device (SF-61DX2; TgK Scientific Limited).

The measurements were performed in triplicate under anoxic conditions in a glove box (Belle Technology) at 25 °C in 50 mM HEPES/NaOH, pH 7.0. The simultaneous

reduction of FAD and the redox dye was monitored with a KinetaScanT diode array detector (MG-6560; TgK Scientific Limited). The reaction was started by mixing a solution containing 300 μM xanthine, 5 μM methyl viologen, and an appropriate amount of enzyme with a solution containing catalytic amounts of xanthine oxidase (approximately 200 nM, from bovine milk, Grade III purity; Sigma-Aldrich) and the redox dye toluidine blue salt (E_0 = 34 mV at pH 7.0, 25 °C). The redox potential was calculated using double logarithmic plots, log(ox/red) of the enzyme versus log(ox/red) of the dye, according to Minnaert. A linear least-squares fit was done with Excel 2010 (Microsoft, Redmond, WA, USA).

References

1. Baccile, J. A., Spraker, J. E., Le, H. H., Brandenburger, E., Gomez, C., Bok, J. W., MacHeleidt, J., Brakhage, A. A., Hoffmeister, D., Keller, N. P., and Schroeder, F. C. (2016) Plant-like biosynthesis of isoquinoline alkaloids in Aspergillus fumigatus. *Nat. Chem. Biol.* **12**, 419–424

2. Macheroux, P. (1999) UV-Visible Spectroscopy as a Tool to Study Flavoproteins. in *Flavoprotein Protocols. Methods in Molecular Biology*, pp. 1–7, 10.1385/1-59259-266-X:1

3. Forneris, F., Orru, R., Bonivento, D., Chiarelli, L. R., and Mattevi, A. (2009) ThermoFAD, a Thermofluor??-adapted flavin ad hoc detection system for protein folding and ligand binding. *FEBS J.* **276**, 2833–2840

4. Kabsch, W. (2010) Integration, scaling, space-group assignment and post-refinement. *Acta Crystallogr. Sect. D Biol. Crystallogr.* **66**, 133–144

5. McCoy, A. J., Grosse-Kunstleve, R. W., Adams, P. D., Winn, M. D., Storoni, L. C., and Read, R. J. (2007) Phaser crystallographic software. *J. Appl. Crystallogr.* **40**, 658–674

6. Emsley, P., and Cowtan, K. (2004) Coot: Model-building tools for molecular graphics. *Acta Crystallogr. Sect. D Biol. Crystallogr.* **60**, 2126–2132

7. Adams, P. D., Afonine, P. V., Bunkóczi, G., Chen, V. B., Davis, I. W., Echols, N., Headd, J. J., Hung, L. W., Kapral, G. J., Grosse-Kunstleve, R. W., McCoy, A. J., Moriarty, N. W., Oeffner, R., Read, R. J., Richardson, D. C., Richardson, J. S., Terwilliger, T. C., and Zwart, P. H. (2010) PHENIX: A comprehensive Python-based system for macromolecular structure solution. *Acta Crystallogr. Sect. D Biol. Crystallogr.* **66**, 213–221

8. Collard, F., Zhang, J., Nemet, I., Qanungo, K. R., Monnier, V. M., and Yee, V. C. (2008) Crystal structure of the deglycating enzyme fructosamine oxidase (Amadoriase II). *J. Biol. Chem.* **283**, 27007–27016

9. Kleywegt, G. J., and Brünger, A. T. (1996) Checking your imagination: Applications of the free R value. *Structure.* **4**, 897–904

10. Chen, V. B., Arendall, W. B., Headd, J. J., Keedy, D. A., Immormino, R. M., Kapral, G. J., Murray, L. W., Richardson, J. S., and Richardson, D. C. (2010) MolProbity: All-atom structure validation for macromolecular crystallography. *Acta Crystallogr. Sect. D Biol. Crystallogr.* **66**, 12–21

11. Schrödinger LLC (2016) The PyMOL Molecular Graphics System. *Schrödinger LLC*. **Version 1.**, http://www.pymol.org

12. Ho, S. N., Hunt, H. D., Horton, R. M., Pullen, J. K., and Pease, L. R. (1989) Site-directed mutagenesis by overlap extension using the polymerase chain reaction. *Gene.* **77**, 51–59

13. Ravindranath, P. A., Forli, S., Goodsell, D. S., Olson, A. J., and Sanner, M. F. (2015) AutoDockFR: Advances in Protein-Ligand Docking with Explicitly Specified Binding Site Flexibility. *PLoS Comput. Biol.* 10.1371/journal.pcbi.1004586

14. Trott, O., and Olson, A. J. (2010) Software news and update AutoDock Vina: Improving the speed and accuracy of docking with a new scoring function, efficient optimization, and multithreading. *J. Comput. Chem.* **31**, 455–461

15. Krieger, E., and Vriend, G. (2014) YASARA View - molecular graphics for all devices - from smartphones to workstations. *Bioinformatics*. **30**, 2981–2982

16. Wolfbeis, O. S. (2015) Luminescent sensing and imaging of oxygen: Fierce competition to the Clark electrode. *BioEssays*. **37**, 921–928

17. Massey, V., and Hemmerich, P. (1978) Photoreduction of Flavoproteins and Other Biological Compounds Catalyzed by Deazaflavins. *Biochemistry*. **17**, 9–17

18. Massey, V. (1991) A simple method for the determination of redox potentials. in *Flavins Flavoproteins Proc. Int. Symp., 10th*, pp. 59–66

Chapter 4: Results

Production, purification and characterization of FsqB

FsqB gene was preceded and ligated to pET21a vector, transformed and expressed successfully in E. coli BL21*. The figure 1 shows the digestion of plasmid by *NdeI* and *NotI* restriction enzymes in order to confirm the identity of both insert and vector.
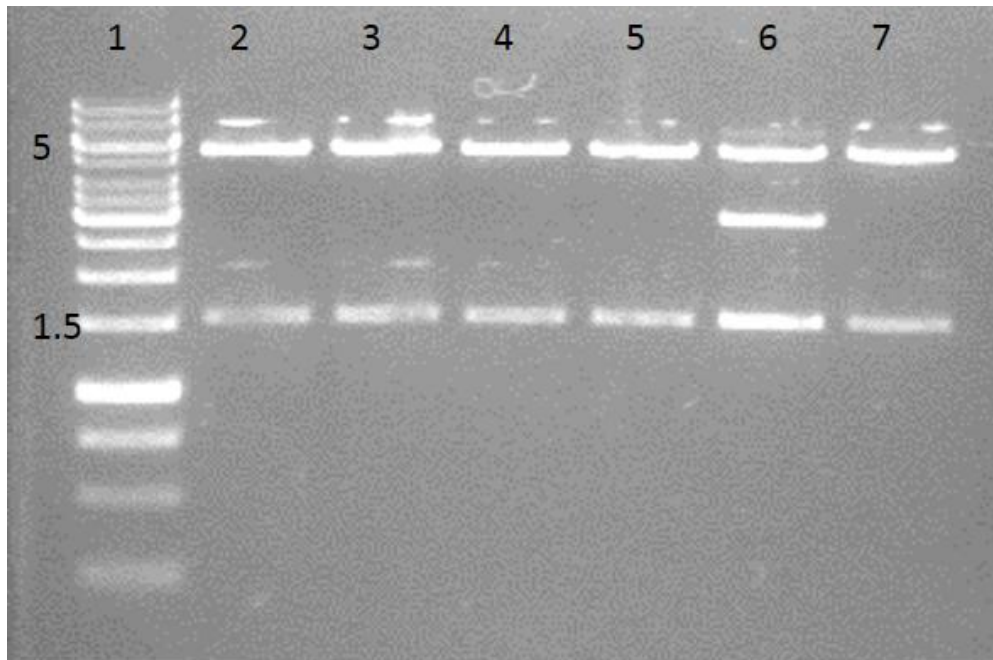
Figure 1. DNA agarose gel (1%) for digested FsqB containing plasmid. Lane 1; 1 KB gene ruler. Lane 2 to 7 digested samples. Sample 6 was excluded since it has 3 bands and other samples were accepted since they contained two bands (the plasmid and the gene). The first band which is about 5 KB is the pET21a vector and the second band which is about 1.5 KB is the gene with sticky ends.

Small scale induction was performed to confirm that FsqB can be expressed in sufficient amount in *E. coli* BL21star (Figure 2).
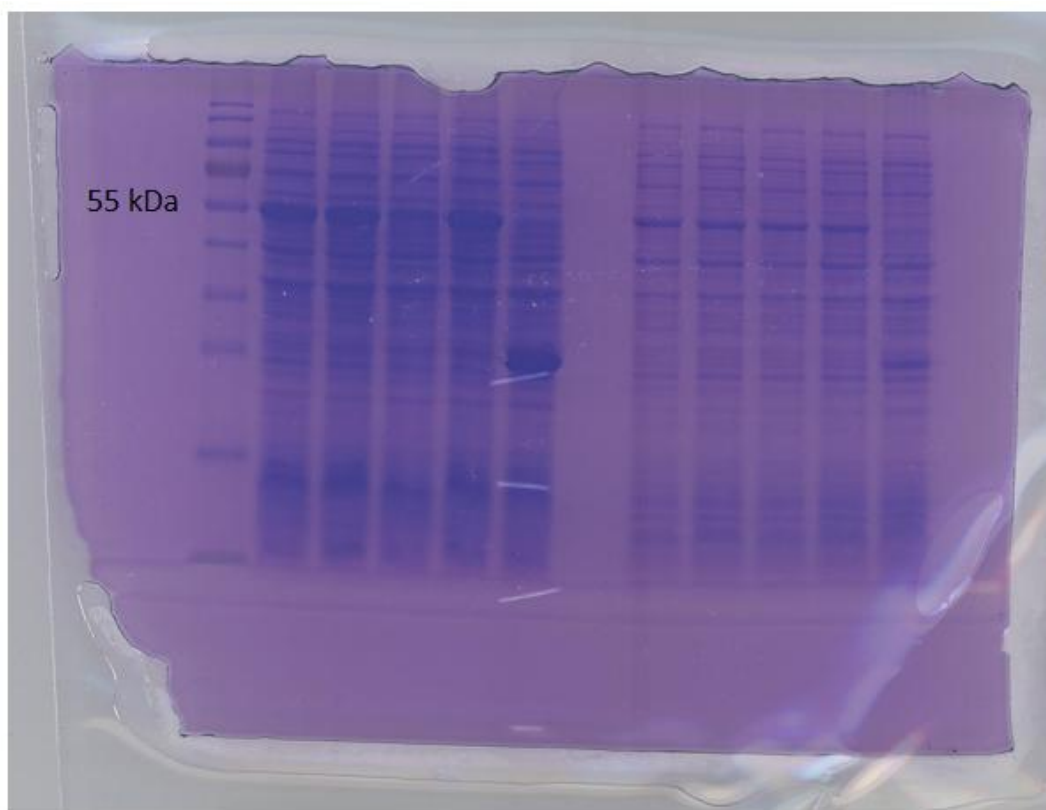
Figure 2. SDS page (12.5% concentration) showing small scale induction of FsqB enzyme. Lane 1; pre-stained protein ruler. Lanes 2-5; induced FsqB lysates. Lane 6; negative control (LuxF enzyme). Lanes 7-10; none induced FsqB lysates. Lane 11; none induced negative control (luxF enzyme). The FsqB enzyme has the molecular weight of 55 kDa.

FsqB was expressed in *E. coli* BL21star at large scale yielding 1 mg of FsqB from 1 g of pellet after purification by Ni-NTA affinity chromatography. For crystallization, the protein was further purified by means of size exclusion chromatography (Figures 3 & 4). The aim of purifying the protein by size exclusion chromatography is to get rid of all impurities and all aggregates that might affect the crystal growth of the enzyme.
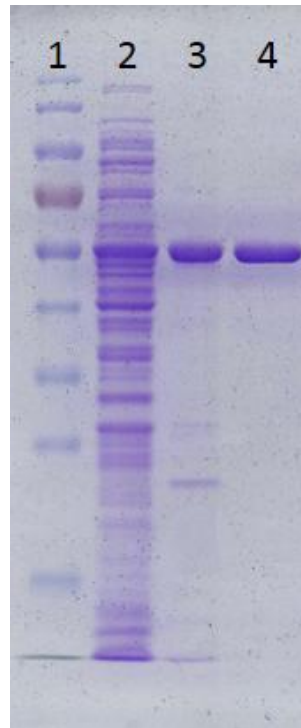
Figure 3. SDS page (12.5%) showing purified FsqB after large scale expression. Lane 1; is pre-stained protein ruller. Lane 2; is FsqB lysate. Lane 3; is purified FsqB by Nickel affinity column. Lane 4; is purified FsqB by size exclusion chromatography.
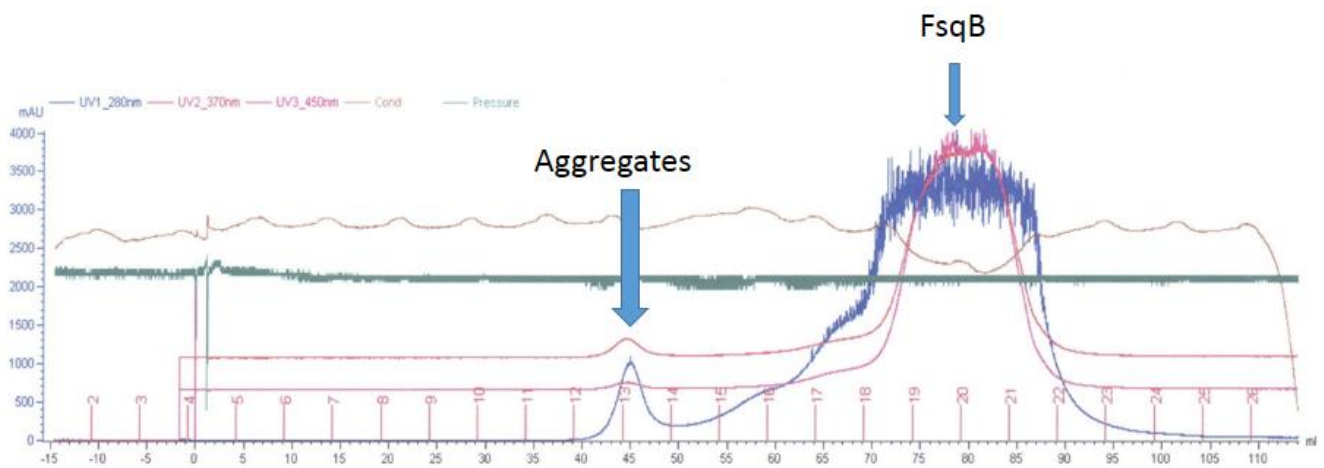
Figure 4. Purification graph of FsqB by size exclusion column connected to FPLC ÄKTA system. Aggregates are eluted first then FsqB is eluted in a later step. The violet line shows the UV absorbance at 280 nm due to the content of aromatic amino acids found in the enzyme.

The UV-Vis absorption spectrum of FsqB possesses the typical features of an FAD containing protein with absorption maxima at 460 and 370 nm, (Figure 5). The bathochromic shift of the long wavelength absorption maximum by about 10 nm

45

compared to free FAD is most likely due to the mono-covalent attachment of the 8α-methyl group to cysteine residue 414. Similar UV-Vis absorption spectra were previously reported for hDMGDH (1) and *N*-methyl-tryptophan oxidase (2), which feature the same covalent linkage. The most distinguished part of the spectrum is between 460 and 500 nm where there is a unique shoulder for the mentioned enzymes.

The extinction coefficient of the FAD bound to FsqB was calculated to be 12,350 M^{-1} cm^{-1} (3) (figure 6).
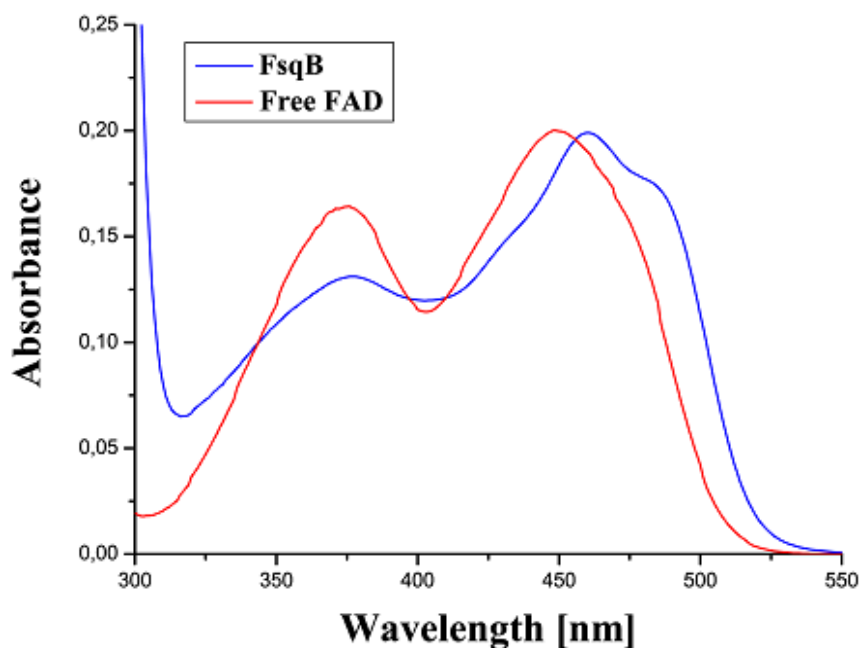
Figure 5. UV-Vis absorption spectrum of FsqB (solid blue line) in comparison with free FAD (solid red line). The absorption spectrum of FsqB was recorded in sodium phosphate buffer, pH 7.6.
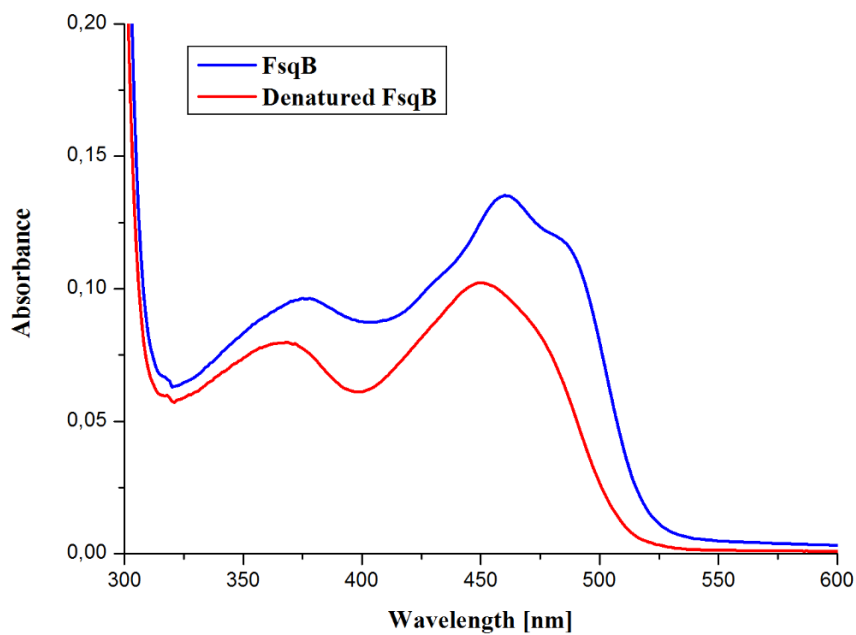
Figure 6. UV-VIS absorption spectrum of FsqB before denaturation (blue line) and after denaturation (red line). This experiment was applied to define the extinction coefficient of FsqB to the extinction coefficient of free FAD.

In order to define the pH optimum of FsqB, the coversion of *N*-methyl-dopa was monitored from pH 4 to 9 using an oxygen sensor to monitor the reaction yielding a bell-shaped profile with an optimum at pH 7.6. (Figure 7)
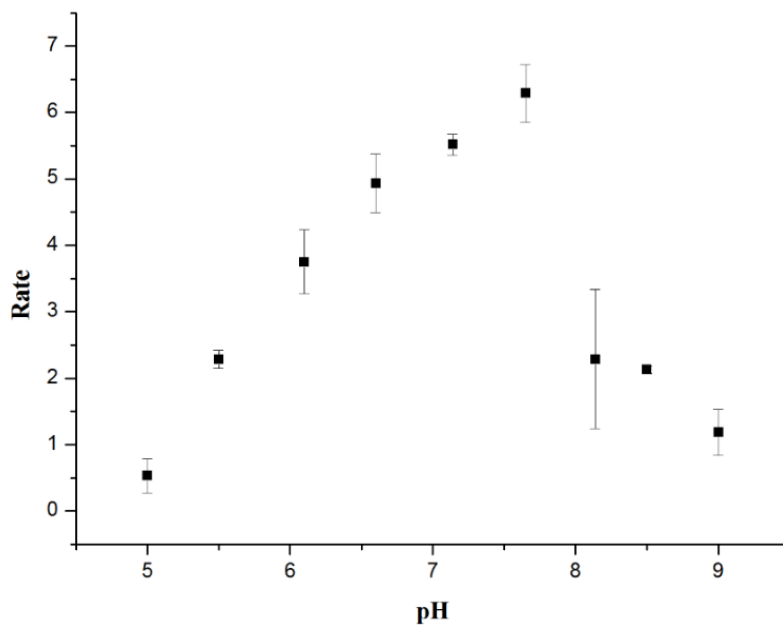
Figure 7. pH optimum experiment showing the rate of *N*-methyl-dopa (applied concentration of 2 mM) at the tested pH spectrum. The results shows that the optimum pH is 7.6.

Photoreduction of FsqB led to the formation of a stable flavin semiquinone with an absorption maximum at 396 nm. Further reduction of the flavin semiquinone to the hydroquinone could not be achieved by light. The flavin semiquinone was reoxidized very slowly by molecular oxygen reaching completion after ca. 70 minutes (Figure 8).
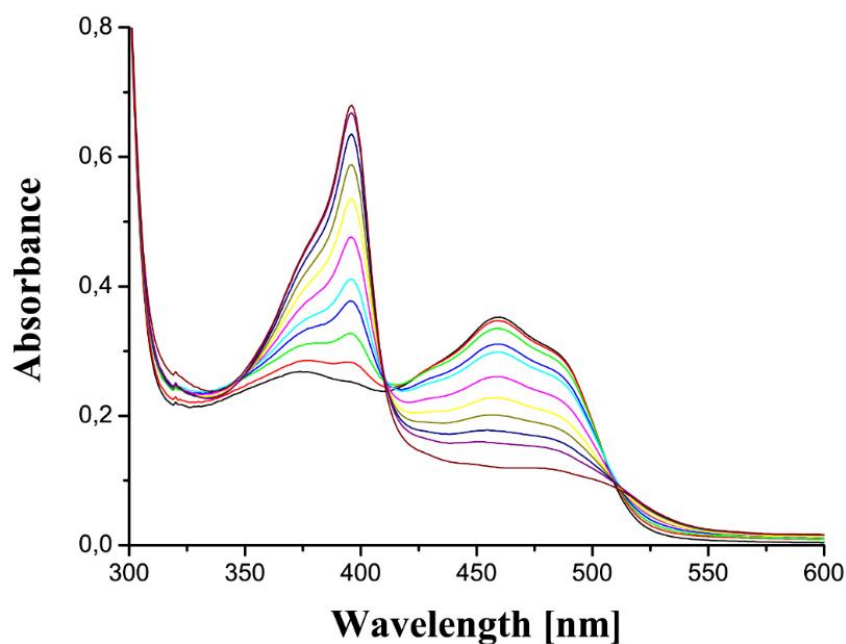
Figure 8. Photoreduction of FsqB as a function of light irradiation, which causes a decrease of absorption at 460 nm and a sharp increase of absorption at 396 nm indicating the formation of the red anionic semiquinone.

Substrate screening

As part of the biosynthetic gene cluster in *Aspergillus fumigatus*, the cognate substrate of FsqB is shown in figure 9. Thus this substrate is neither available nor convenient for the study of reaction kinetics (4).

S-methyl (2*S*,4*S*,5*S*)-2-amino-6-(3,4-dihydroxyphenyl)-4-hydroxy-5-(methylamino)hexanethioate
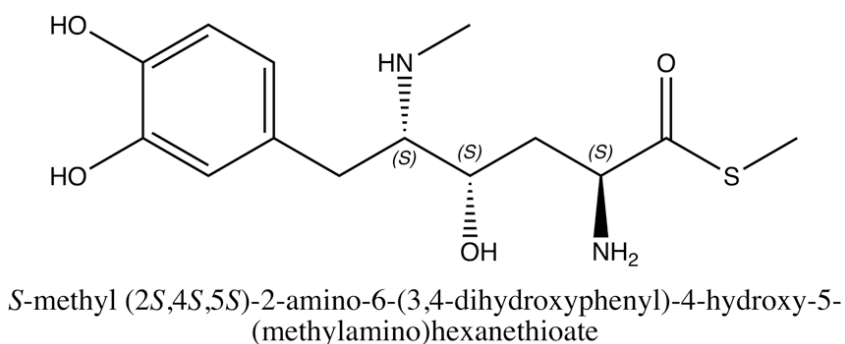
Figure 9. Chemical structure of the truncated, natural substrate used in the docking calculation.

Moreover, we were interested to explore the reaction mechanism of FsqB using substrate analogs. Additionally, we aimed to test the potential use of the enzyme for

biocatalytic applications. The five potential substrates tested with FsqB featured different hydroxylation at the aromatic ring (Figure 10).

Product analysis by HPLC-mass spectrometry, revealed that only *N*-methyl-dopa was oxidized to the corresponding isoquinoline derivative whereas substrates lacking either the *para-* or *meta*-hydroxyl group, *i.e. N*-methyl-*meta*-tyrosine and *N*-methyl-tyrosine, yielded increased amounts of the demethylated product (24 and >99%, respectively, Table 1). On the other hand, adrenalone, epinephrine and phenylephrine were unable to reduce the bound FAD cofactor of FsqB and thus are apparently not accepted as substrates.
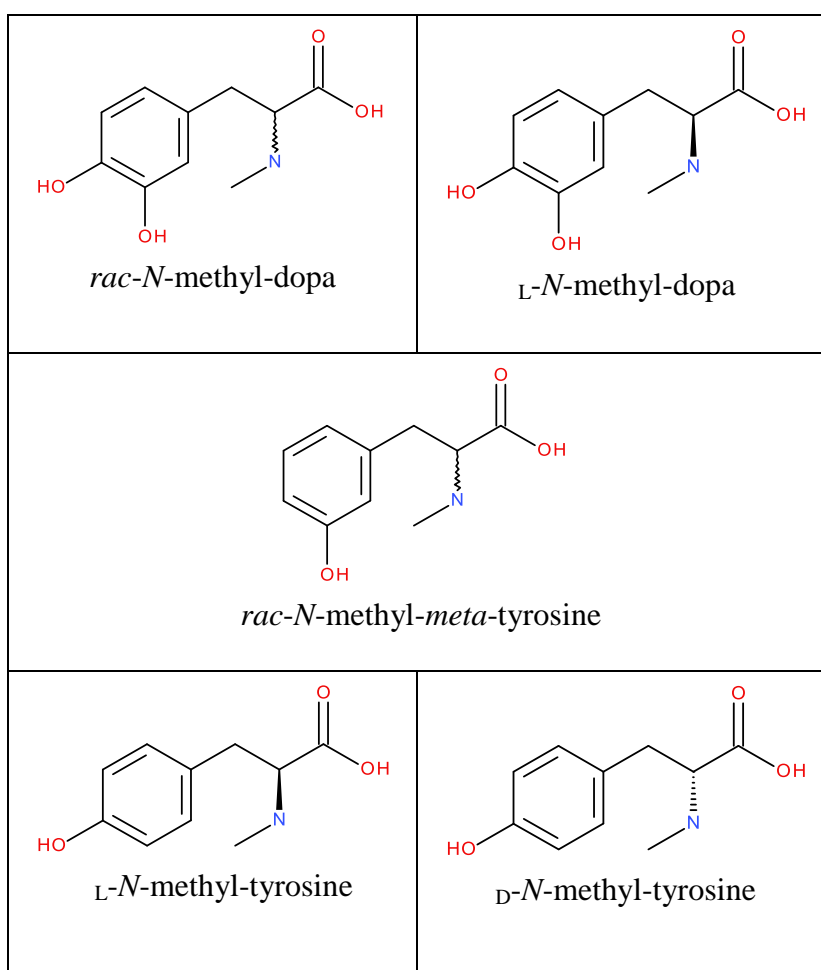
Figure 10. List of tested substrates.

Table 1. Conversions of FsqB-catalyzed biotransformations

Entry	Substrate	Variant	Conversion [%][a]							
			HPLC-MS				HPLC-UV[b]			
			A	B	C	D	A	B	C	D
1	*rac-N*-methyl-dopa	WT	23	76	<1	<1	5	95	<1	<1
2		D444A	91	6	3[c]	<1	94	6	<1	<1
3	L-*N*-methyl-dopa	WT	15	85	<1	<1	11	89	<1	<1
4		D444A	85	15	<1	<1	98	2	<1	<1
5	*rac-N*-methyl-*meta*-tyrosine	WT	49	25[c]	2	24	43	28[c]	5	24
6		D444A	39	27[c]	3	31	54	23[c]	12	16

Entry	Substrate	Variant	Conversion [%][a]					
			HPLC-MS			HPLC-UV[b]		
			E	F	G	E	F	G
7	L-*N*-methyl-tyrosine	WT	<1	<1	>99	3	<1	97
8		D444A	73	<1	27	43	<1	57
9	D-*N*-methyl-tyrosine	WT	>99	<1	<1	>99	<1	<1
10		D444A	>99	<1	<1	>99	<1	<1

WT, wild type enzyme; a) conversions were determined by peak area integration of the corresponding MS or UV response. b) HPLC-UV chromatograms were recorded at 230 nm wavelength. c) no reference material was available, peak identity is assumed in comparison with the other experiments and product formations and the m/z trace of the HPLC-MS peaks.

HPLC chromatograms are shown in the Supplementary section.

Kinetic parameters of FsqB

Following product analysis, we also determined pre-steady state parameters in the stopped-flow apparatus for rac-*N*-methyl-dopa, L-*N*-methyl-dopa, *N*-methyl-*meta*-tyrosine L-*N*-methyl-tyrosine, and D-*N*-methyl-tyrosine. The highest rate of flavin reduction was observed with (racemic) *N*-methyl-dopa whereas (racemic) *N*-methyl-*meta*-tyrosine and L-*N*-methyl-tyrosine were at 10-25 times slower (the k_{obs}-values given in Table 2 were measured at a single fixed concentration of 2.5 mM).

Table 2. Summary of pre-steady state kinetic parameters for wild-type FsqB with different substrates.

Substrate	k_{red}[s^{-1}]	k_{red}(%)^{*2}	k_{red}[s^{-1}]*	k_{red}(%)^{*2}	K_D [mM]
rac-N-methyl-dopa	51 ± 2.7	100	10.4 ± 0.1	100	9.2 ± 0.7
L-*N*-methyl-dopa	21 ± 3	41	4.7 ± 0.01	45	8 ± 1.3
rac-N-methyl-*meta*-tyrosine	6 ± 0.6	12	0.9 ± 0.008	9	15 ± 2
L-*N*-methyl-tyrosine	n.d.^{*3}	-	0.6 ± 0.0004	6	n.d.^{*3}
D-*N*-methyl-tyrosine	n.r.	-	n.r.	-	-

n.d. = not determined; n.r. = no reaction
* For comparison, the values of k_{red} were recorded at 2.5 mM substrate concentration due to the limited solubility of L-*N*-methyl-tyrosine
^{*2} Percentages are given in comparison to the reaction of wild-type FsqB using *rac-N*-methyl-dopa as the substrate.
^{*3} Rate of reaction increased linearly with increasing concentration preventing calculation of a K_D and a limiting rate of reduction.

A more detailed analysis of the reduction of FsqB using *rac-N*-methyl-dopa or the L-stereoisomer yielded limiting rates of 51 ± 2.7 and 21 ± 3 s^{-1}, as well as dissociation constants of 9.2 ± 0.7 and 8 ± 1.3 mM, respectively (Figure 11 & 12). Thus, the limiting rate for L-*N*-methyl-dopa is only ca. 2.5-fold lower than for the racemate indicating that both stereoisomers are accepted by the enzyme. Furthermore, this result also suggests that the enzyme has a preference for D-*N*-methyl-dopa (commercially not available). In order to distinguish the rate of reduction for the D- and L-stereoisomer, we repeated the pre-steady state measurements at a lower concentration of *rac-N*-methyl-dopa (*i.e.* 0.2 mM) and obtained a clear biphasic behavior with observed rates of 1.63 ± 0.04 and 0.61 ± 0.01 s^{-1}, respectively, presumably reflecting the rate of reduction for the two stereoisomers in the racemic mixture. This 2.5-fold difference is similar to the difference observed for the racemate in comparison to the L-stereoisomer (Table 3), supporting our conclusion that the D-stereoisomer is a slightly better substrate than the L-stereoisomer.

Figure 11. Pre-steady state measurement of the conversion of rac-*N*-methyl-dopa by wilt-type FsqB. The standard deviation was calculated based on three measurements for each substrate concentrations.

Figure 12. Pre-steady state measurement of the converstion of L-*N*-methyl-dopa by wild type FsqB. All experiments were done in triplicate.

Interestingly, reduction of the FAD-cofactor was not observed with D-*N*-methyl-tyrosine suggesting that FsqB exhibits a strict stereo-preference for the L-stereoisomer (*S* configuration) (Figure 13) in contrast to what was found with *N*-methyl-dopa. However, the conversion of L-*N*-methyl-tyrosine by FsqB shows does not show any

saturation (linear curve). Therefore, the presteady state kinetic parameter for this substrate could not obtained.
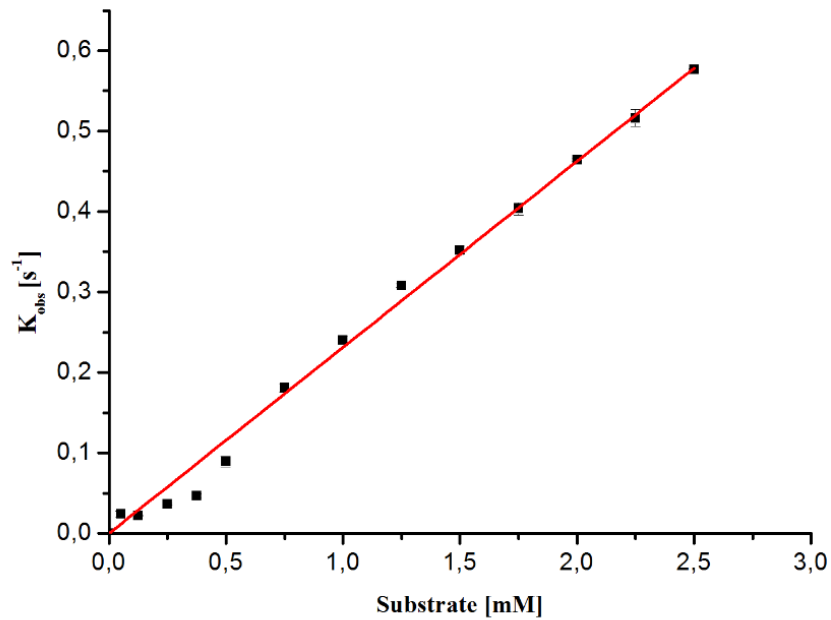
Figure 13. Pre-steady state measurement of the conversion of L-*N*-methyl-tyrosine by wild-type FsqB. All measurements were done in triplicate.

The hyperbolic curve for presteady state kinetics of FsqB wild type against *N*-methyl-meta-tyrosine was also determined (figure 14).
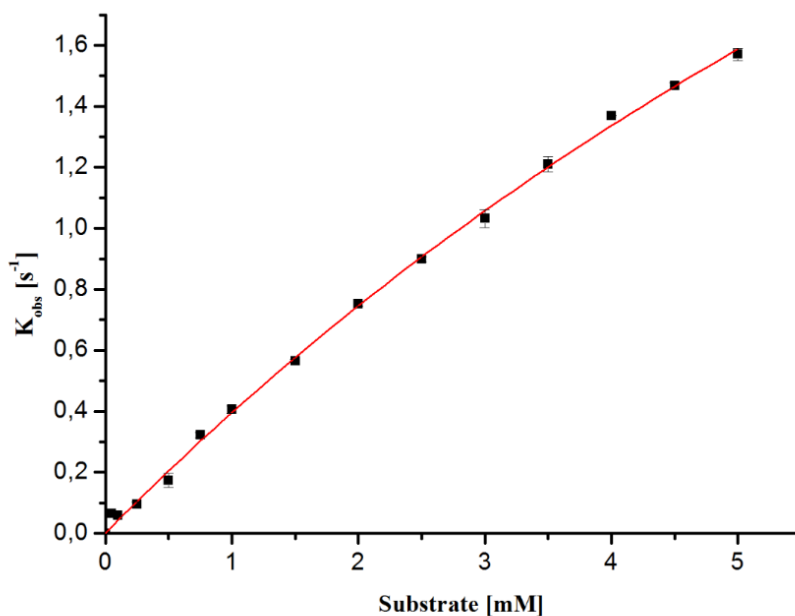
Figure 14. Pre-steady state measurement of the conversion of *rac-N*-methyl-*meta*-tyrosine by wild-type FsqB.

Steady-state kinetics were determined for *N*-methyl-dopa (racemate and the L-stereoisomer), L-*N*-methyl-tyrosine, and *rac-N*-methyl-meta-tyrosine using oxygen depletion to monitor enzyme turnover. Enzyme activity is a function of substrate concentration reaching saturation at ≈ 8 s^{-1}. Similarly, the K_M for the racemate and the L-enantiomer of *N*-methyl-dopa differed only slightly, i.e. 0.16 ± 0.01 and 0.27 ± 0.02 mM, respectively. For L-*N*-methyl-tyrosine and *rac-N*-methyl-meta-tyrosine saturation was reached at ≈ 4 and ≈ 3.5 s^{-1}, respectively. The K_M for these substrates was 2.1 ± 0.2 and 1.6 ± 0.6 mM, respectively. Table 4 summarizes the kinetic parameters for all substrates oxidized by FsqB. As obvious, by the resulting k_{cat}/K_M values, *N*-methyl-dopa (racemate and the L-enantiomere) is more efficiently oxidized by FsqB than L-*N*-methyl-tyrosine and *rac-N*-methyl-meta-tyrosine (Table 3).

Figures 15, 16, and 17 show the hyperbolic behavior of *rac-N*-methyl-dopa, L-*N*-methyl-dopa, and L-*N*-methyl-tyrosine respectively. Kinetic parameters are listed in table 3.
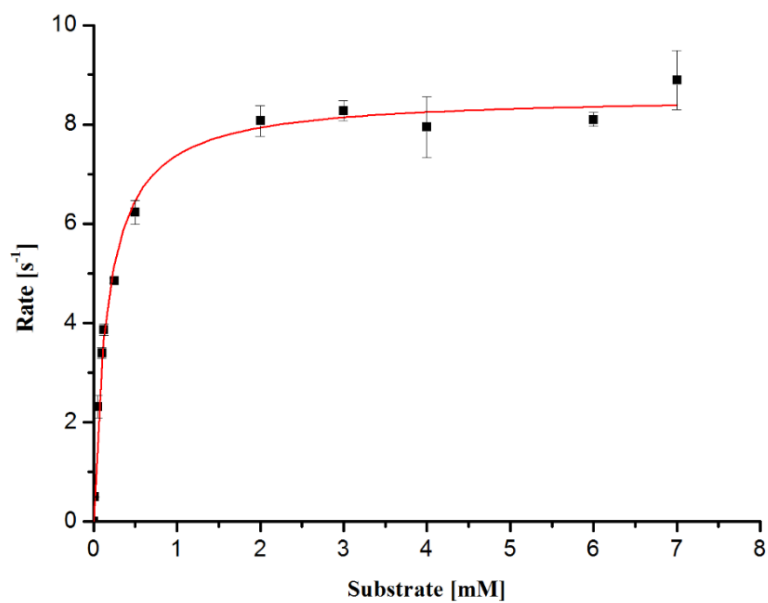
Figure 15. Steady state curve for the conversion of *rac-N*-methyl-dopa by wild type FsqB. The standard deviation was calculated based on three measurements for each substrate concentrating.
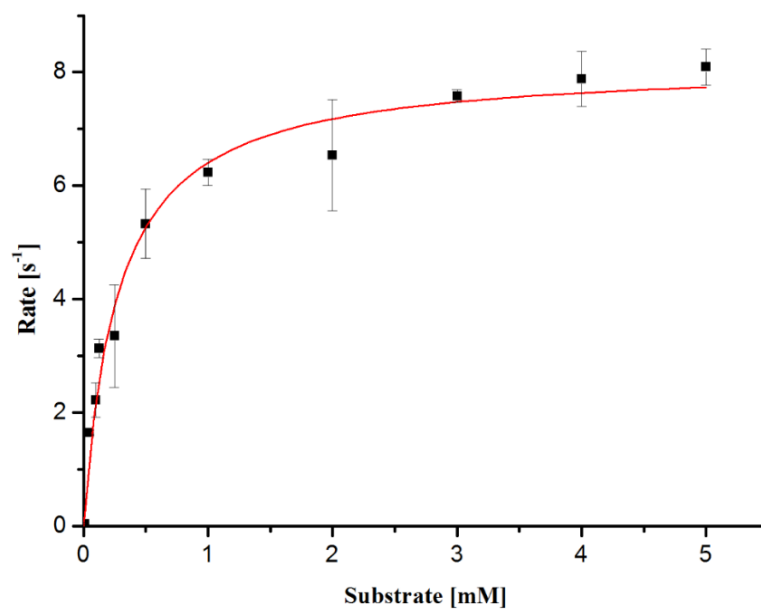
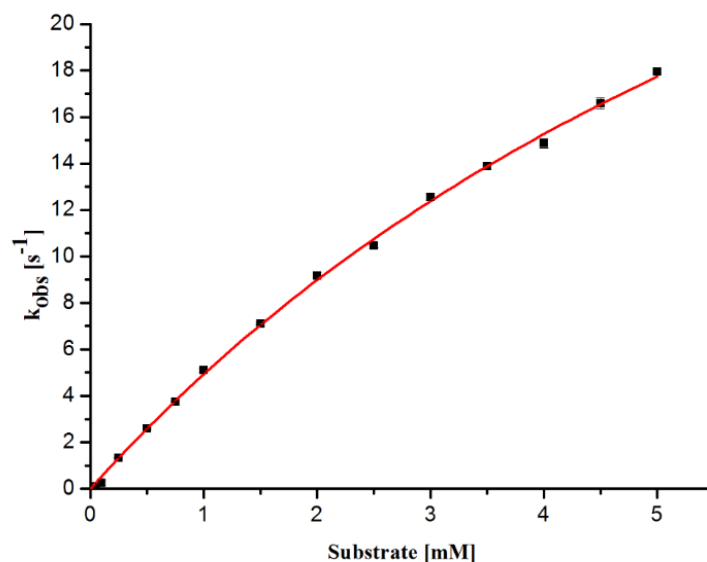**Figure 16.** Steady state measurement of the conversion of L-*N*-methyl-dopa by wild-type FsqB. The standard deviation was calculated based on three measurements for each substrate concentrating.
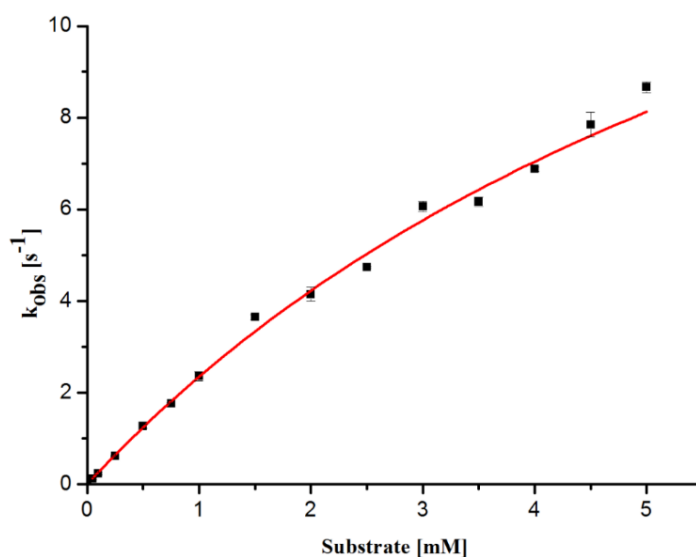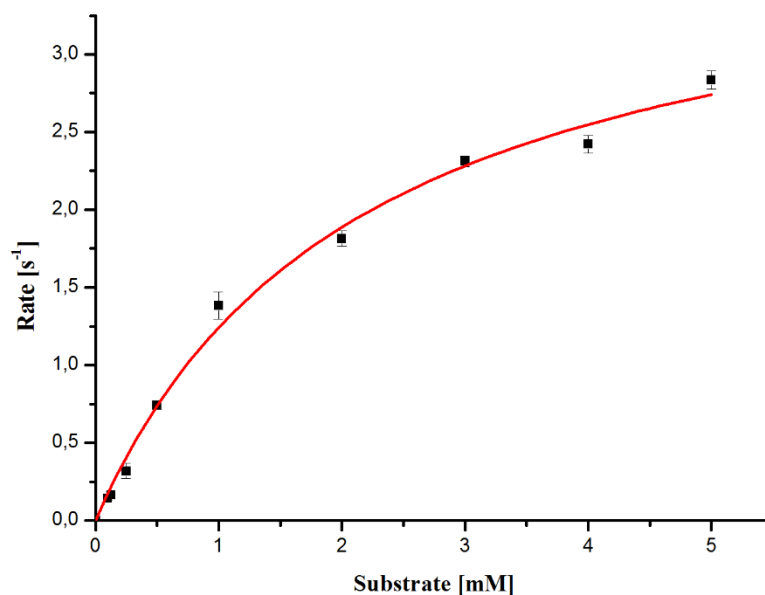
Figure 17. Steady state measurement of the conversion of L-*N*-methyl-tyrosine by wild-type FsqB. The standard deviation was calculated based on three measurements for each substrate concentrating.

Table 3. List of steady-state kinetic parameters of the studied substrates.

Substrate	K_M (mM)	k_{cat} (s^{-1})	k_{cat}/K_M (mM^{-1}.s^{-1})
Rac-*N*-methyl-dopa	0.16 ± 0.01	8.5 ± 0.1	53 ± 4
L-*N*-methyl-dopa	0.27 ± 0.02	8.2 ± 0.2	30 ± 3
Rac-*N*-methyl-*meta*-tyrosine	1.6 ± 0.2	3.5 ± 0.1	2.18 ± 0.04
L-*N*-methyl-tyrosine	2.1 ± 0.2	3.9 ± 0.2	1.91 ± 0.02
D-*N*-methyl-tyrosine	-	-	-

The kinetic parameters were revealed by reacting the listed substrates with the wild type enzyme.

To determine the rate of reoxidation of FsqB, the enzyme was reduced with either (racemic) *N*-methyl-dopa, *N*-methyl-*meta*-tyrosine or L-*N*-methyl-tyrosine under anoxic conditions and reacted with oxygen-containing buffer in the stopped-flow apparatus. This yielded rates for the reoxidation of 20473 ± 852, 4710 ± 121 and 4193 ± 59 M^{-1} s^{-1}, respectively. The results of Kox parameters are listed in table 4.

Table 4. K_{ox} values of FsqB enzymes (Wild type and variants) against different substrates.

Enzyme	Reducing substrate	K_{OX} values
WT	N-methyldopa	20473 $M^{-1}s^{-1}$
WT	N-methyltyrosine	4700 $M^{-1}s^{-1}$
WT	N-methyl-*meta*-tyrosine	4193 $M^{-1}s^{-1}$
D60A	N-methyldopa	4148 $M^{-1}s^{-1}$
K304A	N-methyldopa	183 $M^{-1}s^{-1}$
Y416F	N-methyldopa	13019 $M^{-1}s^{-1}$

X-ray crystallographic structure of FsqB

We determined the crystal structure of FsqB to a resolution of 2.6 Å (Figure 18) (Table 5). The asymmetric unit of the hexagonal crystals contained only one protein chain, but an analysis using the EBI-Pisa server (5) indicated the existence of a dimeric assembly involving a symmetry related molecule generated by a crystallographic two-fold symmetry axis (Figure 19). In this assembly, approximately 2900 $Å^2$ of solvent accessible surface are buried on each protomer predicting that this dimer should also be formed and should be stable in solution.

Figure 18. FsqB crystal exhibiting a yellow color due to the oxidized flavin.
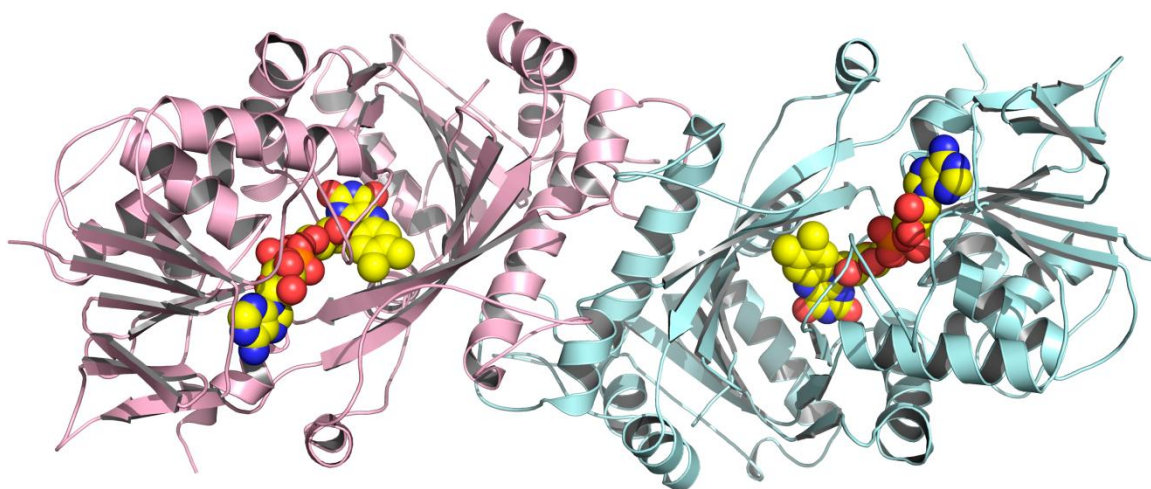
Figure 19. Cartoon representation of the FsqB dimer present in the crystal as predicted by the EBI-Pisa server (5) looking down the crystallographic two-fold symmetry axis. The two protomers are colored pink and light-blue, respectively, the bound flavin cofactors are depicted as spheres.

Table 5. Crystal structure determination: Data collection and refinement statistics.

	FsqB
Wavelength (Å)	0.95
Resolution range (Å)	45.06 - 2.60 (2.69 - 2.60)[a]
Space group	$P6_522$
Unit cell (Å, °)	90.12, 90.12, 266.28 90, 90, 120
Total reflections	316554 (28058)
Unique reflections	20505 (1862)
Multiplicity	15.4 (15.1)
Completeness (%)	98.9 (92.7)
$\langle I/\sigma(I)\rangle$	24.20 (2.66)
Wilson B-factor	65.53
R_{merge}	0.0827 (0.7854)
R_{meas}	0.0856 (0.8121)
R_{pim}	0.0218 (0.2039)
$CC_{1/2}$	1 (0.95)
CC*	1 (0.99)
Reflections used in refinement	20430 (1856)
Reflections used for R_{free}	1022 (93)
R_{work}	0.2123 (0.2647)
R_{free}	0.2432 (0.3362)
CC_{work}	0.95 (0.93)
CC_{free}	0.96 (0.82)
Number of non-H atoms	3945
macromolecule	3856
ligands/cofactors	53

solvent	36
rmsd bonds (Å)	0.006
rmsd bond angles (°)	0.83
Ramachandran favoured (%)	95.73
Ramachandran allowed (%)	4.27
Ramachandran outliers (%)	0.00
Rotamer outliers (%)	0.00
Clashscore	7.89
Average B-factors (Å^2)	71.43
macromolecules	71.68
ligands/cofactors	60.67
solvent	61.05

Statistics for the highest-resolution shell are shown in parentheses.

The FsqB protomer consists of two discontinuous domains (Figure 20), an FAD binding domain (residues 1-97, 183-257 and 419-496) and a substrate binding domain (residues 98-182 and 259-418). The FAD-binding domain exhibits a 3-layer ββα-fold with the diphosphate group of FAD bound at the C-terminal end of a mostly parallel, central β-sheet. The most prominent feature of the substrate binding domain is a seven-stranded, mostly antiparallel β-sheet, which spans across the bound flavin. The two N-terminal strands of this sheet wrap around the dimethyl-benzene part of the isoalloxazine ring system and provide the amino acid residue C414, which is covalently bound to the 8α-methyl group of the FAD cofactor. The substrate binding domain is also responsible for dimer formation. The central portion of the interface between the two protomers is formed by a long α-helix situated on top of the seven-stranded β-sheet as well as by surrounding loop regions (Figure 20).
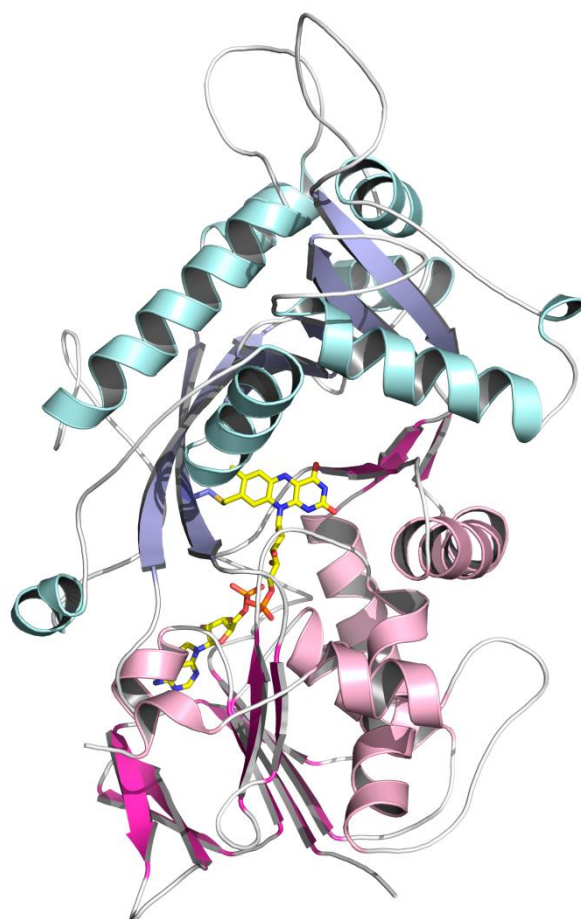
Figure 20. Cartoon representation of the structure of the FsqB protomer. The FAD binding domain is shown in magenta (β-strands) and pink (α-helices) and the substrate binding domain is shown in light blue (β-strands) and light cyan (α-helices). The covalently bound FAD is depicted as sticks (yellow) together with the tethering amino acid Cys414.

A search for structurally similar proteins using the PDBeFold server yielded the fructosamine oxidase from *Aspergillus fumigatus* (PDB-entry 4WCT, (6)) and the fructosyl peptide oxidase from *Eupenicillium terrenum* (PDB-entry 4RSL,) as the closest structural homologs with Q-scores greater than 0.35 and root-mean-square-deviations (rmsd) of approximately 2 Å. A superposition of FsqB with these two structures is shown in figure 21 highlighting the fold similarities.
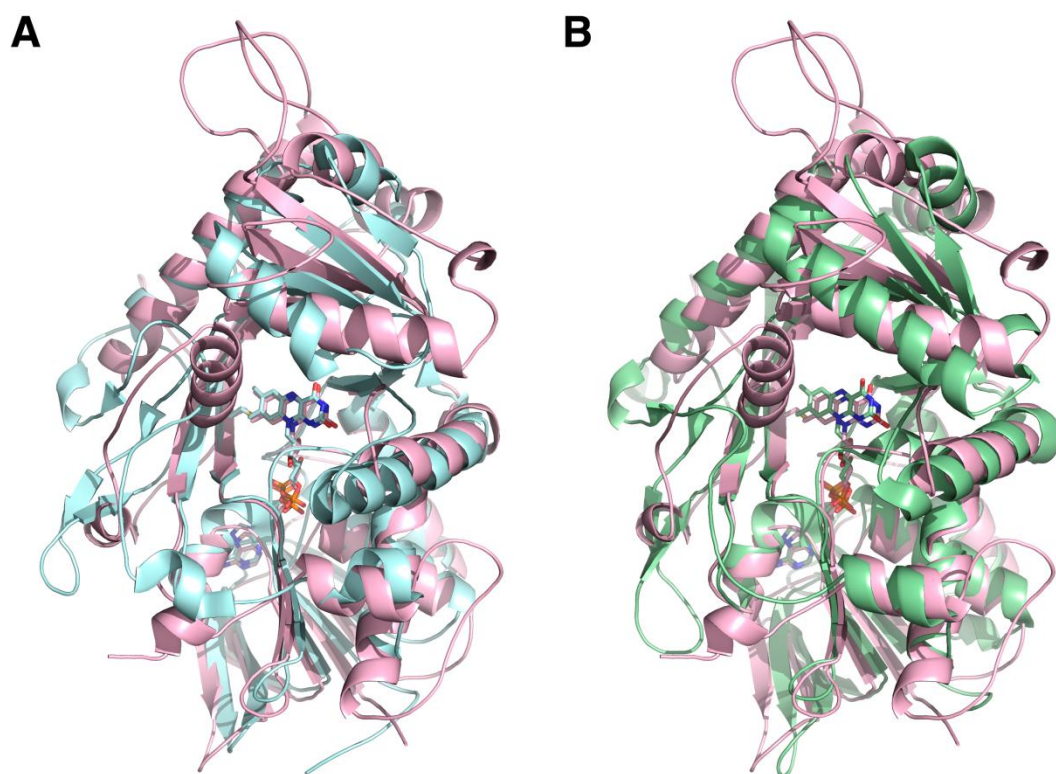
Figure 21. Cartoon representation of FsqB structure (pink) superimposed on the structure of (**A**) fructosamine oxidase from *Aspergillus fumigatus* (cyan) and (**B**) the fructosyl peptide oxidase from *Eupenicillium terrenum* (green).

The active site of FsqB is located at the interface between the FAD binding and the substrate binding domain at the core of the protein and is connected to the solvent by a long and rather broad tunnel. The covalently bound isoalloxazine ring is surrounded on both sides by mostly polar residues, but a hydrophobic pocket – lined by V64, L100, F102, I284, V286, F293 and F308 – is situated on the *re*-side of the cofactor (Figure 22).
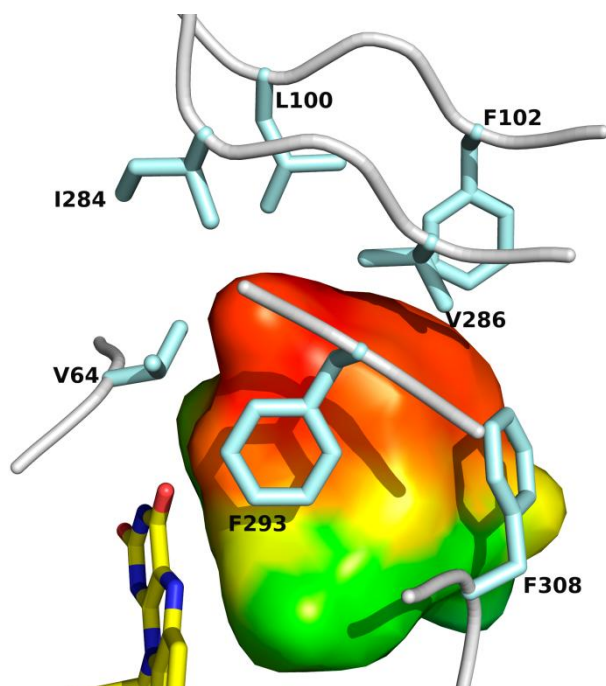
Figure 22. Close-up view of the active site cavity in the vicinity of the flavin cofactor. The cavity volume is depicted as a surface representation colored by hydrophobicity (red: hydrophobic, green: hydrophilic). Cavity points were calculated and annotated using the program CASoX (G. Steinkellner, unpublished). The FAD cofactor as well as the sidechains lining this part of the active site cavity are shown as sticks.

Modeling of the substrate complex

Crystals of FsqB were soaked with various, potential substrates in order to determine the structure of an enzyme substrate complex. However, the treated crystals did either not diffract to high resolution or the resulting difference electron density was not clear enough to be interpreted as a bound substrate. Therefore, we resorted to molecular docking simulations in order to obtain a model of such a complex. For these calculations, we chose a truncated variant of the natural substrate, *S*-methyl (2*S*,4*S*,5*S*)-2-amino-6-(3,4-dihydroxyphenyl)-4-hydroxy-5-(methylamino)-hexanethioate (Figure 23A). A number of active site residues, especially around the hydrophobic pocket (Figure 22) were treated as flexible (see Experimental Procedures). Due to the high number of the resulting internal degrees of freedom, we obtained many different docking poses and analyzed them with respect to mechanistic plausibility, *i.e.* we selected poses where the *N*-methyl group was close (< 4 Å) to the

N(5) atom of the FAD and was appropriately positioned to form a C-C bond with the dihydroxyphenyl moiety in order to form the isoquinoline ring. Out of about twenty different binding modes only one fulfilled these requirements (Figure 23B).

In this model structure, the dihydroxyphenyl group is bound in the hydrophobic pocket and interacts with the side chain of R66. In addition, the 3-OH group forms a hydrogen bond with the C(4)=O of the flavin cofactor. Furthermore, R63 and K304 are near the isoalloxazine ring of the FAD and the dihydroxyphenyl group of the substrate. The resulting positive electrostatic potential could facilitate deprotonation of the substrate or favor the binding of an already deprotonated substrate. In the crystal structure, there is also an ordered water molecule located right between C(4)=O and the amino group of K304, which may be displaced upon substrate binding.

The carbon atom of the *N*-methyl group is close to N(5) of the flavin (required for hydride transfer) and is also appropriately positioned in order to attack C2 of the aromatic ring (3.5 Å). The corresponding nitrogen atom is in hydrogen bonding position to the main chain carbonyl oxygen of D444. The nitrogen atom at the 2-position of the substrate on the other hand forms salt bridges to the side chain carboxylates of D315 and D444. Thus, these two residues are very likely primarily involved in substrate binding and orientation.

The methyl-thioester group of the bound ligand is oriented towards the entrance of the active site tunnel. This binding mode is therefore compatible with a longer chain (*e.g.* as in a CoA-derivative) being attached to the substrate.
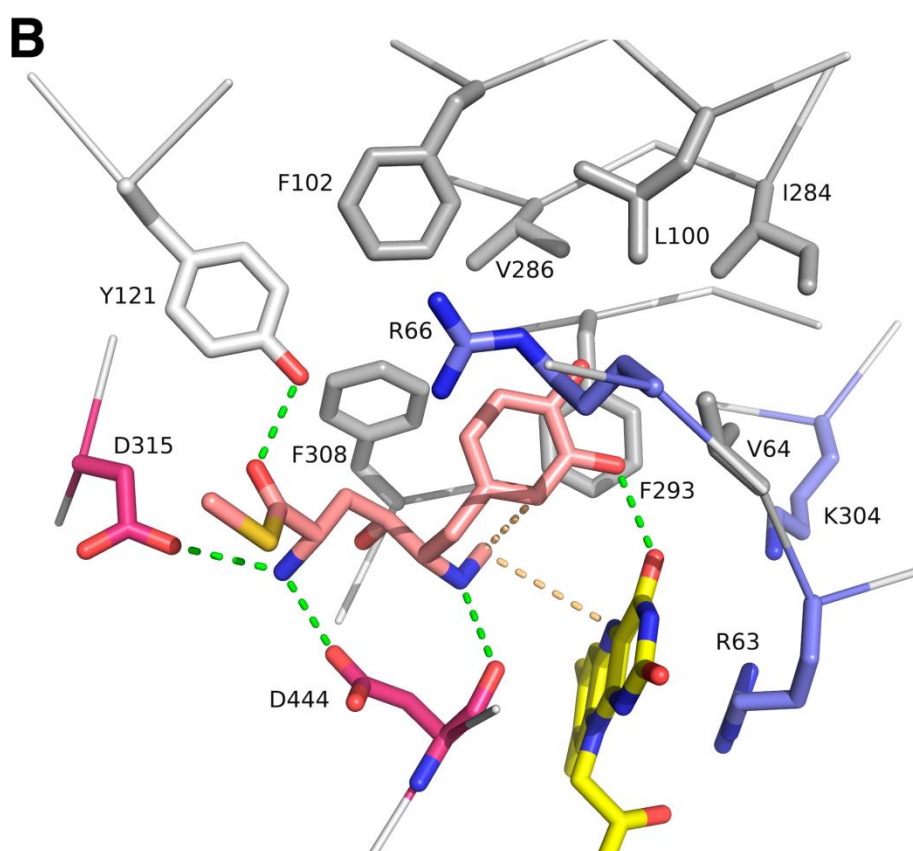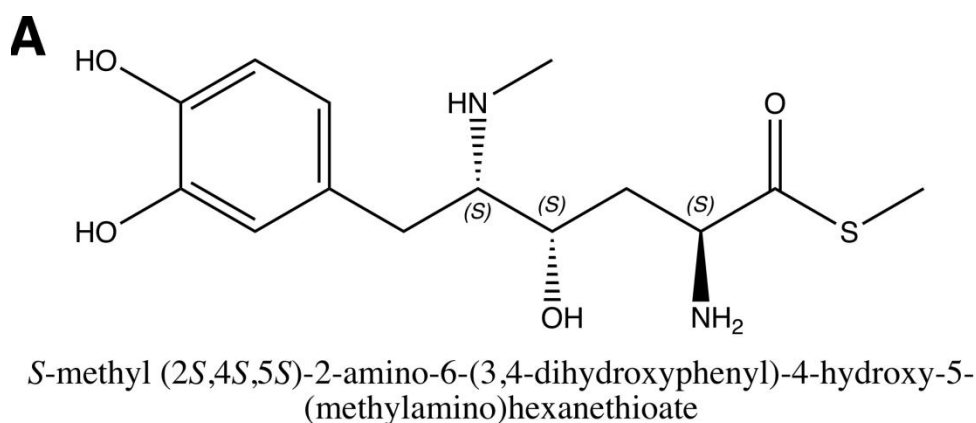
Figure 23. Panel A: Chemical structure of the truncated, natural substrate used in the docking calculations. Panel B: Close up view of the active site of FsqB in the modelled complex with the truncated, natural substrate (pink). The flavin cofactor is shown in yellow. Positively charged residues in vicinity are shown in blue, negatively charged residues in magenta. Residues forming the hydrophobic pocket are shown in grey. Green dashed lines depict hydrogen bonding interactions. The interaction between the N-methyl group of the substrate and N(5) as well as the aromatic moiety are shown as light-orange, dashed lines.

Addionally, we tried a different approach of molecular docking, where the natural substrate was linked with the phosphopantetheine moiety. The crystal structure of

FsqB in complex with the mono-covalently linked FAD co-factor and the docked substrate were used for molecular docking. Molecular docking experiments were performed utilizing the Yasara Structure suite (version 17.3.30, Yasara Biosciences (7). Crystal waters were removed from the structure prior to the docking experiment. Molecular docking was performed utilizing the Autodock Vina Plugin (8) of the Yasara Structure suite. Docking was performed with the rigid receptor while the ligand was flexible with a docking cell lining the cavity of the active center of FsqB. Ligands chosen for docking experiments were the putative non-natural substrates of FsqB, namely the putative natural substrate, N-methyl dopa and potential conversion intermediates. 250 docking runs per experiment were performed with a RMSD cut-off of 1 Å. Resulting docking poses were inspected visually. The natural substrate was generated taking the origin of FsqB into account. FsqB is part of a non-ribosomal peptide synthase pathway. The natural substrate of FsqB is linked to the FsqF NRPS via a thiol ester (1). It is known that in NRPS linker molecules are utilized to fuse the substrate to the carrier protein. The acyl carrier protein (ACP) is a prominent linker moiety (9) During biosynthesis of fatty acids and polyketides the elongated chain of the substrate/product is fused to the ACP via a thiol ester at the distal thiol of the utilized 4'-phosphopantetheine moiety. This utilization of a phosphopantetheine moiety is believed to be a common feature of linker molecules among NRPS systems. Therefore the natural substrate of FsqB determined by Bacille et al. (2016) (4) was generated in-silico linked to a phosphopantetheine moiety. Subsequently this natural substrate-phosphopantetheine molecule was used as ligand for molecular docking experiments. Figure 24 shows the suggested scenario for position of the natural substrate inside the FsqB pocket.
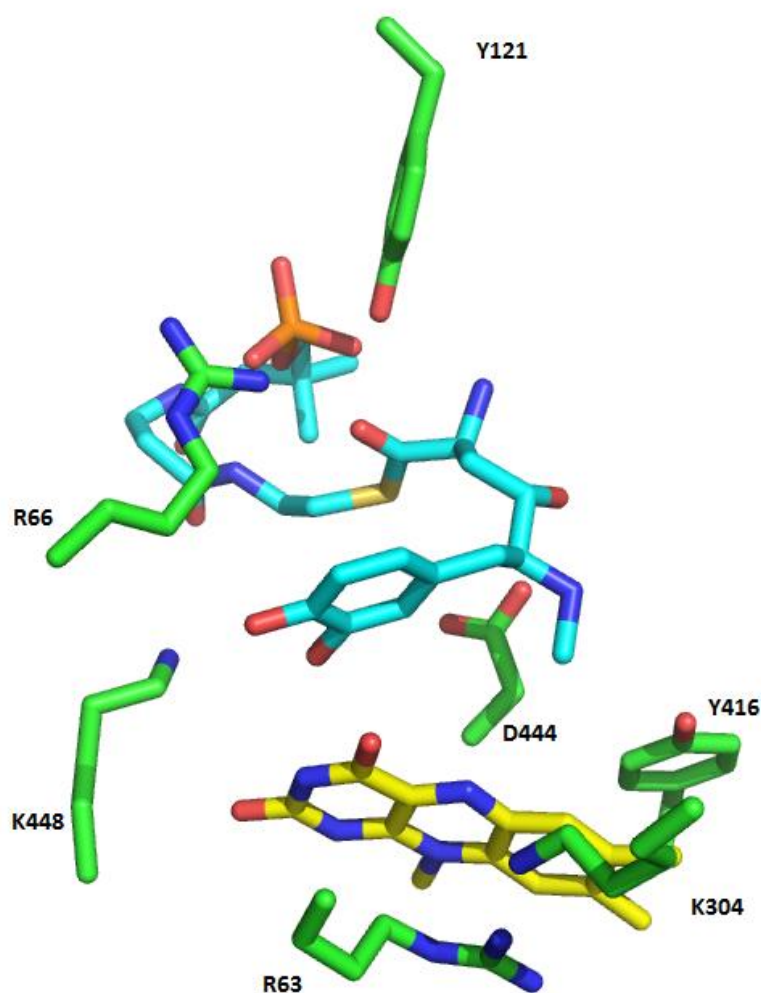
Figure 24. Docking of natural substrate with the phosphopanteine moiety.

In addition, we performed molecular docking simulations with the substrates used in our study, *i.e. N*-methyl-dopa and *N*-methyl-tyrosine. Due to the reduced spatial requirements of these substrates, we found two distinct binding modes that are different to the binding pose for the (truncated) natural substrate. As shown in Figure 25 (panel A), *N*-methyl-tyrosine binds with the carboxylate group oriented toward the pair of positively charged amino acids (R66 and K448) and the phenolate interacts with Y121. This pose also places the *N*-methyl group near N(5) of the isoalloxazine ring thereby allowing the transfer of a hydride. In contrast to the binding pose of *N*-methyl-tyrosine the two stereoisomers of *N*-methyl-dopa may bind in a different orientation with the catechol-ring oriented toward R66 and Y121. In both poses, the *N*-methyl group is placed above N(5) of the flavin to enable hydride transfer (Figure

67

25, panel B and C). In all three docking poses, the amino acid side chain of D444 is within 3-4 Å distance of the *N*-methyl group.
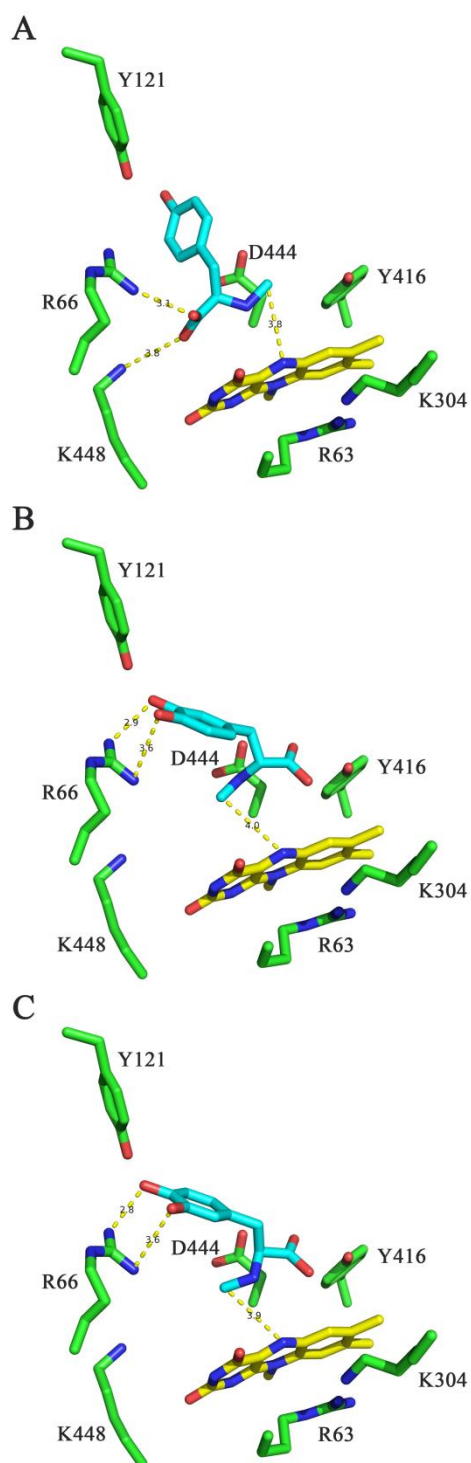
Figure 25. Stick representations of the suggested binding scenarios for L-*N*-methyl-tyrosine (panel A) and the two stereoisomers of *N*-methly-dopa (panel B and C). Amino acid side chains near the binding site are shown in green. The isoalloxazine ring of FAD is shown in yellow. The docked substrates are

shown in cyan. The distances of the carboxylate group of L-*N*-methyl-tyrosine to R66 and K448 and of the catechol to R66 are shown as yellow dashed lines. Panel A, B and C show a model for L-*N*-methyl-tyrosine, D-*N*-methyl-dopa and L-*N*-methyl-dopa bound to the active site of FsqB, respectively.

Site-directed mutagenesis of active site amino acid residues

Based on the crystal structure of FsqB and the molecular docking of the natural substrate, we generated several FsqB variants. (List of primers's sequence are shown in table 5) to probe the involvement of amino acids in catalysis using *N*-methyl-dopa as the substrate. Figure 26 shows the SDS page of small scale expression tests. With the exception of the K448A variant, all variants exhibited a similar thermal melting point (54.5 ± 3 °C) (figure 27 and table 6) and a similar CD-spectrum (figure 28) indicating that the proteins were properly folded and possessed a similar stability. Replacement of the three basic residues R63, R66 and K304 severely compromised enzymatic activity and the R63M and K304A variants showed only residual activity amounting to 0.3 and 3% of the activity of the wild-type enzyme (Table 7). Similarly, replacement of Y121 to phenylalanine resulted in a substantial loss of activity (3% residual activity). Very surprisingly, the D444A variant substantially reduced enzymatic activity of FsqB (0.04% residual activity), suggesting an important role in catalysis. Interestingly, the K304A variant exhibited a very slow rate of reoxidation of 183 ± 37 M^{-1} s^{-1} and thus is apparently involved in the oxidative half reaction, *i.e.* oxidation of the reduced FAD by dioxygen. The role of K448 for covalent flavinylation was probed by replacing this residues with alanine. The resulting K448A variant was completely devoid of FAD confirming earlier findings for MSOX that this residue plays an essential role for establishing the covalent bond between the 8α-methyl group and the corresponding cysteine residue (10). From the results of the mutagenesis study (Table 7), we suggest that the positively charged side chains of residues R66 and K448 are important for substrate binding whereas the carboxyl-group of the side chain of D444 activates the substrate by proton abstraction from the amino-group of the substrate. On the other hand, R63 located on the *si* face stabilizes the negatively charged flavin cofactor after hydride transfer from the substrate.

Finally, K304 was identified as a central player in the reoxidation of the reduced flavin by dioxygen.
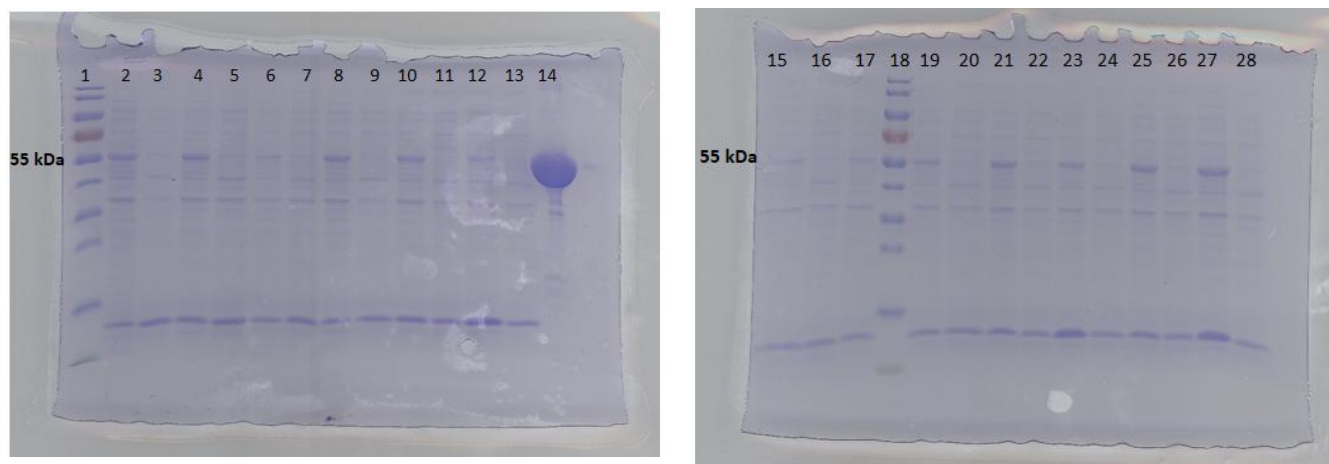
Figure 26. SDS pages (12.5% concentration) showing small scale induction of FsqB. Lane 1; pre-stained protein ruler. Lane 2; induced D60A variant. Lane 3; not induced D60A variant. Lane 4; induced R63M variant. Lane 5; not induced R63M variant. Lane 6; induced R66M variant. Lane 7; not induced R66M variant. Lane 8; induced variant Y69F. Lane 9; not induced variant Y69F. Lane 10; induced Y121F variant. Lane 11; not induced Y121F variant. Lane 12; induced Y266F variant. Lane 13; not induced Y266F variant. Lane 14; FsqB wild type as positive control. Lane 15; induced K304A. Lane 16; not induced K304A. Lane 17; induced K304A (repeated). Lane 18; pre-stained protein ruler. Lane 19; induced Y416F variant. Lane 20; not induced Y416F variant. Lane 21; induced D444A variant. Lane 22; not induced D444A variant. Lane 23; K448A variant. Lane 24; not induced K448A variant. Lane 25; induced Y266F variant (repeated). Lane 26; not induced variant Y266F (repeated). Lane 27; induced K448A variant (repeated). Lane 28; not induced K448A variant (repeated).
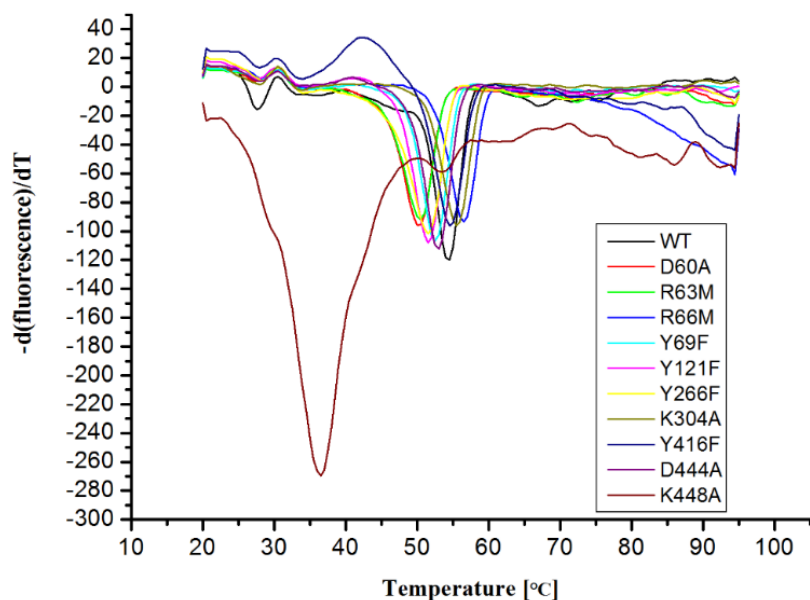
Figure 27. Thermal stability of FsqB WT and variants. ThermoFAD experiment shows that all the variants except for K448A are in the same range as the wild-type protein.

Table 6. Melting points of FsqB wild type and its generated variants.

	FsqB-WT	D60A	R63M	R66M	Y69F	Y121F	Y266F	K304A	Y416F	D444A	K448A
Melting point [°C]	54.5	50.5	50.5	56.5	52.5	51.5	51.5	55.5	54.5	53	36.5
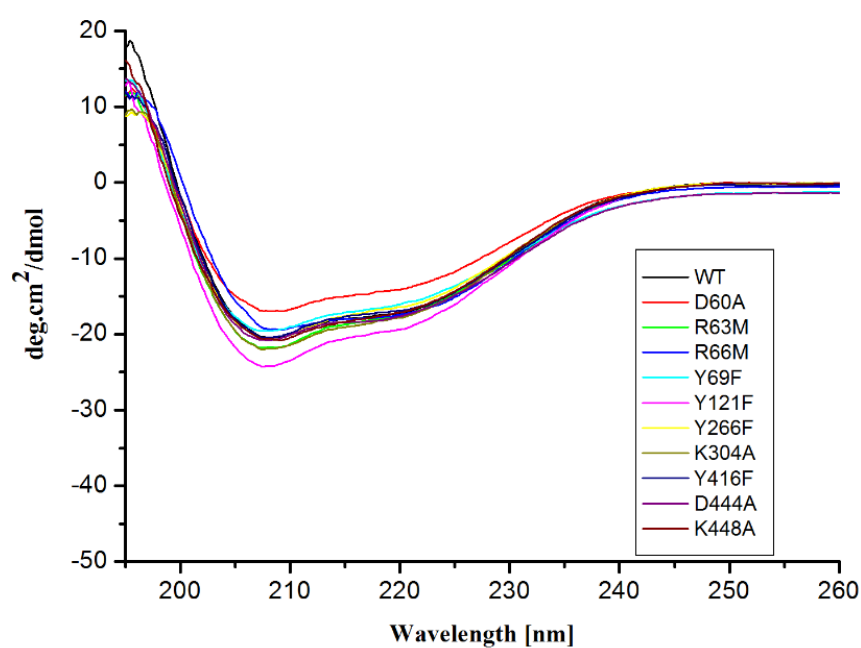
Figure 28. CD experiments show that the content of α helices and β sheets for all variants are comparable to wild-type protein.

Table 7. Summary of pre-steady state kinetic parameters for FsqB variants with *rac-N*-methyl-dopa

Enzyme	k_{obs} [s^{-1}][*]	k_{obs} (%)[*2]
R63M	0.027 ± 0.003	0.3
R66M	n.d.	_
Y121F	0.24 ± 0.03	2
K304A	0.3 ± 0.03	3
Y416F	3.4 ± 0.02	33
D444A	0.0036 ± 0.0004	0.03

[*] the values of k_{obs} were recorded for comparison at 2.5 mM substrate concentrating due to the limited solubility of L-*N*-methyl-tyrosine.

Detection of binding residues in FsqB

Two main experiments were carried out to define the binding residues in the FsqB pocket. In both experiments, changes in spectral properties of the flavin are determined, which occur when the flavin isoalloxazine ring interacts with its environment. In the first experiment, the change in flavin spectrum is observed due to adding an excessive amount of the substrate to the enzyme (10x). In the second experiment, the change in the FAD fluorescence emission is determined by applying the ThermoFAD experiment. It is suggested that residues Arg66, Tyr 69 and Tyr 121 are responsible for coordination the substrate inside the pocket (figure 29). Results of both experiments confirm that these 3 residues are the binding residues.
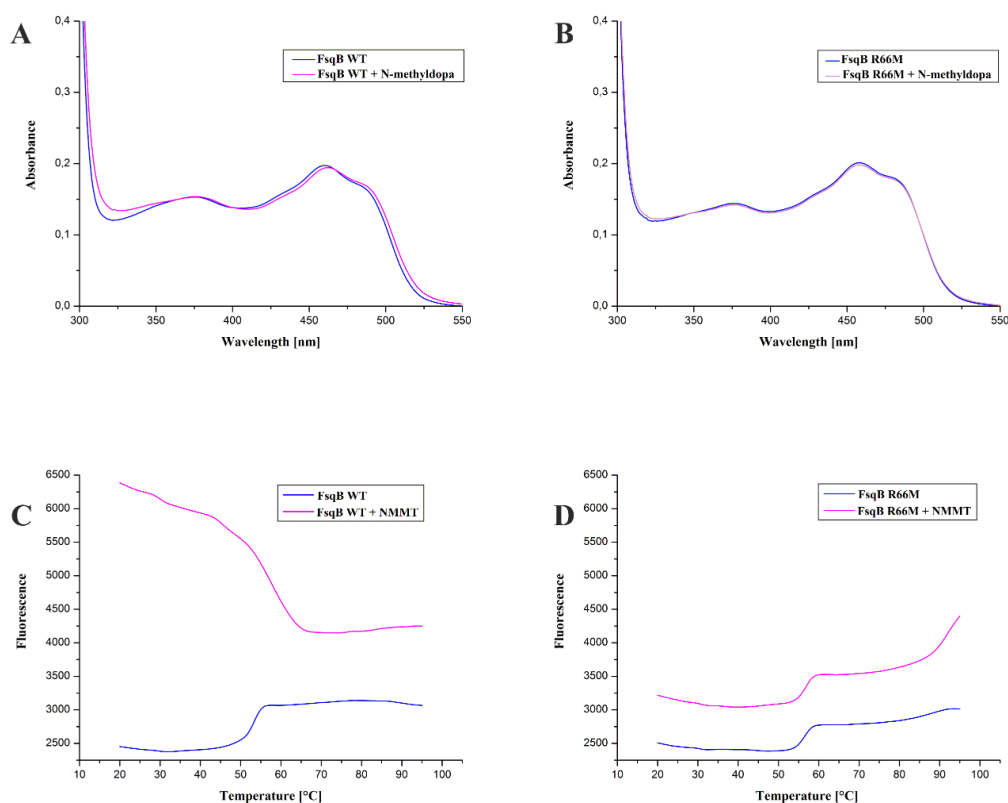
Figure 29. (A) FsqB spectrum without substrate shown as blue line. FsqB spectrum with 10x concentration of *N*-methyldopa in magenta. The graph shows the shift which is due to substrate binding to the flavin. Whereas in (B) the same substrate cannot bind to the flavin because of the mutation in the gene coding for the binding residue Arg 66. (C) ThermoFAD experiment for the wild type enzyme with and without *N*-methyl-*meta*-tyrosine. The blue line shows the enzyme alone where there is an increase in fluorescence due to the release of flavin. The magenta line shows fluorescence signal change of the enzyme with the substrate. (D) There is no change in the R66M variant signal when the substrate is added to this variant.

The redox potential of Flavin bound to FsqB enzyme:

The redox potential of FsqB was calculated to +30mV. The formation of the semiquinon adduct is recorded, where the maximum absorbance of the red product is observed at 396 nm (Figure 30).
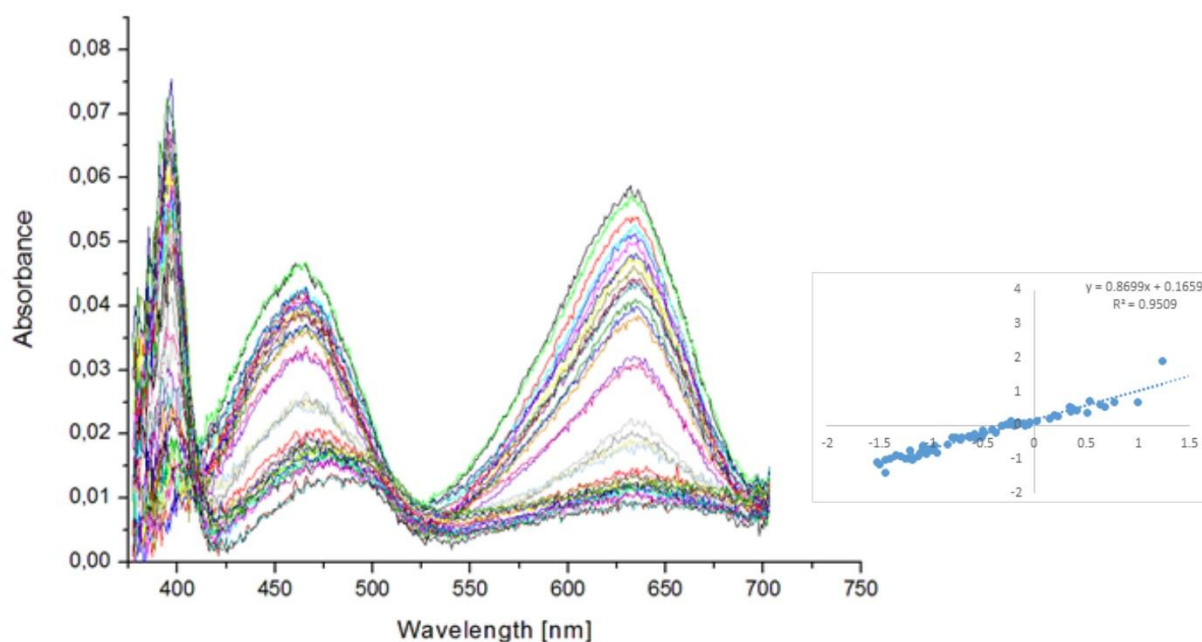
Figure 30. The redox potential (E0) of FsqB-bound FAD. This value was determined by the dye-equilibration method using the xanthine/xanthine oxidase system (11). The measurements took place under anaerobic conditions utilizing a stopped flow device at 25 °C in 25 mM HEPES.NaOH, 150 mM NaCl buffer (pH 7.0). The concentrations of enzyme and redox dye were chosen in a way that their absorption maxima are in the same range. Measurements were done in triplicate. The redox potential was calculated using double logarithmic plots, log (ox/red) of the enzyme versus log(ox/red) of the dye. A linear least-squares fit was done with Excel 2010. ORIGIN 8.6 software was used to produce the figure. The redox potential for the reduction of FAD bound to FsqB was calculated to be 30 ± 1 mV.

This value is common also for other enzymes from the same family (DAAO) which is covalently link to flavin via 8^α position.

References

1. Augustin, P., Hromic, A., Pavkov-Keller, T., Gruber, K., and Macheroux, P. (2016) Structure and biochemical properties of recombinant human dimethylglycine dehydrogenase and comparison to the disease-related H109R variant. *FEBS J.* 10.1111/febs.13828

2. Wagner, M. A., Khanna, P., and Jorns, M. S. (1999) Structure of the flavocoenzyme of two homologous amine oxidases: Monomeric sarcosine oxidase and N-methyltryptophan oxidase. *Biochemistry.* **38**, 5588–5595

3. Macheroux, P. (1999) UV-Visible Spectroscopy as a Tool to Study Flavoproteins. in *Flavoprotein Protocols. Methods in Molecular Biology*, pp. 1–7, 10.1385/1-59259-266-X:1

4. Baccile, J. A., Spraker, J. E., Le, H. H., Brandenburger, E., Gomez, C., Bok, J. W., MacHeleidt, J., Brakhage, A. A., Hoffmeister, D., Keller, N. P., and Schroeder, F. C. (2016) Plant-like biosynthesis of isoquinoline alkaloids in Aspergillus fumigatus. *Nat. Chem. Biol.* **12**, 419–424

5. Krissinel, E., and Henrick, K. (2007) Inference of Macromolecular Assemblies from Crystalline State. *J. Mol. Biol.* **372**, 774–797

6. Rigoldi, F., Spero, L., Dalle Vedove, A., Redaelli, A., Parisini, E., and Gautieri, A. (2016) Molecular dynamics simulations provide insights into the substrate specificity of FAOX family members. *Mol. BioSyst.* **12**, 2622–2633

7. Krieger, E., and Vriend, G. (2014) YASARA View - molecular graphics for all devices - from smartphones to workstations. *Bioinformatics.* **30**, 2981–2982

8. Trott, O., and Olson, A. J. (2010) Software news and update AutoDock Vina: Improving the speed and accuracy of docking with a new scoring function, efficient optimization, and multithreading. *J. Comput. Chem.* **31**, 455–461

9. Crump, M. P., Crosby, J., Dempsey, C. E., Parkinson, J. a, Murray, M., Hopwood, D. a, and Simpson, T. J. (1997) Solution structure of the actinorhodin polyketide synthase acyl carrier protein from Streptomyces coelicolor A3(2). *Biochemistry.* **36**, 6000–6008

10. Trickey, P., Wagner, M. A., Jorns, M. S., and Mathews, F. S. (1999) Monomeric sarcosine oxidase: Structure of a covalently flavinylated amine oxidizing enzyme. *Structure.* **7**, 331–345

11. Massey, V. (1991) A simple method for the determination of redox potentials. in *Flavins Flavoproteins Proc. Int. Symp., 10th*, pp. 59–66

Chapter 5: Discussion

FsqB belongs to the family of D-amino acid oxidases (DAAOs) (1). Based on the sequence similarity to members of the amine oxidase family, *e.g.* MSOX and MTOX, it was recently suggested that FsqB shares the topology of this protein family. FsqB possesses the same fold as P-hydroxybenzoate hydroxylase (PHBH) (2). This fold contains generally two domains; a FAD binding domain consisting of β-sheets sandwiched by α-helices and a catalytic domain consisting of eight β-sheets that form the cavity where FAD-isoalloxazine ring is embedded. These sheets are also surrounded by long α-helices (1–3). The X-ray crystal structure of FsqB reported here supports this assumption. This family of FAD-dependent oxidases was extensively studied in terms of the mechanism of oxidation. Among the discussed mechanisms, a hydride transfer mechanism, entailing the transfer of a hydride from the *N*-methyl group to the N(5)-position of the isoalloxazine ring, appears to be the most favorable (4–6). In addition, recent fragment molecular orbital and mixed quantum mechanics/molecular mechanics calculations have concluded that a hydride transfer mechanism is the most likely scenario (5, 6). Therefore, we assumed that the oxidative cyclization catalyzed by FsqB might be initiated by a hydride transfer, followed by the nucleophilic attack of the catechol moiety of the substrate to yield the isoquinoline product because the electron-rich catechol moiety can be easily deprotonated at the 3-OH (pK_a = 9-9.5,(7)). Moreover, HPLC data (table 2 in the results section) show that FsqB is regioselective. The hydroxyl group on benzene carbon number 3must be close to the oxidized methyl-amine bond (imine species) in order to start the nucleophilic attack. Whereas, in the chemical reaction (the substrate is oxidized by a chemical and not by an enzyme) the 3-OH group is detected on the other side of the imine species. Our results are in agreement with the results of Baccile et. *al* (2016) (8). In fact, docking of the proposed natural substrate to the active site of FsqB suggested that the *N*-methyl group is positioned on the *re*-side of the isoalloxazine ring close to the N(5) in accordance with the steric requirements for a hydride transfer (Figure 21, results section). Although this docking pose is compatible with a hydride transfer mechanism, it fails to explain the effects on catalysis observed in some of the generated FsqB variants, most notably the R66M and D444A variants. Thus, we hypothesized that the substrates tested in our study adopt a different binding pose as suggested for the natural substrate. In fact, docking simulations with L-*N*-methyl-tyrosine and *N*-methyl-dopa showed that both of these substrates can bind in different orientations as compared to

the natural substrate. In the case of L-*N*-methyl-tyrosine the carboxylate group interacts with the side chains of R66 and K448 and the phenolate ring points toward Y121 (Figure 23, panel A, results section). This binding mode is very similar to the binding of substrates in other members of the amine oxidase family (PF01266), notably MTOX, MSOX and NikD (9–11) and is clearly also possible in FsqB because of the conservation of this pair of positively charged amino acid residues. In addition, this binding mode also provides a role for the side chain of D444 as the carboxylate is located near the *N*-methyl group of the substrate and may act as an active site base to promote the transfer of a hydride to the N(5) of the isoalloxazine ring thus accounting for the large effect on catalysis observed in the D444A variant. Interestingly, docking of the two stereoisomers of *N*-methyl-dopa suggested a different binding mode with the catechol ring moiety engaging in a salt bridge with the guanidinium group of R66 and the carboxylate group pointing toward the side chain of Y416 (Figure 23, panel B and C, results section). Again, in these binding poses the side chain of D444 is in close proximity to the *N*-methyl group and may participate in catalysis as an active site base. Overall, the putative binding poses for *N*-methyl-dopa are in agreement with effects observed with the generated FsqB variants: Very low activity for the R66M and D444A variants, a less pronounced effect for the Y121F variant and a very small effect in the case of the Y416F variant. It is also noteworthy that both stereoisomers are productively converted to the isoquinoline product with similar kinetic rates, indicating that both poses are conducive for the ring closure reaction. In this context, it is very interesting to note that the distinct binding poses for L-*N*-methyl-tyrosine and *N*-methyl-dopa also provide a rationale for the finding that FsqB accepts only the L- but not the D-stereoisomer of *N*-methyl-tyrosine whereas both stereoisomers of *N*-methyl-dopa are accepted, albeit with slightly different kinetic rates (Table 3, results section): L-*N*-methyl-tyrosine is anchored to R66 and K448 via its carboxylate group fixing the chiral carbon in the position shown in Figure 23, panel A (results section) and thus binding of the D-stereoisomer would require the rotation of the substrate (by ca. 180°) above the *re*-side of the isoalloxazine ring, which is very unlikely because there are no residues "on the other side" to interact with the carboxylate group. In contrast, a similar rotation is not required for *N*-methyl-dopa because the substrate is anchored to R66 by the catechol moiety and not the carboxylate group and therefore it is sufficient to allow rotation of the C-C bond connecting the chiral carbon atom to the β-carbon atom. In

keeping with this interpretation, *N*-methyl-dopa (and the L-enantiomer) is more efficiently consumed by FsqB than *N*-methyl-tyrosine and *N*-methyl-*meta*-tyrosine (20-fold difference in k_{cat}/K_M, Table 4, results section), suggesting that positioning the catecholate moiety toward R66 is the preferred binding mode for these substrate analogs. In summary, our results suggest that the observed stereospecificity for *N*-methyl-tyrosine (and *N*-methyl-*meta*-tyrosine) is the result of the specific binding mode whereas the different binding mode of *N*-methyl-dopa in combination with the active site plasticity of FsqB accommodates both stereoisomers. Currently, efforts to obtain a crystallographic structure of D- and L-*N*-methyl-tyrosine bound to FsqB are under way to obtain more structural insights into the parameters that control substrate binding and oxidation in particular with regard to the observed stereospecificity.

The demethylation observed with *rac-N*-methyl-*meta*-tyrosine and L-*N*-methyl-tyrosine (Table 2, results section) can be explained by the lack of the *meta*-hydroxyl group in the case of the latter and a lower efficiency for the ring closure reaction in the binding mode adopted by these substrates (Figure 23, panel A, results section). The reduction of the flavin by the substrate results in the formation of an imine that is subsequently attacked by the phenolate ring (see Scheme 1). However, this reaction is not possible in L-*N*-methyl-tyrosine and thus the imine intermediate will hydrolyze to the demethylated product, *i.e.* L-tyrosine. The lack of the *para*-hydroxyl group, on the other hand, may also slow down the ring closure step and therefore lead to an efficient competition by hydrolysis yielding a mixture of cyclized and demethylated product in the case of *rac-N*-methyl-*meta*-tyrosine as substrate.

The oxidation of reduced FAD by molecular oxygen in the family of amine oxidases has been subject of several detailed studies revealing the importance of a positive charge near the site of reoxidation, the C(4a)-position of the isoalloxazine ring (12, 13). In accordance with these studies, we have identified K304 as a central amino acid residue for the oxidative half reaction since the K304A variant exhibited a more than 100-fold decreased rate. The importance of this residue for the reactivity of the reduced FAD with oxygen was also observed with the related MSOX (14) thus our finding adds further support to the current concept of oxygen activation in flavoprotein amine oxidases. Jorns et. *al.* (2010), reported that replacing the lysine residue responsible for flavin reoxidation results in the elimination or displacement of a positive charge from the pocket above the *si* face of the flavin ring. This results in the loss of a charge-

stabilized binding site for the superoxide anion, an intermediate in the oxidative half-reaction of MSOX, and greatly reduces the rate of oxygen reduction. At the same time, the mutation disrupts a water relay system near the flavin N(5) atom that probably catalyzes the ionization of a protonated sarcosine intermediate, leading to a transient accumulation of a charge-transfer intermediate along the pathway of product release from the reoxidized enzyme (15). We have also observed different rates for the reoxidation of reduced FsqB depending on the substrate used for the reduction, *i.e* a fast reaction with *N*-methyl-dopa and five-fold lower reaction with L-*N*-methyl-tyrosine and *rac*-*N*-methyl-*meta*-tyrosine. In the case of MSOX, it was proposed that oxygen reacts with the enzyme-product complex (16). The reoxidation proceeds via a modified ping pong mechanism in which the oxygen reacts with Enzyme-FADred-Product prior to the dissociation of the imino acid product (16). Thus the observed differences in the kinetic rates may reflect the differences of the enzyme-product complex obtained with L-*N*-methyl-tyrosine (only demethylated product, *i.e.* tyrosine) and *rac*-*N*-methyl-*meta*-tyrosine (demethylated and isoquinoline product) on the one hand and *N*-methyl-dopa (only isquinoline product) on the other hand.

Different studies show that the anionic form of sarcosine is the active form that can be converted by MSOX (17–19). We suggest that all tested substrates, that are oxidized by FsqB, are also in their anionic form. The anionic form the substrate forms a charge transfer complex with the oxidized form of the flavin, which serves as charge acceptor (9, 11, 20). Moreover, this complex is stabilized by R66/K448 on the *re* face of flavin and R63/K304 on the *si* face of the flavin (21). The variant Y121F leads to a sharp decrease in the activity of FsqB (2% of the original activity). The primary tests show that Y121F is responsible for coordinating the substrate inside the pocket. In the study of Ewing et. *al.* (2017) they proved that the tyrosine residues in VAO's pocket might play a role in deprotonating the substrate (22). Thus, it is suggested in FsqB that the Y121 residue might have the same role.

In the study of Trickey et. *al.* (1999), it is proved in MSOX that K348 (the same residue as K448 in FsqB) is responsible for the covalent flavinylation (23). FsqB K448M also led to the same conclusion since this variant was only obtained as apoenzyme without the cofactor.

Photoreduction of FsqB shows the anionic semiquinone (1+1 electron reduction). When the redox potential of the FsqB is determined in stopped flow experiments, the cofactor

is clearly reduced in a two electron transfer system. This feature is common for the amine oxidase family (4, 24). Moreover, it is proved that the electron transfer type can be changed in a given flavoenzyme with different conditions and upon substrate binding to the pocket (25).

In summary, our study has shown that FsqB is a member of the family of amine oxidases, but in contrast to previously characterized members of this family it combines the oxidation of a *N*-methyl group with the generation of a heterocyclic ring system. Although FsqB is the first characterized representative of this group of "oxidative cyclases" data base searches using the FsqB sequence revealed many more putative enzymes that may catalyze a similar ring closure reaction in natural product biosynthesis, in particular in fungi. Also, the plasticity of the active site of FsqB, and potentially of other yet uncharacterized homologs, may encourage further developments to improve the substrate scope of the enzyme for biocatalytic applications.

Scheme 1

Proposed reaction mechanism for the ring closure reaction with *N*-methyl-dopa (top) and for the demethylation via hydrolysis of the imine with *N*-methyl-tyrosine (R_1= OH, R_2 = H) and partially with *N*-methyl-*meta*-tyrosine (R_1= H, R_2 = OH) (bottom)
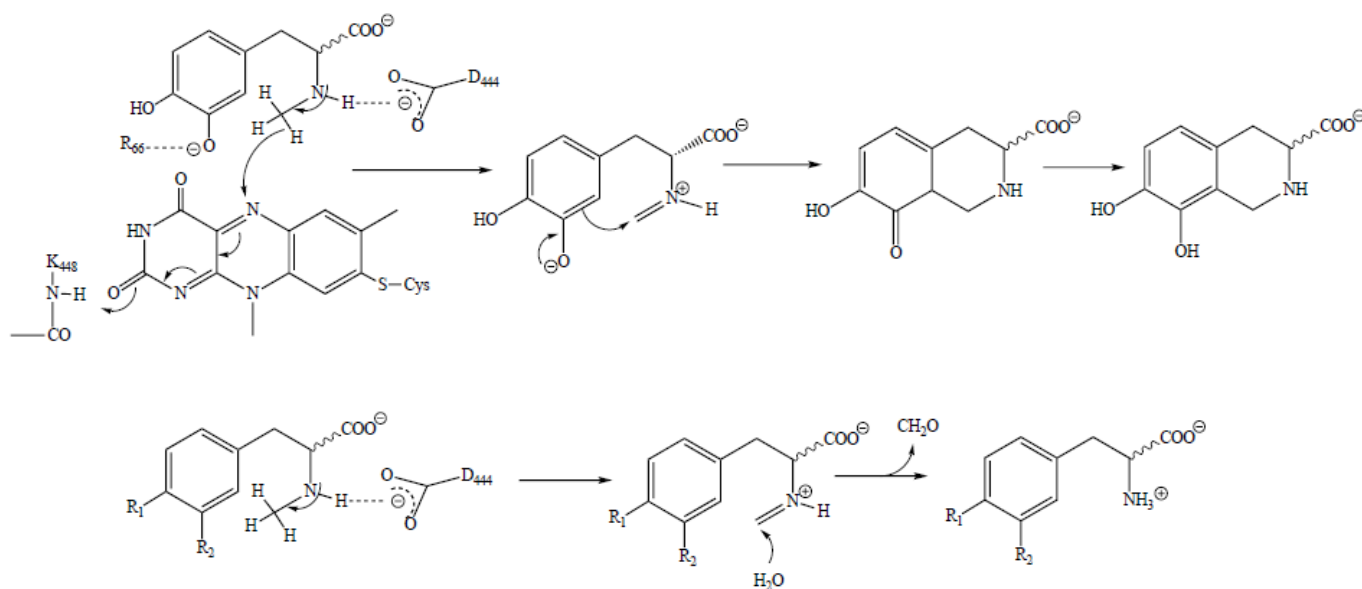
References

1. Collard, F., Zhang, J., Nemet, I., Qanungo, K. R., Monnier, V. M., and Yee, V. C. (2008) Crystal structure of the deglycating enzyme fructosamine oxidase (Amadoriase II). *J. Biol. Chem.* **283**, 27007–27016

2. MATTEVI, A., VANONI, M. A., TODONE, F., RIZZI, M., and ALEX TEPLYAKOV ALESSANDRO CODA, M. B. B. C. (1996) Crystal structure of D -amino acid oxidase: A case of active site mirror-image convergent evolution with flavocytochrome b 2. *Proc. Natl. Acad. Sci. USA.* **93**, 7496–7501

3. Rigoldi, F., Spero, L., Dalle Vedove, A., Redaelli, A., Parisini, E., and Gautieri, A. (2016) Molecular dynamics simulations provide insights into the substrate specificity of FAOX family members. *Mol. BioSyst.* **12**, 2622–2633

4. Fitzpatrick, P. F. (2010) Oxidation of amines by flavoproteins. *Arch. Biochem. Biophys.* **493**, 13–25

5. Karasulu, B., and Thiel, W. (2015) Amine oxidation mediated by N-methyltryptophan oxidase: Computational insights into the mechanism, role of active-site residues, and covalent flavin binding. *ACS Catal.* **5**, 1227–1239

6. Abe, Y., Shoji, M., Nishiya, Y., Aiba, H., Kishimoto, T., and Kitaura, K. (2017) The reaction mechanism of sarcosine oxidase elucidated using FMO and QM/MM methods. *Phys. Chem. Chem. Phys.* **19**, 9811–9822

7. Herrero-Martínez, J. M., Sanmartin, M., Rosés, M., Bosch, E., and Ràfols, C. (2005) Determination of dissociation constants of flavonoids by capillary electrophoresis. *Electrophoresis.* **26**, 1886–1895

8. Baccile, J. A., Spraker, J. E., Le, H. H., Brandenburger, E., Gomez, C., Bok, J. W., MacHeleidt, J., Brakhage, A. A., Hoffmeister, D., Keller, N. P., and Schroeder, F. C. (2016) Plant-like biosynthesis of isoquinoline alkaloids in Aspergillus fumigatus. *Nat. Chem. Biol.* **12**, 419–424

9. Carrell, C. J., Bruckner, R. C., Venci, D., Zhao, G., Jorns, M. S., and Mathews, F. S. (2007) NikD, an Unusual Amino Acid Oxidase Essential for Nikkomycin Biosynthesis: Structures of Closed and Open Forms at 1.15 and 1.90 Å Resolution. *Structure.* **15**, 928–941

10. Ilari, A., Bonamore, A., Franceschini, S., Fiorillo, A., Boffi, A., and Colotti, G. (2008) The X-ray structure of N-methyltryptophan oxidase reveals the structural determinants of substrate specificity. *Proteins Struct. Funct. Genet.* **71**, 2065–2075

11. Wagner, M. A., Trickey, P., Che, Z. W., Mathews, F. S., and Jorns, M. S. (2000) Monomeric sarcosine oxidase: 1. Flavin reactivity and active site binding determinants. *Biochemistry.* **39**, 8813–8824

12. Gadda, G. (2012) Oxygen activation in flavoprotein oxidases: The importance of being positive. *Biochemistry.* **51**, 2662–2669

13. Kommoju, P. R., Chen, Z. W., Bruckner, R. C., Mathews, F. S., and Jorns, M. S. (2011) Probing oxygen activation sites in two flavoprotein oxidases using chloride as an oxygen surrogate. *Biochemistry*. **50**, 5521–5534

14. Zhao, G., Bruckner, R. C., and Jorns, M. S. (2008) Identification of the oxygen activation site in monomeric sarcosine oxidase: Role of Lys265 in catalysis. *Biochemistry*. **47**, 9124–9135

15. Jorns, M. S., Chen, Z. W., and Mathews, F. S. (2010) Structural characterization of mutations at the oxygen activation site in monomeric sarcosine oxidase. *Biochemistry*. **49**, 3631–3639

16. Wagner, M. A., and Jorns, M. S. (2000) Monomeric sarcosine oxidase: 2. Kinetic studies with sarcosine, alternate substrates, and a substrate analogue. *Biochemistry*. **39**, 8825–8829

17. Zhao, G., and Jorns, M. S. (2006) Spectral and kinetic characterization of the Michaelis charge transfer complex in monomeric sarcosine oxidase. *Biochemistry*. **45**, 5985–5992

18. Zhao, G., and Jorns, M. S. (2002) Monomeric sarcosine oxidase: Evidence for an ionizable group in the E·S complex. *Biochemistry*. **41**, 9747–9750

19. Zhao, G., and Jorns, M. S. (2005) Ionization of zwitterionic amine substrates bound to monomeric sarcosine oxidase. *Biochemistry*. **44**, 16866–16874

20. Ralph, E. C., and Fitzpatrick, P. F. (2005) pH and kinetic isotope effects on sarcosine oxidation by N-methyltryptophan oxidase. *Biochemistry*. **44**, 3074–3081

21. Hassan-Abdallah, A., Zhao, G., and Jorns, M. S. (2006) Role of the covalent flavin linkage in monomeric sarcosine oxidase. *Biochemistry*. **45**, 9454–9462

22. Ewing, T. A., Nguyen, Q. T., Allan, R. C., Gygli, G., Romero, E., Binda, C., Fraaije, M. W., Mattevi, A., and Van Berkel, W. J. H. (2017) Two tyrosine residues, Tyr-108 and Tyr-503, are responsible for the deprotonation of phenolic substrates in vanillyl-alcohol oxidase. *J. Biol. Chem.* **292**, 14668–14679

23. Trickey, P., Wagner, M. A., Jorns, M. S., and Mathews, F. S. (1999) Monomeric sarcosine oxidase: Structure of a covalently flavinylated amine oxidizing enzyme. *Structure*. **7**, 331–345

24. Khanna, P., and Jorns, M. S. (2001) Characterization of the FAD-containing N-methyltryptophan oxidase from Escherichia coli. *Biochemistry*. **40**, 1441–1450

25. Hu, J., Chuenchor, W., and Rokita, S. E. (2015) A switch between one- And two-electron chemistry of the human flavoprotein iodotyrosine deiodinase is controlled by substrate. *J. Biol. Chem.* **290**, 590–600

Author contributions and financing

Chapter 6: Supplementary data

The chemical synthesis of substrates

Preparation of (*S*)-3-(3,4-dihydroxyphenyl)-2-(methylamino)propanoic acid (4):

(*S*)-Benzyl 2-(benzylamino)-3-(3,4-bis(benzyloxy)phenyl)propanoate (2). L-DOPA (1, 1.3 g, 6.6 mmol), potassium carbonate (3.0 g, 21.7 mmol), tetrabutylammonium iodide (420 mg, 1.14 mmol) and sodium iodide (100 mg, 0.67 mmol) were suspended in acetone (40 mL) and benzylbromide (3.0 mL, 4.3 g, 25.3 mmol) was added. The mixture was refluxed for 16 h, cooled to room temperature and filtered. The filter cake was washed with additional acetone (40 mL) and the combined filtrate was concentrated. The obtained crude product was purified via flash chromatography (SiO_2, hexanes/EtOAc 3/1) to give compound 2 as yellow oil (952 mg, 1.71 mmol, 26%).

$[\square]D20 = -6.4$ (c 1.2, CHCl3); 1H-NMR (300 MHz, $CDCl_3$): 7.50-7.19 (m, 20H), 6.84 (d, J = 8.3, 1H), 6.80 (d, J = 2.0, 1H), 6.67 (dd, J1 = 8.3, J2 = 2.0, 1H),5.16 (s, 2H), 5.09 (s, 2H), 5.07 (s, 2H), 3.81 (d, J = 13.2, 1H), 3.64 (d, J = 13.2, 1H), 3.55 (t, J =7.0, 1H), 2.91 (d, J = 7.0, 2H); 13C-NMR (75 MHz, $CDCl_3$): 174.5, 148.8, 147.8, 139.5, 137.4, 137.3, 135.7, 128.6, 128.5, 128.4, 128.32, 128.29, 128.2, 127.8, 127.33, 127.29, 122.2, 116.1, 115.1, 71.4, 71.2, 66.4, 62.0, 52.0, 39.2; IR (film) $\tilde{\upsilon}$ = 1730, 1588, 1510, 1454, 1262, 1214, 1162, 1135, 1023, 906, 725, 694; HRMS(APCI): m/z: calc. for $C_{37}H_{36}NO_4{+}$: 558.2639 [M+H]+, found: 558.2634.

(*S*)-Benzyl 2-(benzyl(methyl)amino)-3-(3,4-bis(benzyloxy)phenyl)propanoate (3). Compound 2 (883 mg, 1.58 mmol) was dissolved in dichloromethane (22 mL). Anhydrous sodium sulfate (898 mg, 6.32 mmol), sodium triacetoxyborohydride (2.35 g, 11.1 mmol) and formaldehyde (37 wt-% solution in water, 552 µL, 11.7 mmol) were added. The mixture was stirred for 16 h at room temperature. The reaction was quenched by the addition of saturated aqueous ammonium chloride solution (10 mL), the phases were separated, the aqueous phase was washed with

EtOAc (2 x 15 mL) and the combined organic phase was dried over sodium sulfate, filtered and concentrated. The crude product was purified via flash chromatography (SiO$_2$, hexanes/EtOAc 3/1) to give the target compound 3 as pale yellow oil (881 mg, 1.54 mmol, 98%).

[□]D20 = -25.3 (c 0.66, CHCl3); 1H-NMR (300 MHz, CDCl$_3$): 7.44-7.10 (m, 20H), 6.82 (d, J = 8.2, 1H), 6.76 (d, J = 2.0, 1H), 6.66 (dd, J1 = 8.2, J2 = 2.0, 1H), 5.13 (s, 2H), 5.10 (s, 1H), 5.08 (s, 1H), 5.04 (s, 2H), 3.76 (d, J =13.9, 1H), 3.58-3.53 (m, 2H), 3.07 (dd, J1 = 13.9, J2 = 7.8, 1H), 2.27 (s, 3H); 13C-NMR (75 MHz, CDCl$_3$): 171.8, 148.9, 147.6, 139.3, 137.7, 137.5, 136.0, 131.9, 128.8, 128.63, 128.58, 128.55, 128.4, 128.33, 128.27, 127.84, 127.82, 127.4, 127.0, 122.3, 116.3, 115.2, 71.6, 71.3, 67.4, 66.1, 58.8, 38.1, 35.6; IR (film) ṽ = 1727, 1510, 1454, 1262, 1214, 1155, 1167, 1023, 906, 725, 694; HRMS(APCI): m/z: calc. for C$_{38}$H$_{38}$NO$_4$+: 572.2795 [M+H]+, found: 572.2790.

(*S*)-3-(3,4-dihydroxyphenyl)-2-(methylamino)propanoic acid (4). Compound 3 (398 mg, 0.69 mmol) was dissolved in MeOH (10 mL) and Pd/C (10 wt-%, 40 mg) was added. The reaction mixture was stirred vigorously under a hydrogen atmosphere (1 atm.) for 24 h. After removal of the hydrogen atmosphere, HCl (2 vol-% in H$_2$O, 10 mL) was added and the mixture was centrifuged and the supernatant was filtered through a syringe filter (0.45 μm). The filter was washed with additional HCl (2 vol-% in H$_2$O, 2 x 10 mL). The obtained filtrate was immediately frozen in liquid nitrogen and lyophilized again. Compound 4 was obtained as a colorless solid (112 mg, 0.53 mmol, 77%).

[□]D20 = -18.2 [c 1.0, HCl (2 vol-% in H2O)]; 1H-NMR (300 MHz, CDCl3): 6.56 (d, J = 8.1, 1H), 6.48 (d, J = 2.1, 1H), 6.40 (dd, J1 = 8.1, J2 = 2.1, 1H), 3.76 (t, J =6.0, 1H), 2.88 (dd, J1 = 6.0, J2 = 5.6, 2H), 2.42 (s, 3H); 13C-NMR (75 MHz, CDCl3): 170.2, 144.0, 143.4, 125.4, 121.6, 116.6, 116.3, 61.5, 33.8, 31.6; IR (film) ṽ = 3426 (br), 3132 (br); 1570, 1481, 1386, 1294, 1200, 780, 542, 527; HRMS(APCI): m/z: calc. for C$_{10}$H$_{14}$NO$_4$+: 212.0917 [M+H]+, found: 212.0917.

Preparation of (*rac*)- 3-(3-hydroxyphenyl)-2-(methylamino)propanoic acid (9):

(*rac*)-2-{[(benzyloxy)carbonyl]amino}-3-(3-{[(benzyloxy)carbonyl]oxy}phenyl)propanoic acid (6). meta-Tyrosine (5, 1.0 g, 5.5 mmol) was dissolved in NaOHaq. solution (11 mL, 0.5 M) and cooled to 4 °C. A solution of benzyl chloroformate (1.88 g, 11 mmol, 1.57 mL, 2 equiv.) in Et_2O (15 mL) and a NaOHaq. solution (19 mL, 1.00 M) were added dropwise simultaneously over a period of one hour. The reaction mixture was stirred for 1 h at 4 °C and 2 h at room temperature. The obtained slurry was filtered and the filtrate's pH was adjusted to 1-2 by the addition of solid citric acid. The aqueous phase was extracted with Et_2O (3 x 50 mL), the combined organic phase was dried over Na_2SO_4, filtered and concentrated to give a yellow oil (2.3 g), which was directly used for the next reaction step without further purification.

(*rac*)-methyl 2-{[(benzyloxy)carbonyl](methyl)amino}-3-(3-{[(benzyloxy)carbonyl]oxy}phenyl)propanoate (7). Crude product 6 (2.3 g, 5.1 mmol) was dissolved in DMF (10 mL), Cs_2CO_3 (5.4 g, 16.5 mmol) and iodomethane (4.68 g, 33 mmol, 2.05 mL) were added. The reaction mixture was stirred for 16 h at 90 °C. The reaction mixture was cooled to room temperature and quenched by the addition of NH_4Claq., sat. solution (10 mL). The mixture was extracted with EtOAc (3 x 50 mL), the combined organic phase was dried over Na_2SO_4, filtered and concentrated to give a crude product oil, which was purified via flash chromatography (SiO_2, hexanes/EtOAc 3/1) to give the 7 as colorless oil (245 mg, 0.51 mmol, 10%), which was inseparable from EtOAc (ca. 25% according to NMR). The low yield is due to partial deprotection of the carbonate group and methylation of the deliberated phenol under the reaction conditions.

1H-NMR (300 MHz, $CDCl_3$): 7.43-7.21 (m, 11H), 7.09-6.99 (m, 3H), 5.25 (s, 2H), 5.09 (s, 1.2H, rotamer 1), 5.04 (s, 0.8H, rotamer 2), 4.91 (dd, J1 = 10.6, J2 = 5.4, 0.6H, rotamer 1), 4.73 (dd, J1 = 10.4, J2 = 4.9, 0.4H, rotamer 2), 3.73 (s, 1.8H, rotamer 1), 3.65 (s, 1.2H, rotamer 2), 3.39-3.27 (m, 1H), 3.12-2.94 (m, 1H), 2.82 (s, 1.2H, rotamer 2), 2.79 (s, 1.8H, rotamer 1); 13C-NMR (75 MHz, CDCl3): 171.3 (rotamer 1), 171.1 (rotamer 2), 156.6 (rotamer 1), 155.9 (rotamer 2), 153.7 (rotamer 1), 153.6 (rotamer 2), 151.33 (rotamer 2),

151.26 (rotamer 1), 139.2 (rotamer 2), 139.1 (rotamer 1), 136.7, 136.4, 134.9, 129.7, 128.9 (rotamer 2), 128.8 (rotamer 1), 128.7 (rotamer 1), 128.6 (rotamer 2), 128.2 (rotamer 2), 128.1 (rotamer 1), 128.0, 127.7, 126.70 (rotamer 2), 126.67 (rotamer 1), 121.7 (rotamer 1), 121.6 (rotamer 2), 119.6 (rotamer 2), 119.5 (rotamer 1), 70.4, 67.6 (rotamer 2), 67.4 (rotamer 1), 60.8 (rotamer 2), 60.4 (rotamer 1), 52.5, 35.2 (rotamer 1), 34.8 (rotamer 2), 32.6 (rotamer 1), 32.2 (rotamer 2); IR (film) $\tilde{\upsilon}$ = 1730, 1588, 1510, 1454, 1262, 1214, 1162, 1135, 1023, 906, 725, 694; HRMS(APCI): m/z: calc. for $C_{37}H_{36}NO_4^+$: 558.2639 [M+H]+, found: 558.2634.

(*rac*)-methyl2-{[(benzyloxy)carbonyl](methyl)amino}-3-(3-{[(benzyloxy)carbonyl]oxy}phenyl)propanoate (6). 7 (225 mg, 0.47 mmol) was dissolved in THF (5 mL) and NaOHaq. solution (1.8 mL, 3.5M) was added. The reaction mixture was stirred for 32 h at room temperature. The pH of the mixture was adjusted to 1 with HCl (6 M) and the slurry was extracted with Et_2O (3 x 20 mL). The combined organic phase was dried over Na_2SO_4, filtered and concentrated. The obtained crude product was directly used for the next reaction step, without further purification.

(*rac*)- 3-(3-hydroxyphenyl)-2-(methylamino)propanoic acid (9). Crude product 8 (153 mg, 0.47 mmol) was dissolved in MeOH (5 mL). Pd/C (10 wt-% Pd, 20 mg) was added and the reaction mixture was vigorously stirred under a hydrogen atmosphere (1 atm.). After 6 h the hydrogen atmosphere was removed and hydrochloric acid (2 M, 2 mL) was added. The obtained slurry was filtered through a syringe filter (0.45 μm). The filter was washed with additional hydrochloric acid (2 M, 2 x 4 mL) and the combined filtrate was frozen in liquid nitrogen and lyophilized. Compound 9 was obtained as a pale yellow solid (72 mg, 0.37 mmol, 79% over 2 steps).

1H-NMR (300 MHz, D_2O + DCl): 7.26 (t, J = 7.9, 1H), 6.85 (d, J = 2.1, 1H), 6.82 (d, J = 2.0, 1H), 6.76 (t, J = 1.9, 1H), 4.17 (t, J = 4.2, 1H), 3.73 (dd, J1 = 6.1, J2 = 4.3, 1H), 2.71 (s, 3H); 13C-NMR (75 MHz, D_2O + DCl): 170.9, 155.9, 135.4, 130.5, 121.4, 116.1, 114.9,

62.3, 34.8, 31.9; IR (film) $\tilde{\upsilon}$ = 1730, 1588, 1510, 1454, 1262, 1214, 1162, 1135, 1023, 906, 725, 694; HRMS(APCI): m/z: calc. for $C_{37}H_{36}NO_4^+$: 558.2639 [M+H]+, found: 558.2634.

Scheme 1: NMR data to confirm the identity of synthesised substrates

L-Benzyl 2-(benzylamino)-3-(3,4-bis(benzyloxy)phenyl)propanoate (2).
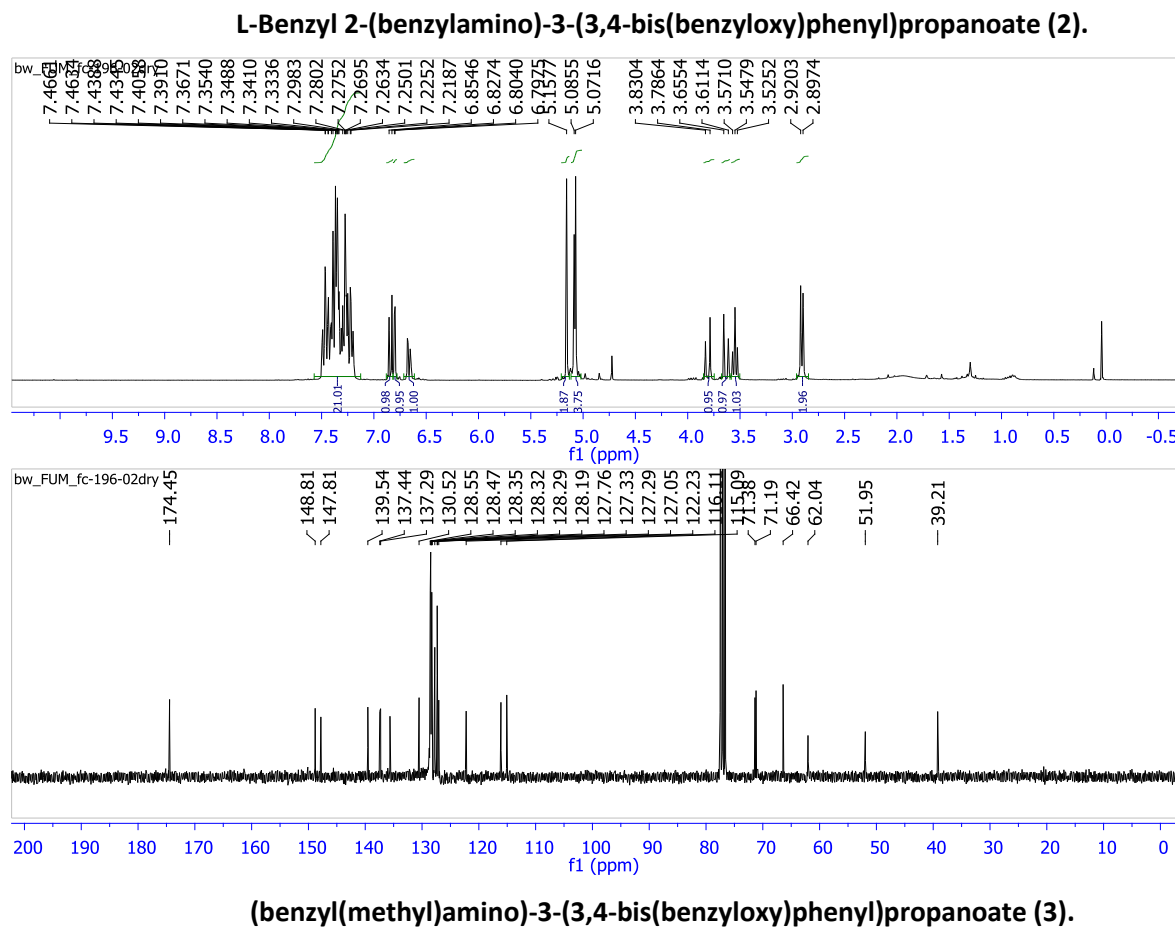
L-Benzyl 2-(benzyl(methyl)amino)-3-(3,4-bis(benzyloxy)phenyl)propanoate (3).

bw_FUM_fc-222-o1dry
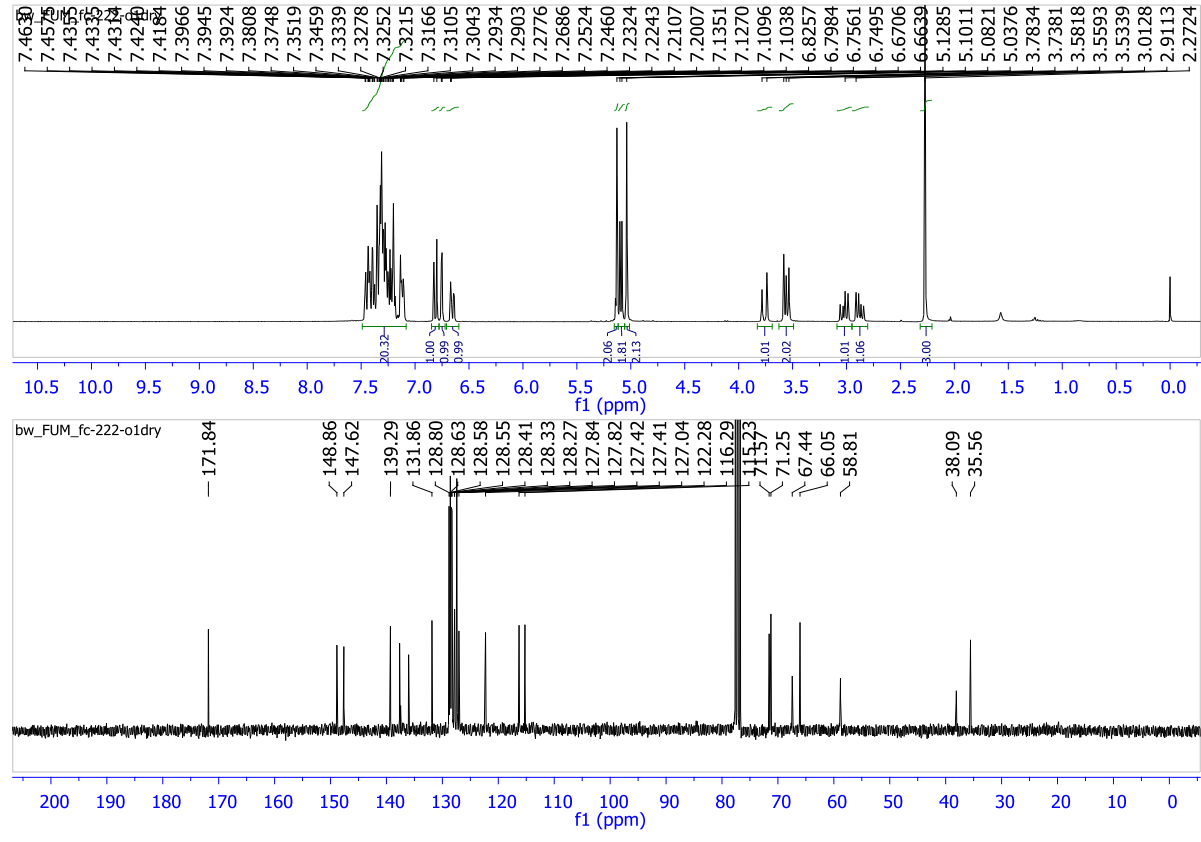
***L*-3-(3,4-dihydroxyphenyl)-2-(methylamino)propanoic acid (4).**
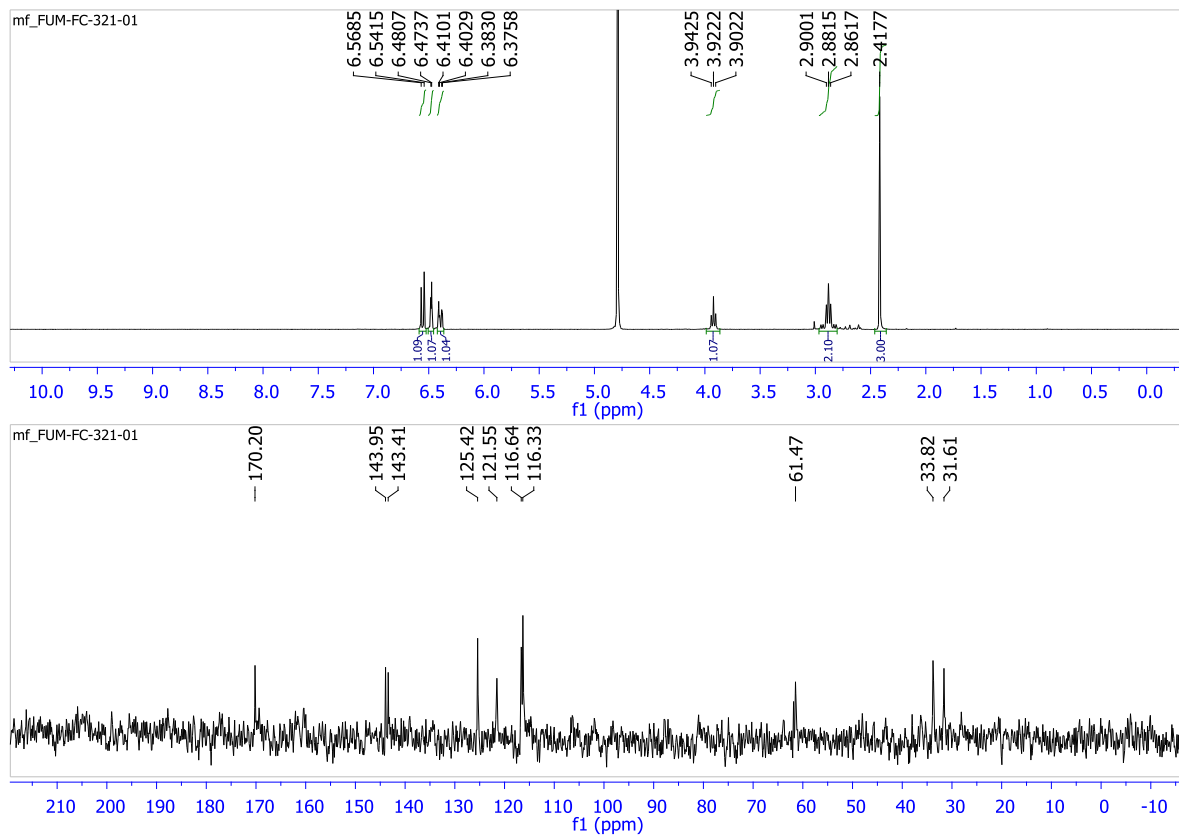
(*rac*)-methyl 2-{[(benzyloxy)carbonyl](methyl)amino}-3-(3-{[(benzyloxy)carbonyl]oxy}phenyl)propanoate (7).

(*rac*)- 3-(3-hydroxyphenyl)-2-(methylamino)propanoic acid (9).

93

mf_FUM-FC-407-01

7.2860
7.2593
7.2335
6.8498
6.8429
6.8233
6.8166
6.7695
6.7635
6.7570

4.1881
4.1674
4.1468

3.2476
3.2337
3.2279
3.2130
2.7115

1.04
1.04
0.97
0.95

1.04

2.01

3.00

f1 (ppm)

mf_FUM-FC-407-01

170.90

155.86

135.35
130.52
121.35
116.08
114.88

62.27

34.77
31.86

f1 (ppm)

94

Conversions of FsqB-catalyzed biotransformations

Entry	Substrate	Variant	Conversion [%]							
			HPLC-MS				HPLC-UV[b]			
			A	B	C	D	A	B	C	D
1	*rac-N*-methyl-dopa	WT	23	76	<1	<1	5	95	<1	<1
2		D444A	91	6	3[c]	<1	94	6	<1	<1
3	L-*N*-methyl-dopa	WT	15	85	<1	<1	11	89	<1	<1
4		D444A	85	15	<1	<1	98	2	<1	<1
5	*rac-N*-methyl-*meta*-tyrosine	WT	49	25[c]	2	24	43	28[c]	5	24
6		D444A	39	27[c]	3	31	54	23[c]	12	16

Entry	Substrate	Variant	Conversion [%]					
			HPLC-MS			HPLC-UV[b]		
			E	F	G	E	F	G
7	L-*N*-methyl-tyrosine	WT	<1	<1	>99	3	<1	97
8		D444A	73	<1	27	43	<1	57
9	D-*N*-methyl-tyrosine	WT	>99	<1	<1	>99	<1	<1
10		D444A	>99	<1	<1	>99	<1	<1

HPLC chromatograms

Compound 4.

HPLC-UV method. HPLC-UV chromatograms were measured on a Phenomenex Luna 5 μ C18 100A column. Water/acetonitrile (+0.1 vol-% of trifluoroacetic acid) was used as eluent starting with 100% water for 2 min, going to 100% acetonitrile within 16 min and hold it at 100% acetonitrile for 2 min.

PDA Ch2 230nm

Peak#	Ret. Time	Name	Area	Height	Area%
1	10,304		7636546	1042815	100,000
Total			7636546	1042815	100,000

Fig SI01. HPLC-UV chromatogram of compound **4**

PDA Ch2 230nm

Peak#	Ret. Time	Name	Area	Height	Area%
1	9,982		12356904	1226556	94,975
2	10,356		653784	128730	5,025
Total			13010688	1355286	100,000

Fig SI02. HPLC-UV chromatogram of the biotransformation of substrate **4** with fsqB-WT (reaction time 1h)

PDA Ch2 230nm

Peak#	Ret. Time	Name	Area	Height	Area%
1	10,110		922659	165604	5,901
2	10,270		14713013	1498017	94,099
Total			15635673	1663621	100,000

Fig. SI03. HPLC-UV chromatogram of the biotransformation of substrate **4** with fsqB-Var9 (reaction time 1h)

HPLC-MS Method. Samples were measured on a Kinetex 2.6 μ C-18 100A column (50 x 4.6 mm, 2.6 micron). Water/acetonitrile (+0.1 vol-% of formic acid) was used as eluent starting with 100% water and going to 100% of acetonitrile within 10 min at a flow rate of 0.2 mL/min (40°C oven temperature). MS spectra were recorded in positive mode (API-ES, 3000 V capillary voltage).

MSD2 TIC, MS File (D:\CHEM32\1\DATA\MAJD\2017-11-17_DIHYDROXYSUB_02 2017-11-17 10-57-17\10MM_DI_OH_SUB.D)   ES-API, P

Signal 2: MSD2 TIC, MS File

```
Peak  RetTime  Type   Width     Area       Area     Name
  #    [min]          [min]                  %
----|--------|------|-------|----------|--------|---------------------
   1   4.475  VV     0.3786  2.55956e7  100.0000  ?
```

99

Fig SI04. HPLC-MS chromatogram and *m/z* trace of compound **4**
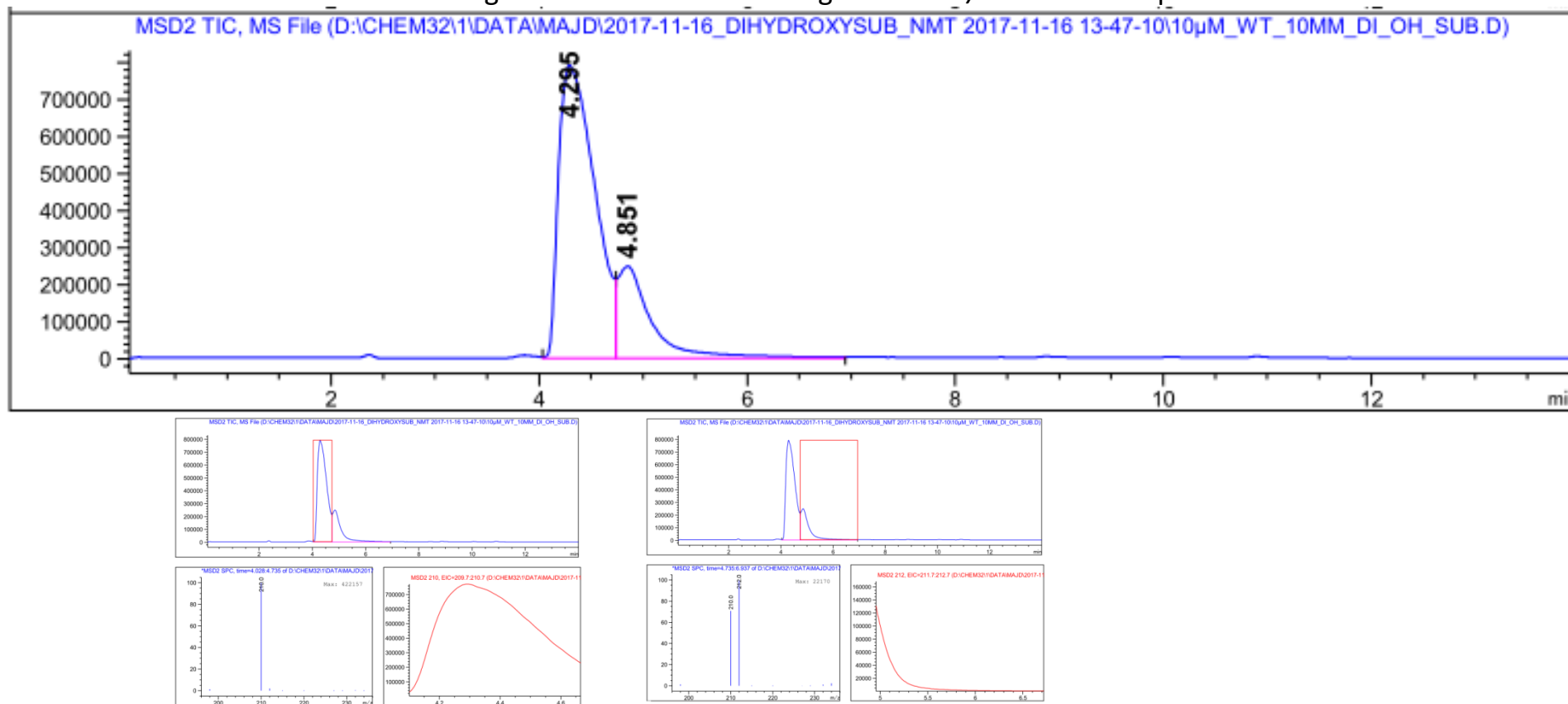
```
Signal 2: MSD2 TIC, MS File

Peak RetTime  Type   Width      Area       Area      Name
 #    [min]          [min]                   %
----|-------|------|-------|----------|--------|--------------------
  1   4.295  VV     0.3700 1.89985e7   76.8191 ?
  2   4.851  VV     0.3171 5.73296e6   23.1809 ?
```

Fig SI05. HPLC-MS chromatogram and *m/z* traces of the biotransformation of substrate **4** with fsqB-WT (reaction time 1h)
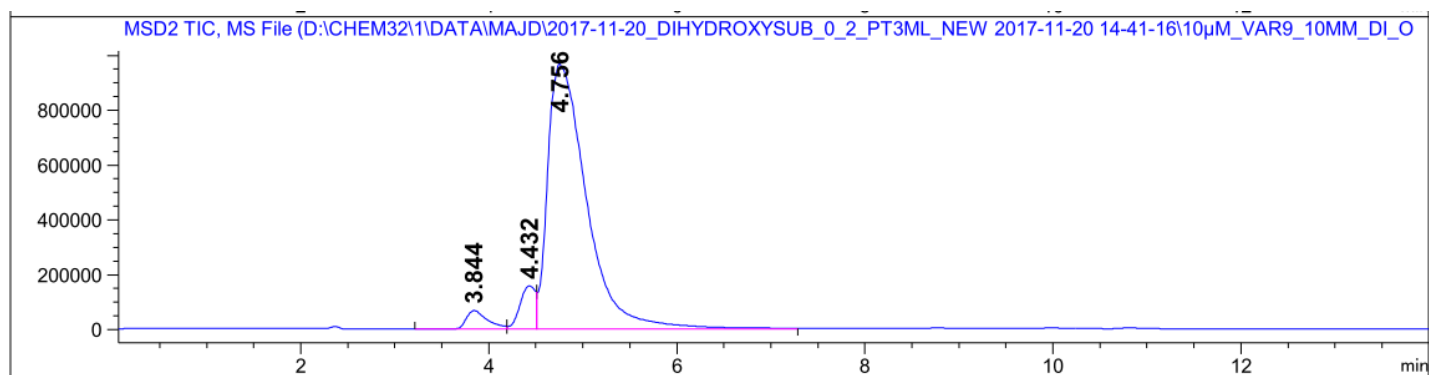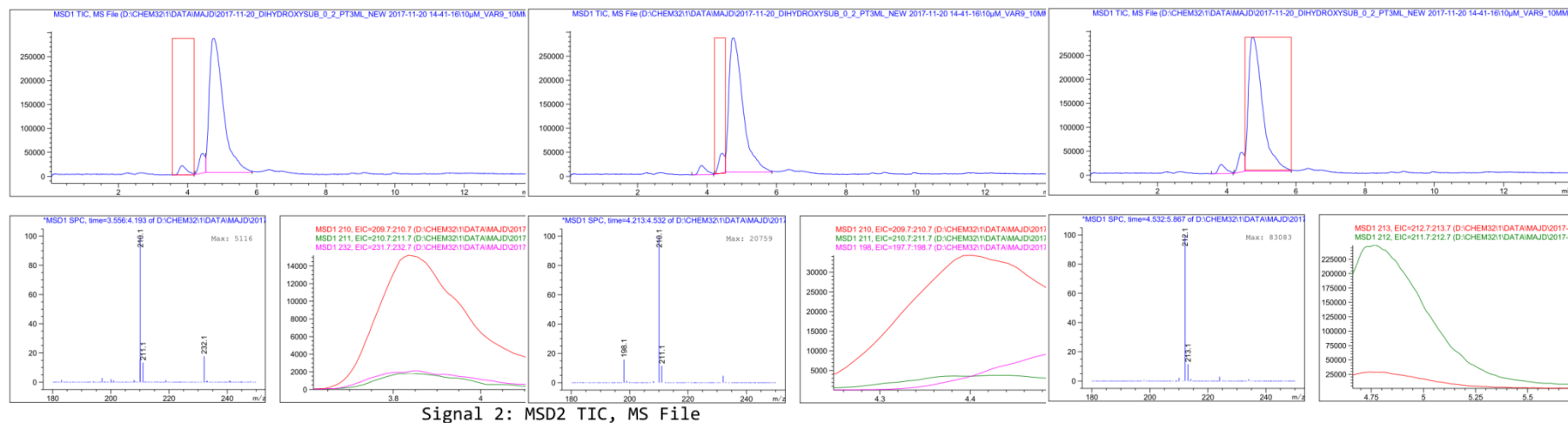
Signal 2: MSD2 TIC, MS File

Peak #	RetTime [min]	Type	Width [min]	Area	Area %	Name
1	3.844	BV	0.2336	1.05754e6	3.4379	?
2	4.432	VV	0.1749	1.76017e6	5.7221	?
3	4.756	VV	0.4237	2.79432e7	90.8400	?

Fig. SI06. HPLC-MS chromatogram and *m/z* traces of the biotransformation of substrate **4** with fsqB-var9 (reaction time 1h)

Compound 7.

HPLC-UV method. HPLC-UV chromatograms were measured on a Phenomenex Luna 5 μ C18 100A column. Water/acetonitrile (+0.1 vol-% of trifluoroacetic acid) was used as eluent starting with 100% water for 2 min, going to 100% acetonitrile within 16 min and hold it at 100% acetonitrile for 2 min.
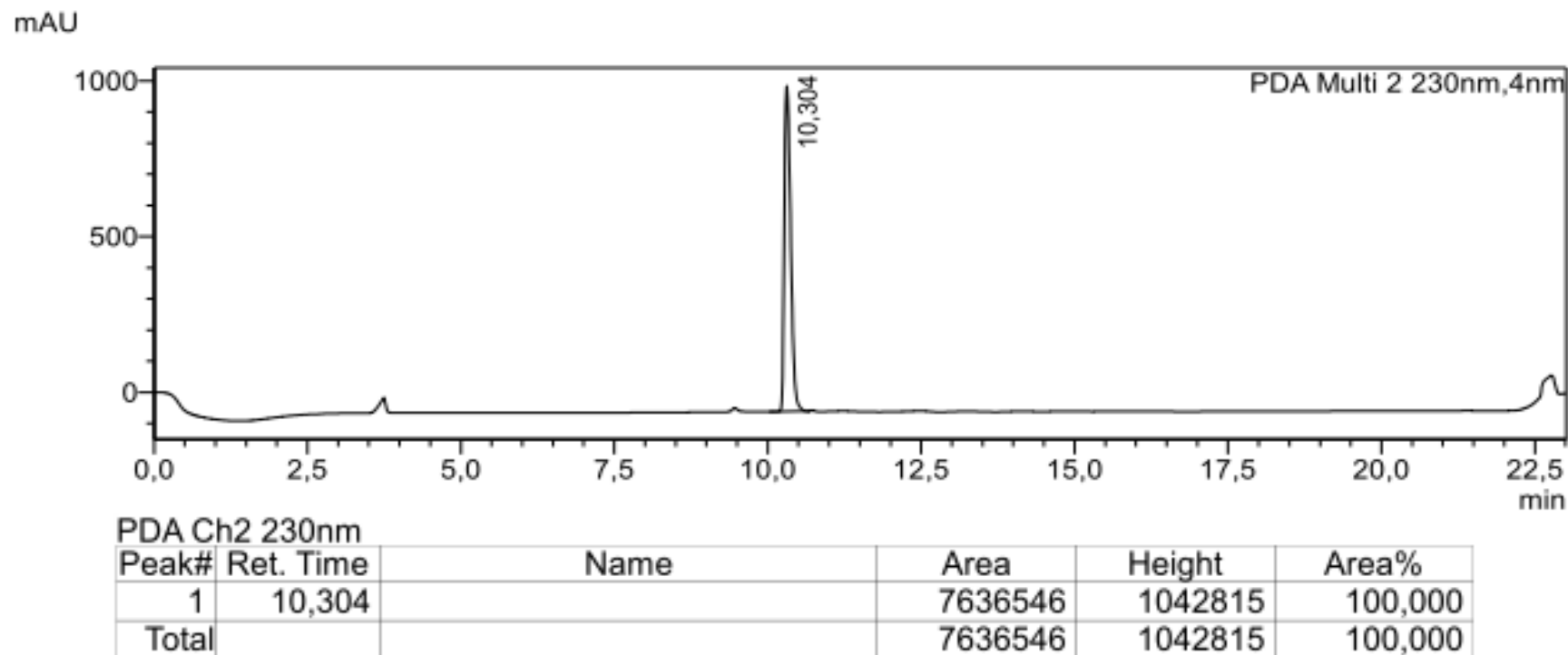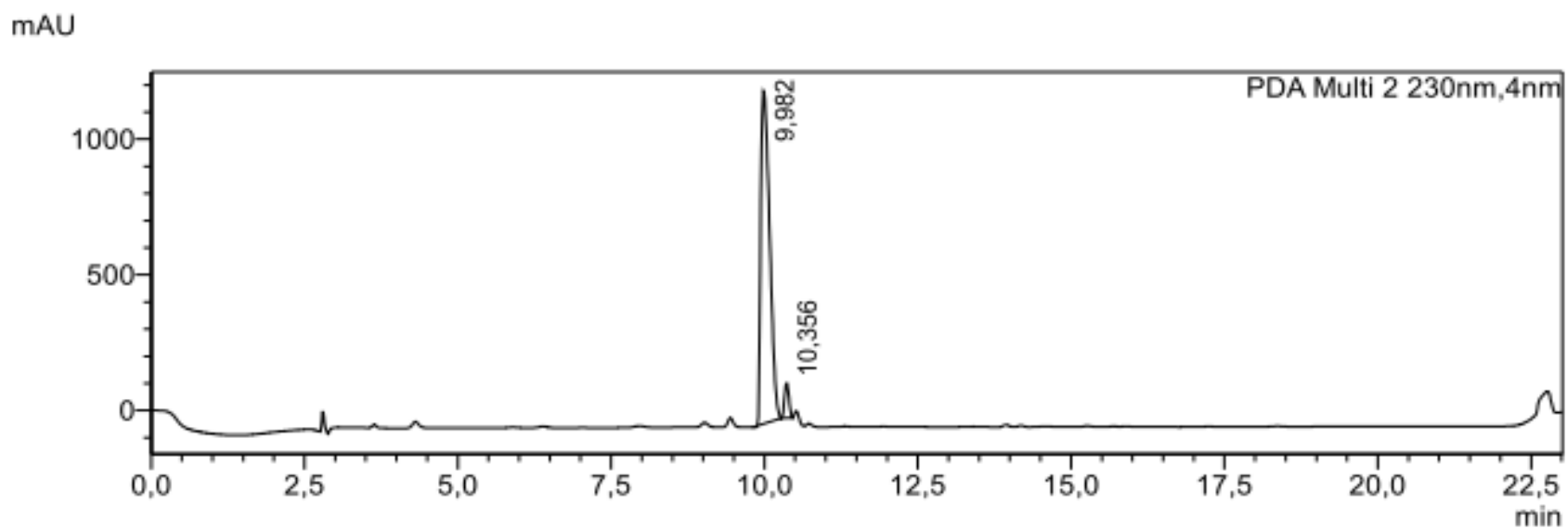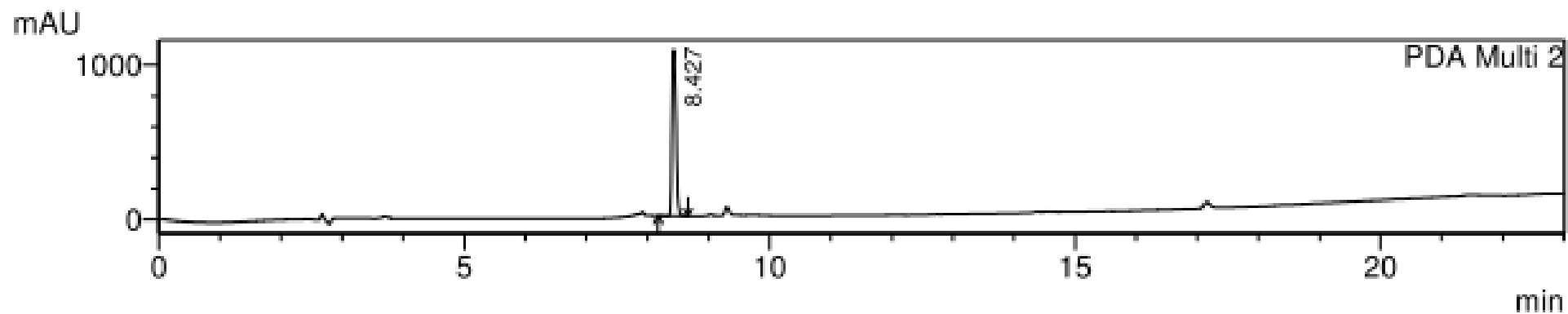
PeakTable

PDA Ch2 230nm 4nm

Peak#	Ret. Time	Area	Height	Area %	Height %
1	8.427	5079422	1072057	100.000	100.000
Total		5079422	1072057	100.000	100.000

Fig. SI07. HPLC-UV chromatogram of compound **7**

PeakTable

PDA Ch2 230nm 4nm

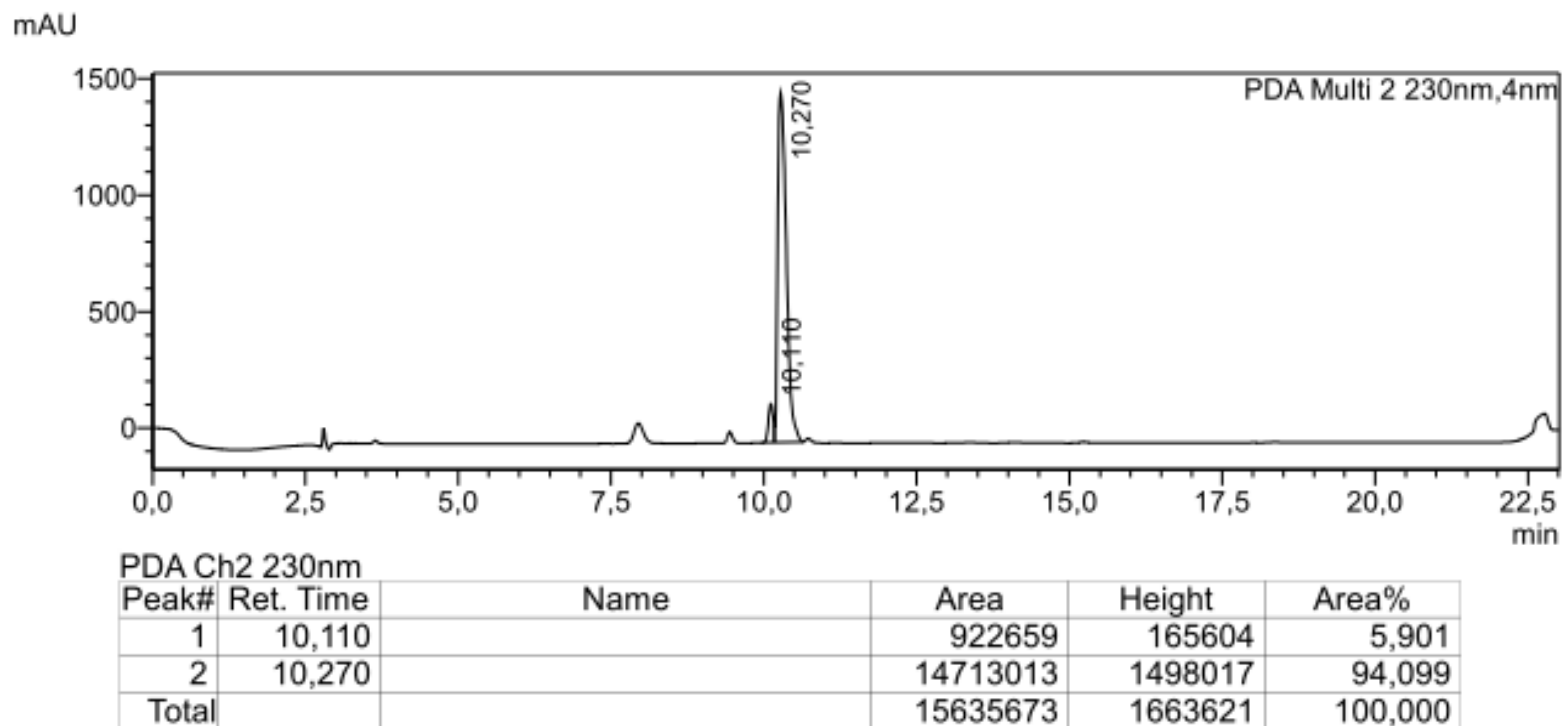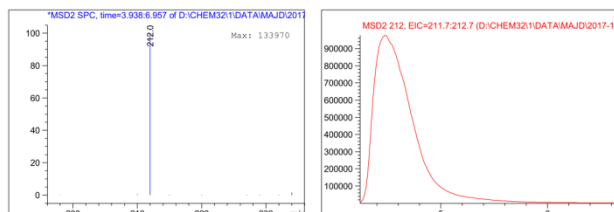| Peak#	Ret. Time	Area	Height	Area %	Height %
1	8.430	172011	45588	5.265	6.372
2	8.614	913297	218778	27.957	30.578
3	9.015	1408754	320041	43.123	44.732
4	9.325	772748	131063	23.655	18.318
Total		3266810	715469	100.000	100.000

Fig. SI08. HPLC-UV chromatogram of the biotransformation of substrate **7** with fsqB-WT (reaction time 2h)
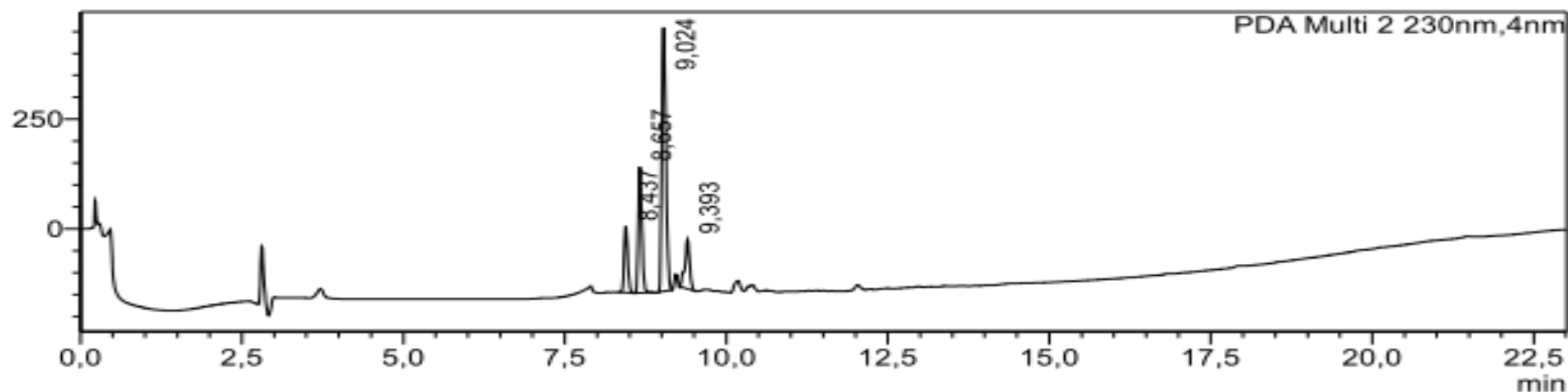
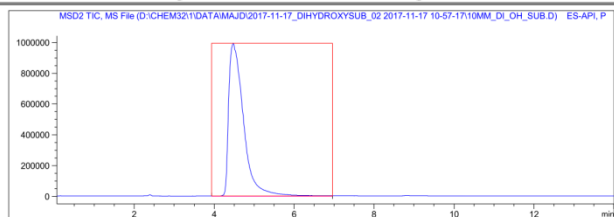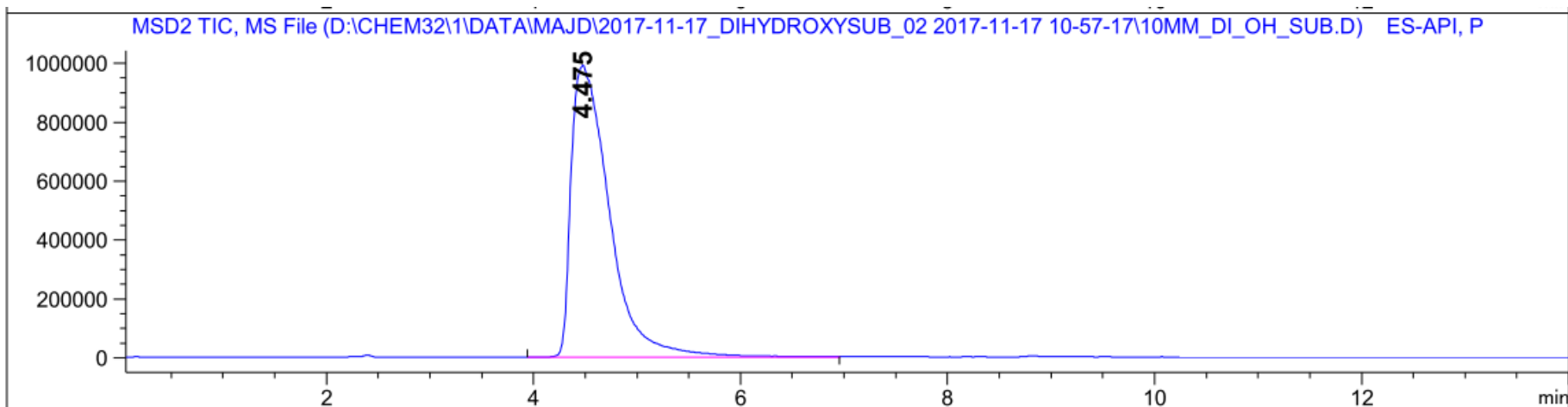| Peak#	Ret. Time	Name	Area	Height	Area%
1	8,437		583675	149507	11,732
2	8,657		1126331	286488	22,639
3	9,024		2689548	600168	54,060
4	9,393		575604	111430	11,570
Total			4975158	1147593	100,000

Fig. SI09. HPLC-UV chromatogram of the biotransformation of substrate **7** with fsqB-Var9 (reaction time 2h)

HPLC-MS Method. Samples were measured on an Agilent Zorbax 300-SCX column (250 x 4.6 mm, 5 micron). Water/acetonitrile (+0.1 vol-% of formic acid) was used as eluent starting with 100% water for 2 min, and going to 100% of acetonitrile within 15 min at a flow rate of 2.0 mL/min (40°C oven temperature) and stay at 100% acetonitrile for 2.5 min. MS spectra were recorded in positive mode (API-ES, 3000 V capillary voltage).

MSD2 TIC, MS File (D:\CHEM32\1\DATA\2017-11-29_MONO-HYDROXY_ZORBAX_LONG_2ML 2017-11-29 17-46-15\MONO-OH_WT.D)   ES-AP

Signal 2: MSD2 TIC, MS File

Peak #	RetTime [min]	Type	Width [min]	Area	Area %	Name
1	2.541	MM	0.7825	2.48580e6	49.0510	?
2	4.586	MM	0.5202	1.20961e6	23.8687	?
3	5.992	MM	0.4454	9.28586e4	1.8323	?
4	9.024	MM	0.5690	1.27951e6	25.2479	?

Fig. SI10. HPLC-MS chromatogram and *m/z* traces of the biotransformation of substrate **7** with fsqB-WT (reaction time 2h)
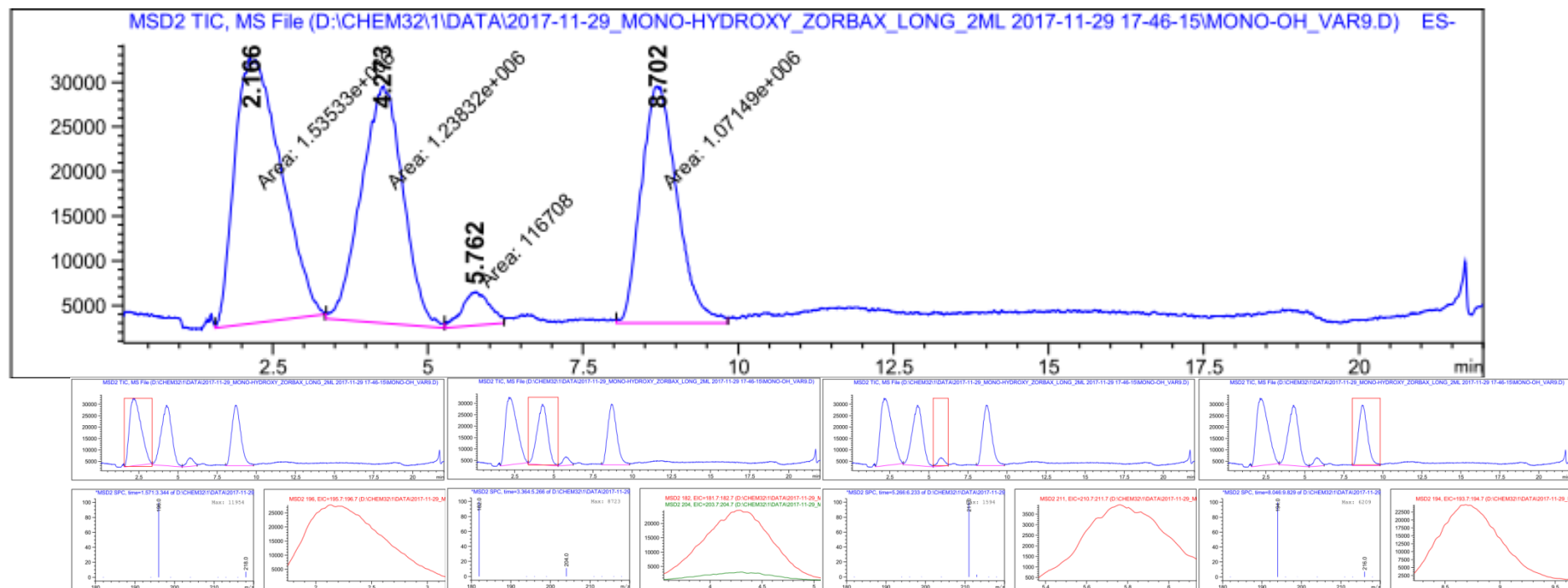
```
Signal 2: MSD2 TIC, MS File

Peak RetTime  Type    Width       Area       Area      Name
 #   [min]           [min]                     %
----|-------|------|-------|----------|--------|--------------------
 1    2.166 MM      0.8535 1.53533e6   38.7528 ?
 2    4.273 MM      0.7846 1.23832e6   31.2562 ?
 3    5.762 MM      0.5201 1.16708e5    2.9458 ?
 4    8.702 MM      0.6668 1.07149e6   27.0452 ?
```

Fig. SI11. HPLC-MS chromatogram and *m/z* traces of the biotransformation of substrate **7** with fsqB-Var9 (reaction time 2h)

*Compound **10**.*

HPLC-UV method. HPLC-UV chromatograms were measured on a Phenomenex Luna 5 μ C18 100A column. Water/acetonitrile (+0.1 vol-% of trifluoroacetic acid) was used as eluent starting with 100% water for 2 min, going to 20% acetonitrile within 16 min and increasing to 100% of acetonitrile within 2 min.
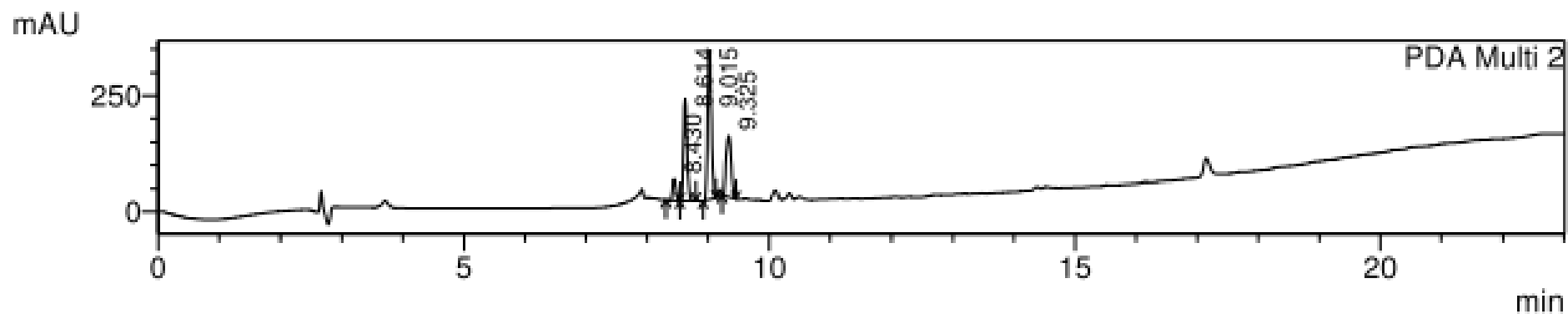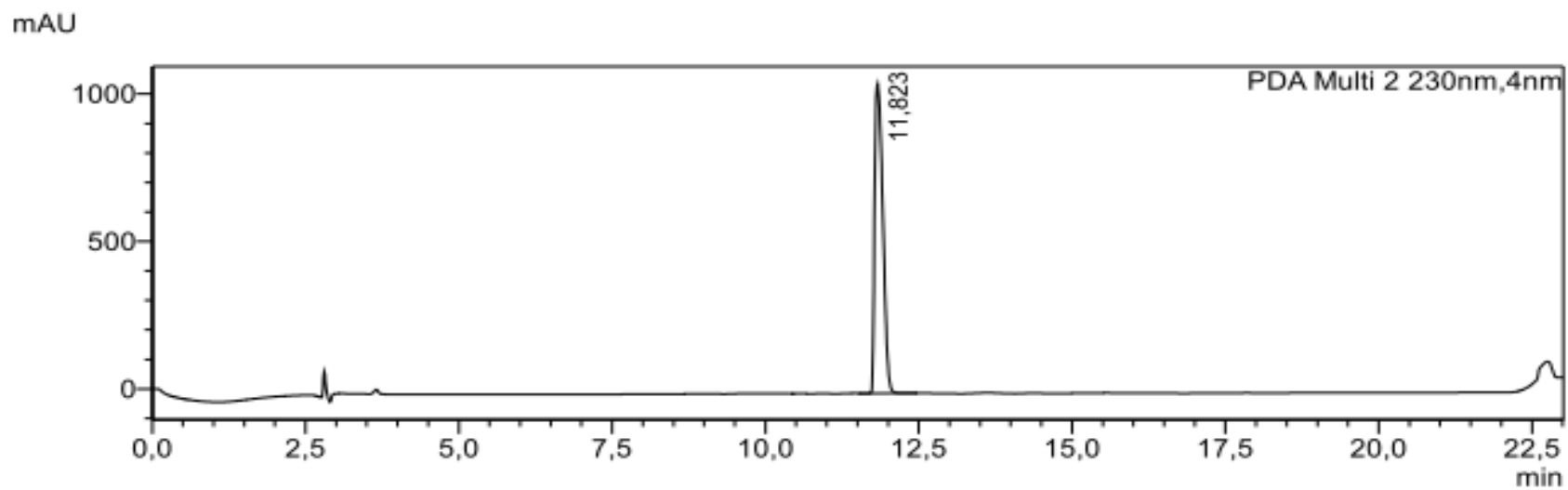
PDA Ch2 230nm

Peak#	Ret. Time	Name	Area	Height	Area%
1	11,823		9755352	1047571	100,000
Total			9755352	1047571	100,000

Fig. SI12. HPLC-UV chromatogram of compound **10**
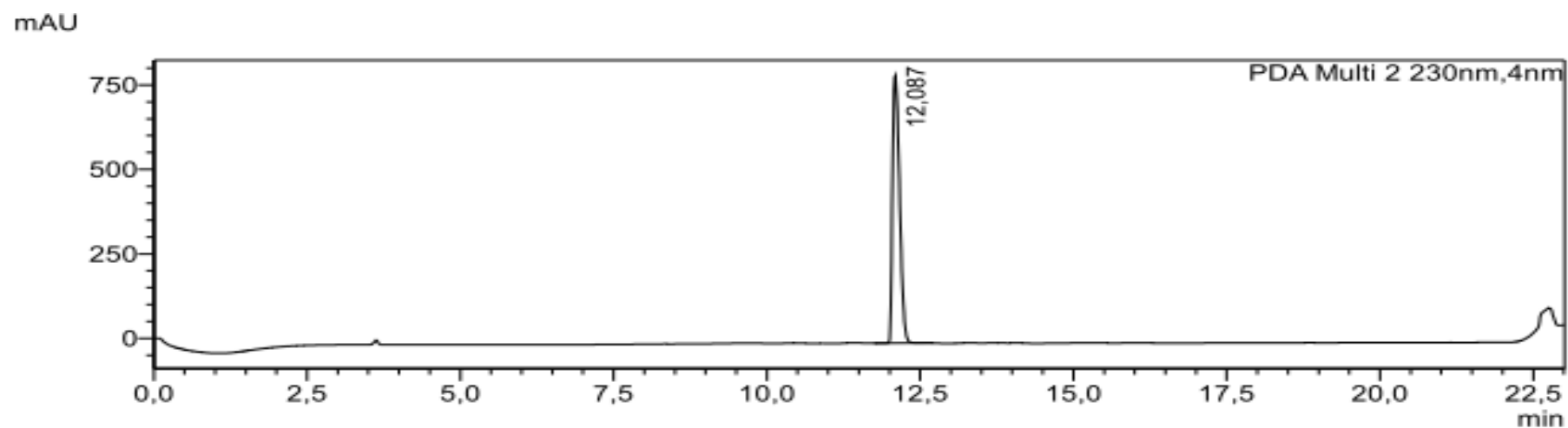
PDA Ch2 230nm

Peak#	Ret. Time	Name	Area	Height	Area%
1	12,087		6442894	791322	100,000
Total			6442894	791322	100,000

Fig. SI13. HPLC-UV chromatogram of tyrosine (**11**)
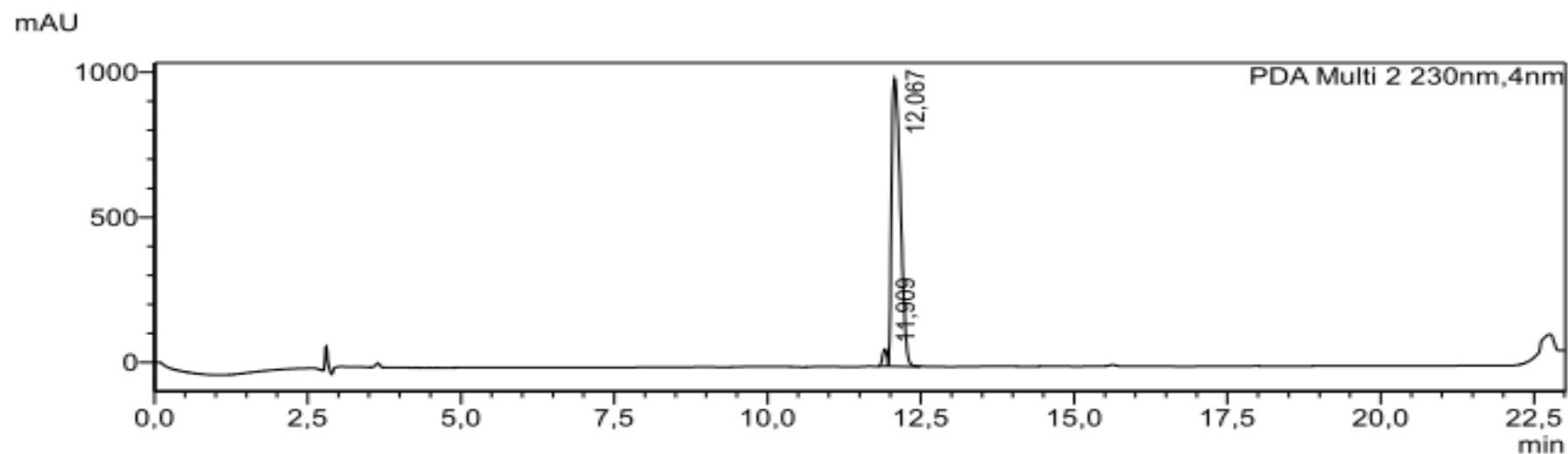
PDA Ch2 230nm

Peak#	Ret. Time	Name	Area	Height	Area%
1	11,909		306367	58519	2,982
2	12,067		9966675	988820	97,018
Total			10273042	1047338	100,000

Fig. SI14. HPLC-UV chromatogram of the biotransformation of substrate **10** with fsqB-WT (reaction time 2h)
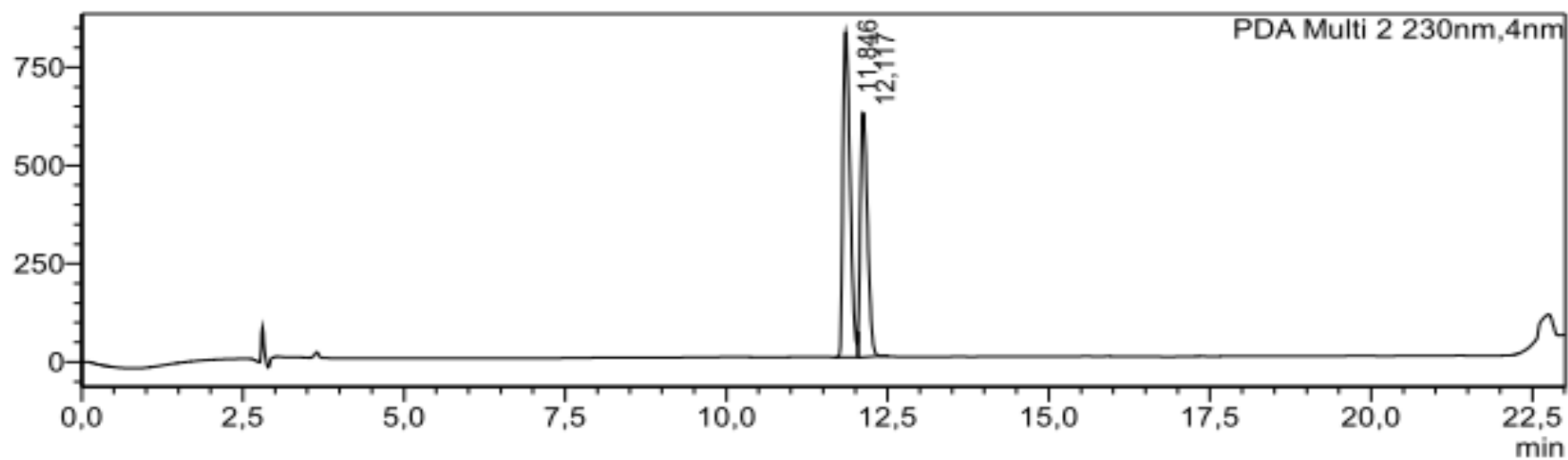
PDA Ch2 230nm

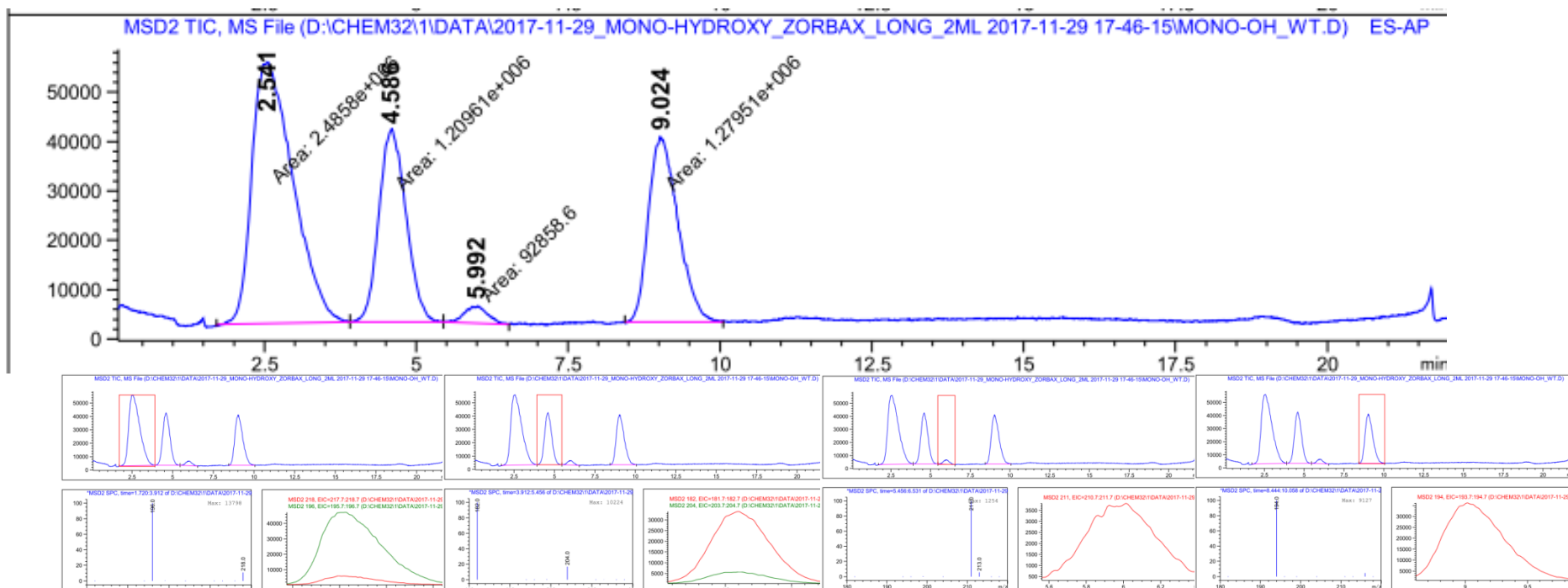| Peak#	Ret. Time	Name	Area	Height	Area%
1	11,846		6421675	825572	57,376
2	12,117		4770603	621491	42,624
Total			11192278	1447063	100,000

Fig. SI15. HPLC-UV chromatogram of the biotransformation of substrate **10** with fsqB-Var9 (reaction time 2h)

**HPLC-MS Method.** Samples were measured on a Kinetex 2.6 μ C-18 100A column (50 x 4.6 mm, 2.6 micron). Water/acetonitrile (+0.1 vol-% of formic acid) was used as eluent starting with 100% water and going to 100% of acetonitrile within 10 min at a flow rate of 1.5 mL/min (40°C oven temperature). MS spectra were recorded in positive mode (API-ES, 3000 V capillary voltage).
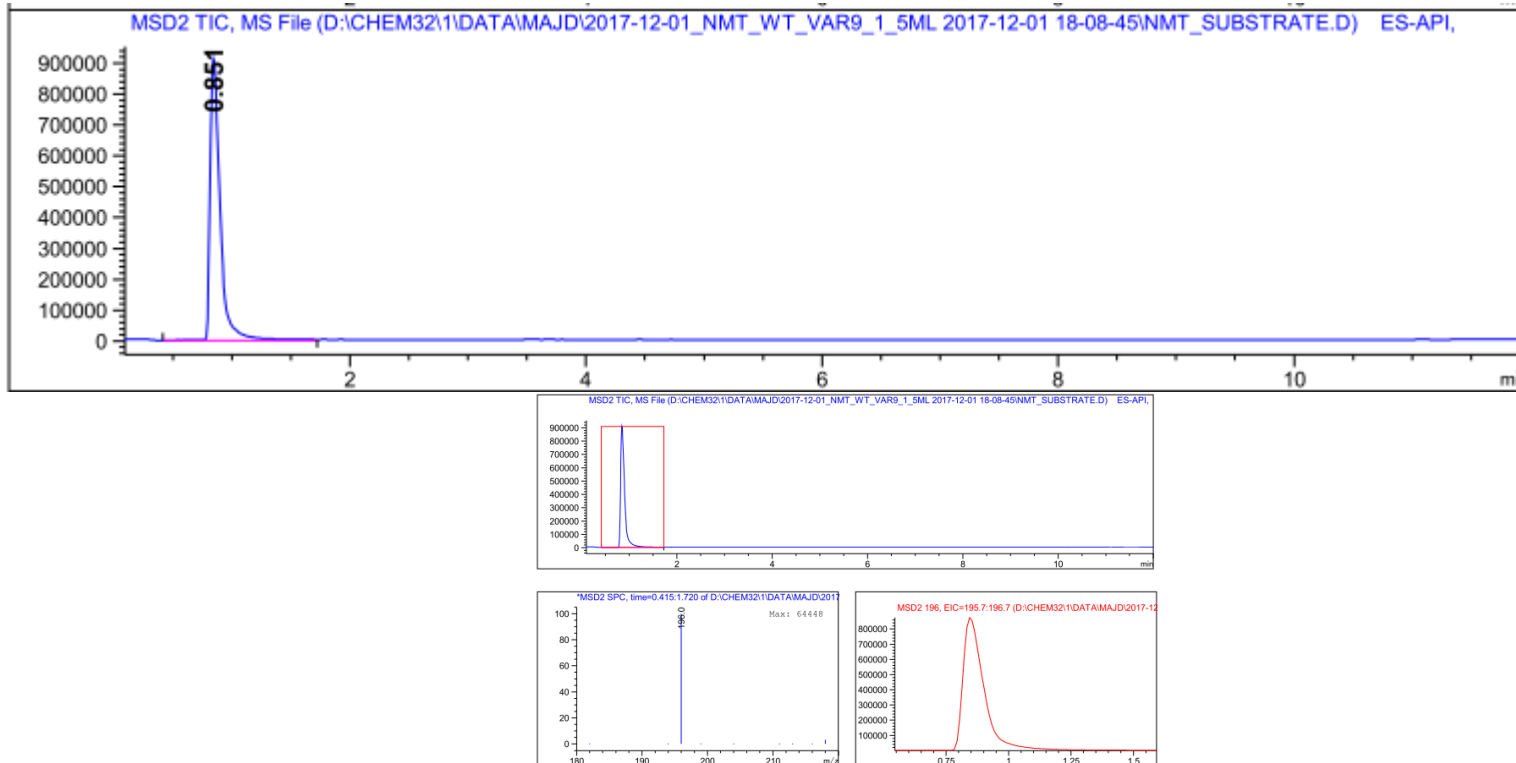
```
Peak RetTime  Type    Width      Area       Area      Name
  #   [min]          [min]                   %
----|-------|------|-------|----------|--------|---------------------
  1   0.851  VV     0.0915 5.36367e6  100.0000 ?
```

Fig. SI16. HPLC-MS chromatogram and *m/z* traces of substrate **10** (reaction time 2h)
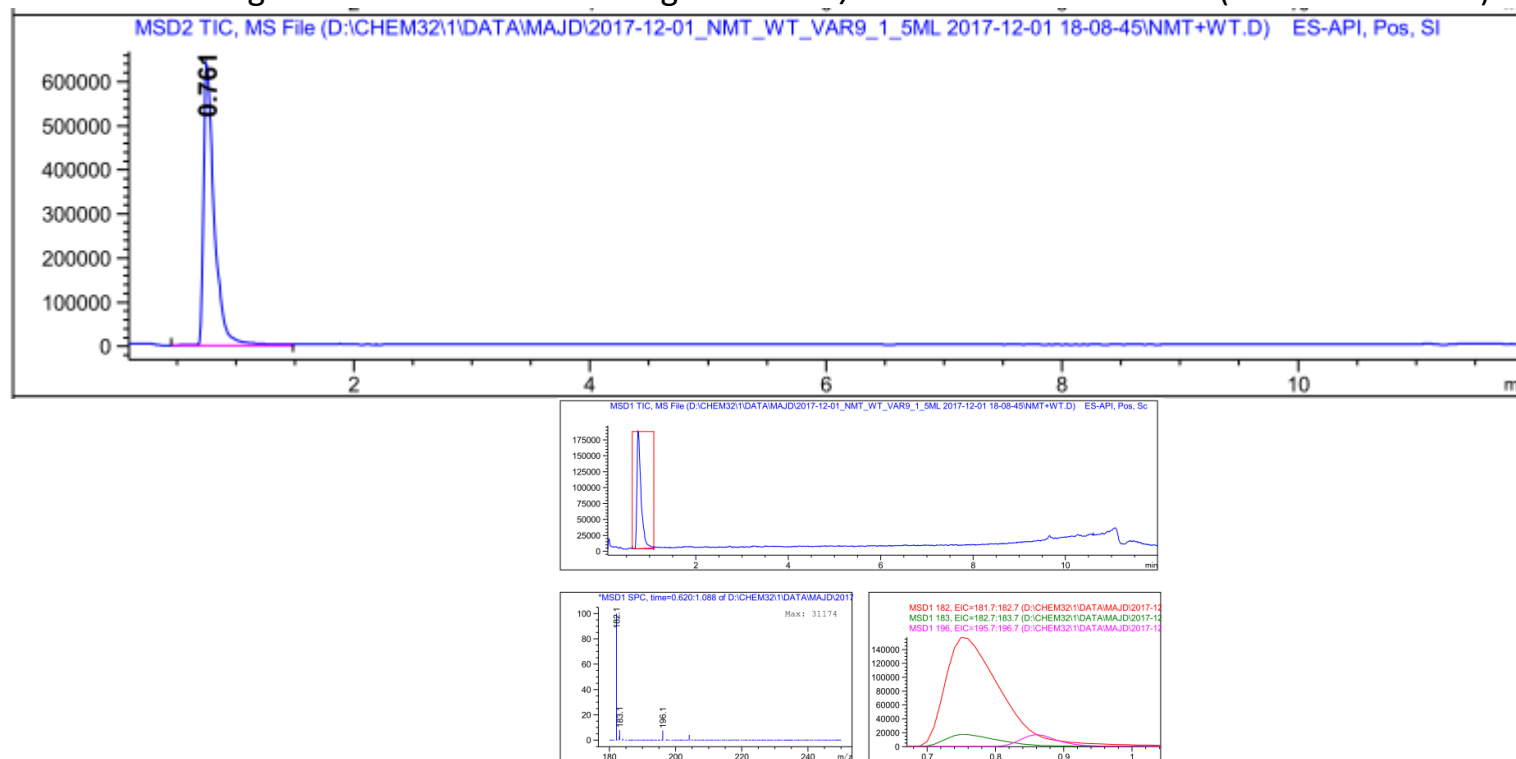
```
Signal 2: MSD2 TIC, MS File

Peak RetTime  Type    Width      Area       Area      Name
 #    [min]           [min]                   %
----|-------|-------|-------|-----------|--------|--------------------
  1   0.761 BV       0.0999 4.02498e6  100.0000 ?

Totals :                       4.02498e6
```

Fig. SI17. HPLC-MS chromatogram and *m/z* traces of the biotransformation of substrate **10** with fsqB-WT (reaction time 2h)
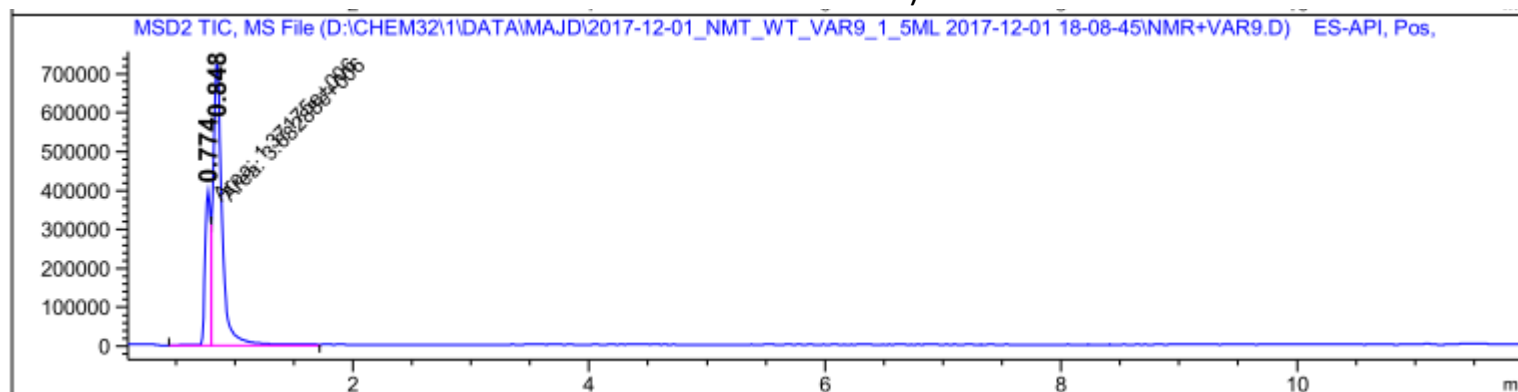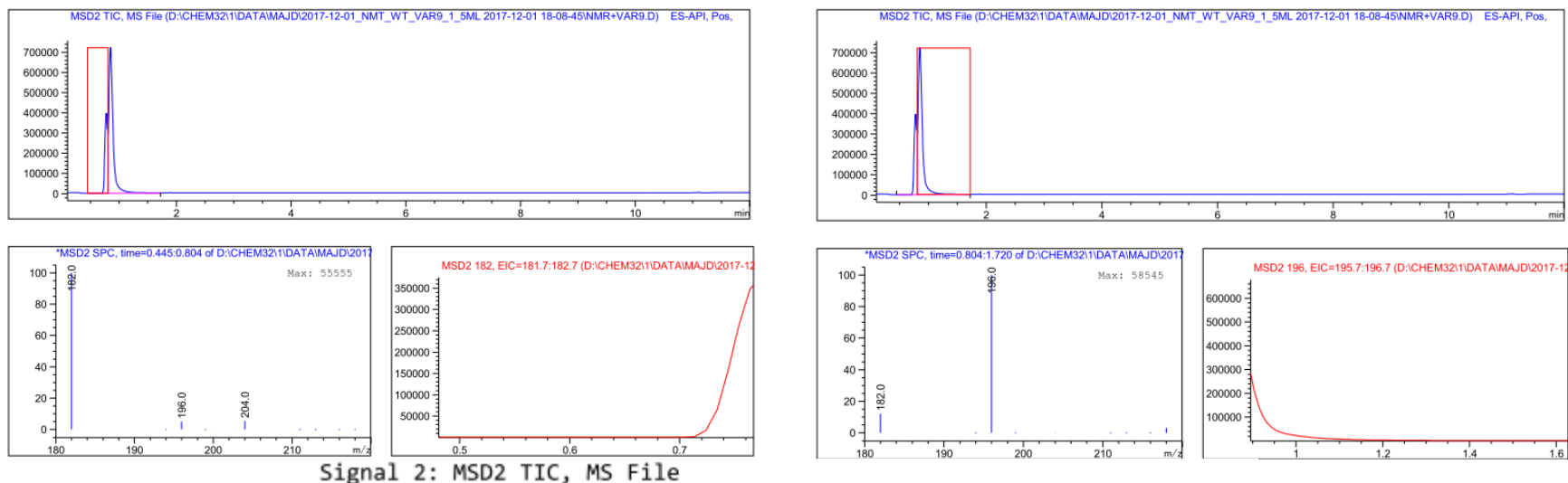
Fig. SI18. HPLC-MS chromatogram and *m/z* traces of the biotransformation of substrate **10** with fsqB-Var9 (reaction time 2h)

**^{1}H-NMR of biotransformation.** Substrate **4** (15 mg, 0.071 mmol) were dissolved in buffer (100 mM P_i buffer in D_2O, pH = 7.6) and purified fsqB enzyme was added (50 µL, enzyme conc. ???). The reaction was shaken for 16 h in horizontal position at 30°C before it was transferred to a NMR tube and analysed.
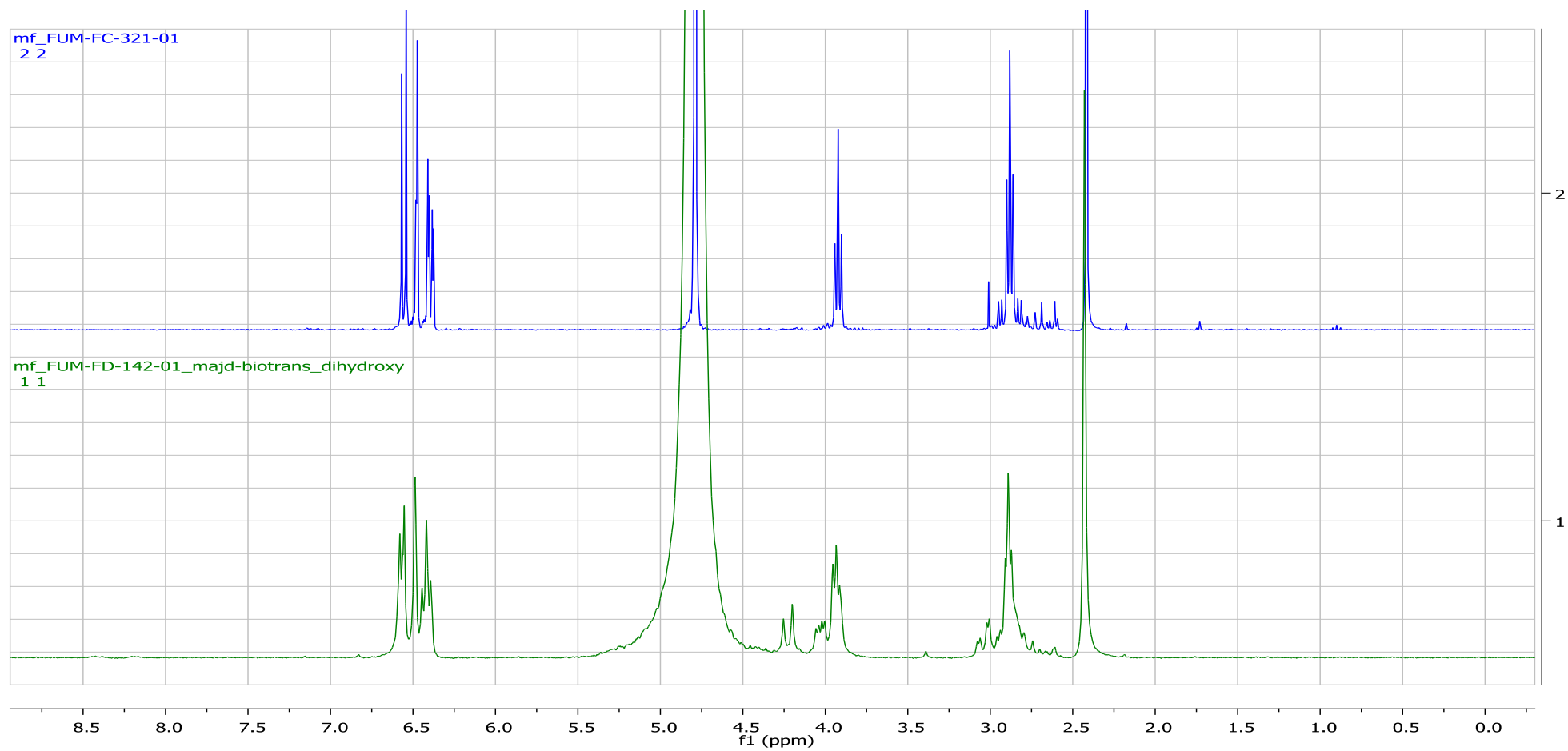
Fig SI19. ^{1}H-NMR spectra of substrate (top) and biotransformation (bottom).
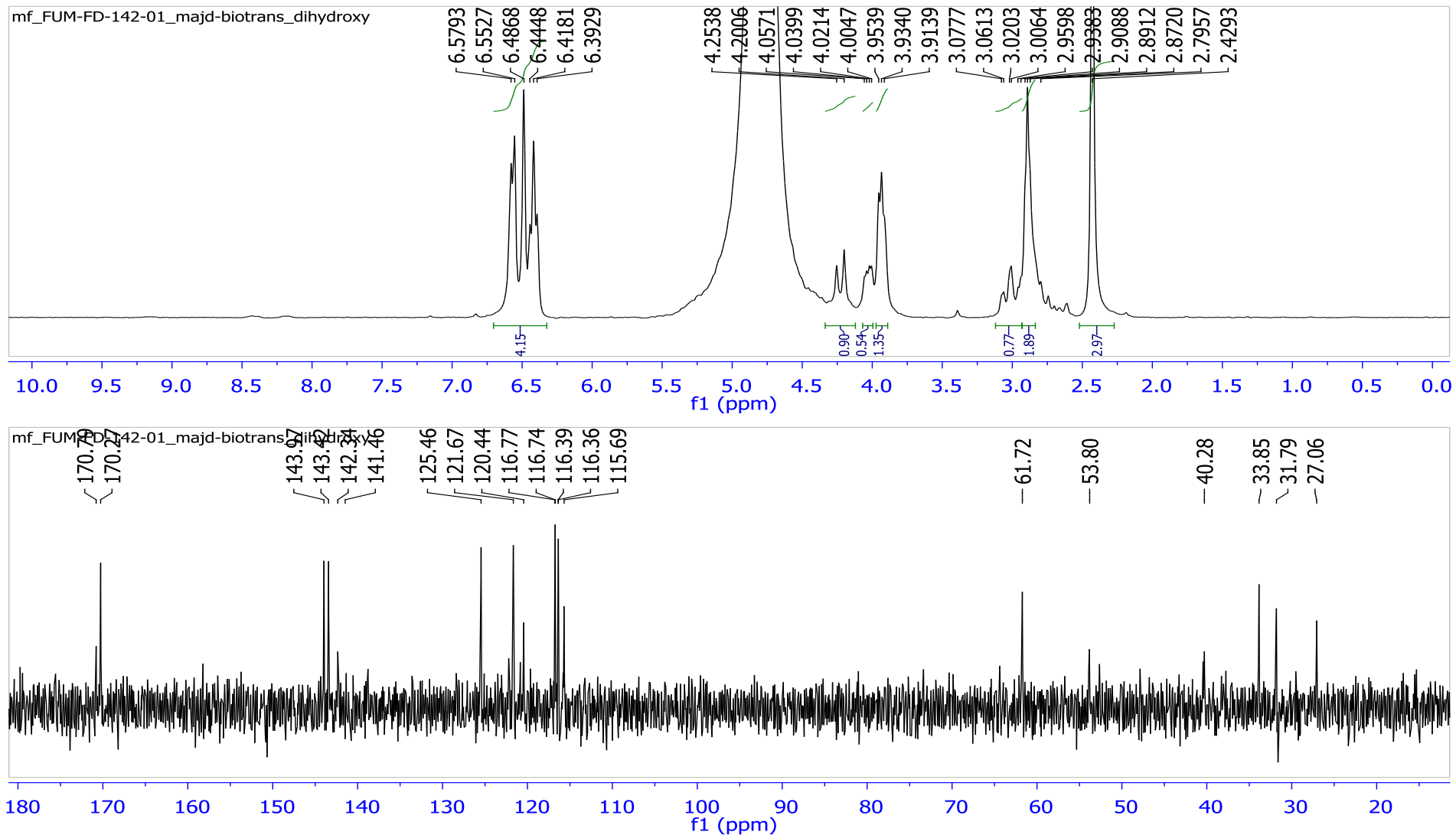
Fig SI20. ^{1}H- and ^{13}C-NMR of biotransformation of compound **4**.

Section II

The characterization of the wild type of
Electron transferring flavoprotein from
Saccharomyces cerevisiae

Chapter 1: Introduction

Electron transfer flavoprotein

Electron transfer flavoproteins (ETFs) are a group of enzymes, which employ flavin as a cofactor and which are located on the matrix face of the inner mitochondrial membrane. The main role of these enzymes is to accept electrons from primarily nine mitochondrial matrix dehydrogenases and to transfer the electrons to the terminal respiratory system in eukaryotic (1, 2). Reduced ETF is then reoxidized by the ETF ubiquinone oxide ETF/ETF:QO that functions as a short electron transfer pathway (3) (Figure 1).
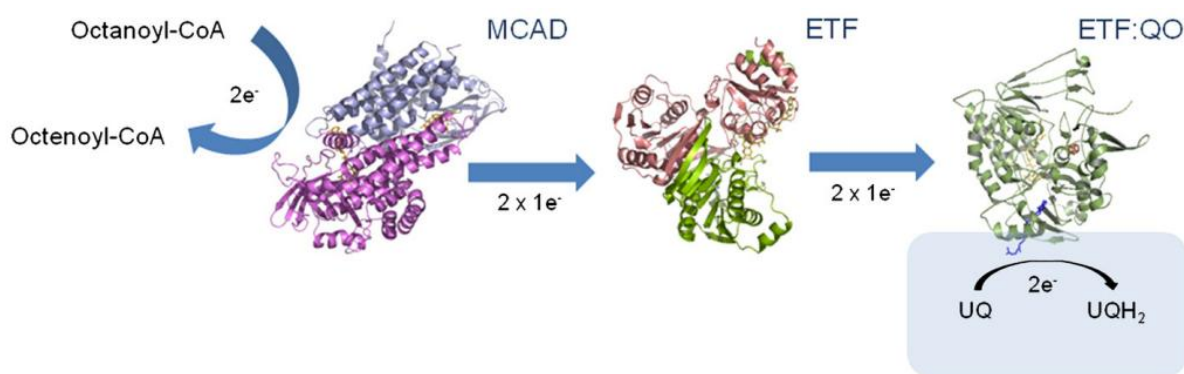
Figure 1. Electron-transfer from Octanoyl-CoA to Ubiquinone is mediated by ETF and ETF-QO. The two electron reduced flavin cofactor (FADH2) of MCAD is reoxidized by two equivalents of the electron-transfer flavoprotein, which is a one electron carrier. The ETF flavin semiquinone is in turn reoxidized by ETF-QO, which catalyses the transfer of the electrons to the mitochondrial ubiquinone pool. The ETF/ETF-QO system serves as the electron acceptor for nine mitochondrial flavoprotein dehydrogenases: short-chain acyl-CoA dehydrogenase (EC 1.3.99.2); medium-chain acyl-CoA dehydrogenase (EC 1.3.99.3); long-chain acyl-CoA dehydrogenase (EC 1.3.99.13); very long-chain acyl-CoA dehydrogenase; ACAD-9; isovaleryl-CoA dehydrogenase (EC 1.3.99.10); 2-methyl-butyryl-CoA dehydrogenase; isobutyryl-CoA dehydrogenase and glutaryl-CoA dehydrogenase (EC 1.3.99.7). The same pathway is also responsible for accepting electrons from sarcosine dehydrogenase (EC 1.5.99.1) and dimethylglycine dehydrogenase (EC 1.5.99.2). The figure is drawn with Pymol (v0.99 using the following pdb files 3MDD (MCAD), 1EFV (ETF) and 2GMH (ETF-QO). Figure and legend are quoted from the review of Watmough and Frerman (3).

The human ETF was characterized by Roberts *et al.* (Figure 2). This structure has provided insight into the amino acid side chains that may be involved in stabilization of the anionic ETF semiquinone and hydroquinone and suggested a possible structure for a binary complex of ETF and medium chain acyl-CoA dehydrogenase (4). ETFs are heterodimeric enzymes consisting of two subunits: alpha and beta. The protein consists of

three domains, two contributed by the α subunit (aI and aII), and a third contributed entirely by the β subunit, which contains the noncovalently bound AMP. ETFs employ a flavin adenine dinucleotide (FAD) as cofactor (4–6). In human, defects in either ETF or ETF:QO lead to glutaric acidemia type II (2).

Figure 2. A cartoon representation of the human ETF structure (PDB code: 1EFV). FAD (yellow) binds in a cleft formed by the α (orange) and β (cyan) subunits. The AMP (salmon) is located entirely within the b subunit.

Electron transfer flavoprotein in Yeast

The budding yeast *Saccharomyces cerevisiae* is considered a simple eukaryotic organism, which has been proven to be a good model for the investigation of many aspects of cell biology, including the study of mitochondria at genetic, molecular, and physiological level (7). This facultative aerobe organism is an important tool for energetic studies, because this yeast is still able to grow under fermentative conditions after generating deficient mutations, thus allowing the isolation and study of deficient mitochondria. When grown on a non-fermentable carbon source, such as lactate, yeast mitochondria exhibit a general organization and function very similar to mammalian mitochondria (8).

Botstein et al. (1997) proved that 31% of yeast open reading frames (ORF) have a homologue in mammalian genomes (9). It is estimated that 30% of human genes involved in human diseases have a yeast homologues (10). Moreover, *S. cerevisiae* played a central role in the discovery of the first flavoenzyme (11) .The yeast orthologues of ETFα, ETFβ and ETF-dH were reported to be mitochondrial proteins and are encoded by, respectively, *AIM45*, *YGR207c/CIR1* and *YOR356w/CIR2* (Scheme 1) (11, 12, 8). The study of Grandier-Vazeille *et al.* (2001) suggests that yeast ETF and ETF-dH could play additional roles in mitochondrial metabolism. By the analysis of yeast cell extracts by two-dimensional electrophoresis and identification by mass spectrometry, it was hypothesized that Ypr004c/Aim45 and Yor356w/Cir2 are associated in a mitochondrial dehydrogenases supramolecular complex (8). The close interaction of ETF and ETF-dH with mitochondrial dehydrogenases and their role in electron transfer from metabolic reactions to the electron transfer chain (ETC) suggests that they play a role in the oxidative stress response and they can be a source of reactive oxygen species (ROS) under impairment of mitochondrial function (7).
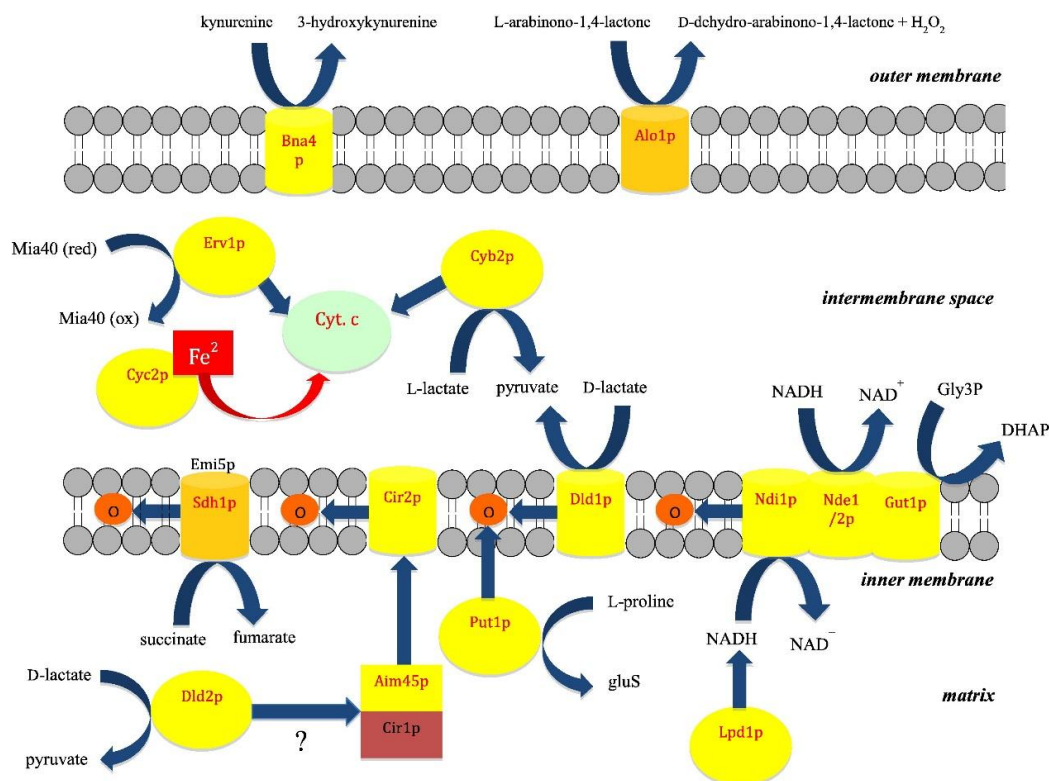
Scheme 1. Shows the ortholog ETF enzymes in *S. cerevisiae,* which are Aim45p (the α subunit) and Cir1p (the β subunit. This enzyme receives electrons from D-lactate-dehydrogenase (DLD2) in the matrix part of mitochondria (11).

According to the study of Gudipati *el al.* (2014), the yeast ETF (yETF) receives the electron from D-lactate dehydrogenase (DLD2) (11). *S. cerevisiae* possesses three DLDs that operate in different compartments of the cell. Dld1p is located in the inner mitochondrial membrane, Dld2p in the matrix and Dldl3 in the cytosol (13, 14). D-lactate dehydrogenase activity is required in these compartments to oxidize D-lactate to pyruvate. Oxidation of D-lactate by the D-lactate dehydrogenase (Dld2p) localized in the mitochondrial matrix is coupled to ATP synthesis and therefore Dld2p apparently donates substrate-derived electrons to the ETC (15).

References

1. Weidenhaupt, M., Rossi, P., Beck, C., Fischer, H. M., and Hennecke, H. (1996) Bradyrhizobium japonicum possesses two discrete sets of electron transfer flavoprotein genes: FixA, fixB and etfS, etfL. *Arch. Microbiol.* **165**, 169–178

2. Frerman, F. E., and Goodman, S. I. (1985) Deficiency of electron transfer flavoprotein or electron transfer flavoprotein:ubiquinone oxidoreductase in glutaric acidemia type II fibroblasts. *Proc. Natl. Acad. Sci.* **82**, 4517–4520

3. Watmough, N. J., and Frerman, F. E. (2010) The electron transfer flavoprotein: Ubiquinone oxidoreductases. *Biochim. Biophys. Acta - Bioenerg.* **1797**, 1910–1916

4. Roberts, D. L., Frerman, F. E., and Kim, J. J. (1996) Three-dimensional structure of human electron transfer flavoprotein to 2.1-A resolution. *Proc. Natl. Acad. Sci. U. S. A.* **93**, 14355–60

5. Tsai, M. H., and Saier, M. H. (1995) Phylogenetic characterization of the ubiquitous electron transfer flavoprotein families ETF-α and ETF-β. *Res. Microbiol.* **146**, 397–404

6. Sato, K., Nishina, Y., and Shiga, K. (1994) Preparation of separated α and β subunits of electron-transferring flavoprotein in unfolded forms and their restoration to the native holoprotein form. *J. Biochem.* **116**, 147–155

7. Lopes, J., Pinto, M. J., Rodrigues, A., Vasconcelos, F., and Oliveira, R. (2010) The Saccharomyces cerevisiae Genes, AIM45, YGR207c/CIR1 and YOR356w/CIR2, Are Involved in Cellular Redox State Under Stress Conditions. *Open Microbiol. J.* **4**, 75–82

8. Grandier-vazeille, X., Bathany, K., Chaignepain, S., Camougrand, N., Manon, S., and Schmitter, J. (2001) Yeast Mitochondrial Dehydrogenases Are Associated in a Supramolecular Complex Articles Yeast Mitochondrial Dehydrogenases Are Associated in a Supramolecular Complex †. *Situ.* **40**, 9758–9769

9. Botstein, D., Chervitz, S. A., and Cherry, J. M. (1997) Yeast as a model organism. *Science (80-.).* **277**, 1259–1260

10. Foury, F. (1997) Human genetic diseases: A cross-talk between man and yeast. *Gene.* **195**, 1–10

11. Gudipati, V., Koch, K., Lienhart, W.-D., and Macheroux, P. (2014) The flavoproteome of the yeast Saccharomyces cerevisiae. *Biochim. Biophys. Acta - Proteins Proteomics.* 10.1016/j.bbapap.2013.12.015

12. Sickmann, A., Reinders, J., Wagner, Y., Joppich, C., Zahedi, R., Meyer, H. E., Schonfisch, B., Perschil, I., Chacinska, A., Guiard, B., Rehling, P., Pfanner, N., and Meisinger, C. (2003) The proteome of Saccharomyces cerevisiae mitochondria. *Proc. Natl. Acad. Sci.* **100**, 13207–13212

13. Chelstowska, A., Liu, Z., Jia, Y., Amberg, D., and Butow, R. A. (1999) Signalling

between mitochondria and the nucleus regulates the expression of a new D-lactate dehydrogenase activity in yeast. *Yeast*. **15**, 1377–1391

14. Rojo, E. E., Guiard, B., Neupert, W., and Stuart, R. A. (1998) Sorting of D-lactate dehydrogenase to the inner membrane of mitochondria. Analysis of topogenic signal and energetic requirements. *J. Biol. Chem.* **273**, 8040–8047

15. Pallotta, M. L., Valenti, D., Iacovino, M., and Passarella, S. (2004) Two separate pathways for D-lactate oxidation by Saccharomyces cerevisiae mitochondria which differ in energy production and carrier involvement. *Biochim. Biophys. Acta - Bioenerg.* **1608**, 104–113

16. Kim, H. J., and Winge, D. R. (2013) Emerging concepts in the flavinylation of succinate dehydrogenase. *Biochim. Biophys. Acta - Bioenerg.* **1827**, 627–636

17. Tzagoloff, A., Jang, J., Glerum, D. M., and Wu, M. (1996) FLX1 codes for a carrier protein involved in maintaining a proper balance of flavin nucleotides in yeast mitochondria. *J. Biol. Chem.* **271**, 7392–7397

18. Pallotta, M. L., Brizio, C., Fratianni, A., De Virgilio, C., Barile, M., and Passarella, S. (1998) Saccharomyces cerevisiae mitochondria can synthesise FMN and FAD from externally added riboflavin and export them to the extramitochondrial phase. *FEBS Lett.* **428**, 245–249

19. Bafunno, V., Giancaspero, T. A., Brizio, C., Bufano, D., Passarella, S., Boles, E., and Barile, M. (2004) Riboflavin uptake and FAD synthesis in saccharomyces cerevisiae mitochondria. Involvement of the flx1p carrier in fad export. *J. Biol. Chem.* **279**, 95–102

20. Pallotta, M. L. (2011) Evidence for the presence of a FAD pyrophosphatase and a FMN phosphohydrolase in yeast mitochondria: A possible role in flavin homeostasis. *Yeast*. **28**, 693–705

21. Torchetti, E. M., Brizio, C., Colella, M., Galluccio, M., Giancaspero, T. A., Indiveri, C., Roberti, M., and Barile, M. (2010) Mitochondrial localization of human FAD synthetase isoform 1. *Mitochondrion*. **10**, 263–273

Chapter 2: Aim of study

The human electron transfer protein (hETF) functions as electron acceptor for thirteen mitochondrial dehydrogenases (1). It is known that the ETF protein from *Saccharomyces cerevisiae* (yETF) receives electrons from only one protein named D-lactate dehydrogenase 2 (DLD2) (2). This simple eukaryotic system of yeast makes it a good model for the investigation of many aspects of cell biology, including the study of mitochondria at genetic, molecular, and physiological level (3). Augustin et *al.* proved that the flavin cofactor in hETF forms a special adduct named 8-formyl-FAD that plays a crucial role in interaction between ETF and the corresponding nine electron donors (4). This study aims to express and purify the wild type of yETF. In later stage, the purified protein will be characterized in order to reveal if it possesses 8-formyl-FAD as well and to compare it to its human homologue.

References

1. Watmough, N. J., and Frerman, F. E. (2010) The electron transfer flavoprotein: Ubiquinone oxidoreductases. *Biochim. Biophys. Acta - Bioenerg.* **1797**, 1910–1916

2. Gudipati, V., Koch, K., Lienhart, W.-D., and Macheroux, P. (2014) The flavoproteome of the yeast Saccharomyces cerevisiae. *Biochim. Biophys. Acta - Proteins Proteomics*. 10.1016/j.bbapap.2013.12.015

3. Lopes, J., Pinto, M. J., Rodrigues, A., Vasconcelos, F., and Oliveira, R. (2010) The Saccharomyces cerevisiae Genes, AIM45, YGR207c/CIR1 and YOR356w/CIR2, Are Involved in Cellular Redox State Under Stress Conditions. *Open Microbiol. J.* **4**, 75–82

4. Augustin, P., Toplak, M., Fuchs, K., Gerstmann, E. C., Prassl, R., Winkler, A., and Macheroux, P. (2018) Oxidation of the FAD cofactor to the 8-formyl-derivative in human electron-transferring flavoprotein. *J. Biol. Chem.* **293**, 2829–2840

Chapter 3: Materials and Methods

Chemicals

The gene encoding *yETF* in *Saccharomyces cerevisiae* was synthesized by Invitrogen Life Technologies (Carlsbad, CA, USA). Restriction enzymes, ligases, were from Thermo Fisher Scientific (Waltham, MA, USA). Pre-packed nickel sepharose fast flow columns were from GE Healthcare (Little Chalfont, UK). Solvents, media components and buffer salts were from Carl Roth GmbH (Karlsruhe, Germany).

Molecular cloning

On ordering, the gene sequence of yETF (listed below) was codon optimized for expression in *E. coli.* The gene was designed to be flanked with *NcoI* and *NotI* restriction sites at the 5' and 3'-end, respectively (figure 1). Since yETF consists of two subunits (α and β), the gene sequence that was ordered contains the sequence coding for the two subunits with a linker region in between.

More information about the genes coding for yETF subunits can be found in NCBI under the following links:

https://www.ncbi.nlm.nih.gov/nuccore/NC_001148.4?report=genbank&from=564007&to=565041&strand=true

https://www.ncbi.nlm.nih.gov/nuccore/NC_001139.9?report=genbank&from=910843&to=911628&strand=true

The DNA string was cloned into a shuttle vector (pJET) and transformed into *E. coli* Top 10 cells for strain preservation and plasmid propagation. After digestion with *NcoI* and *NotI* to create sticky ends, the gene was cloned into the expression vector pETM-11 (figure2), conferring Kanamycin resistance. This vector contains a N-terminal hexa-His tag. Correct insertion of the gene sequence was verified by sequencing. The yETF containing plasmid was transformed to different strains of *E. coli* to find the best expression strain for this gene.
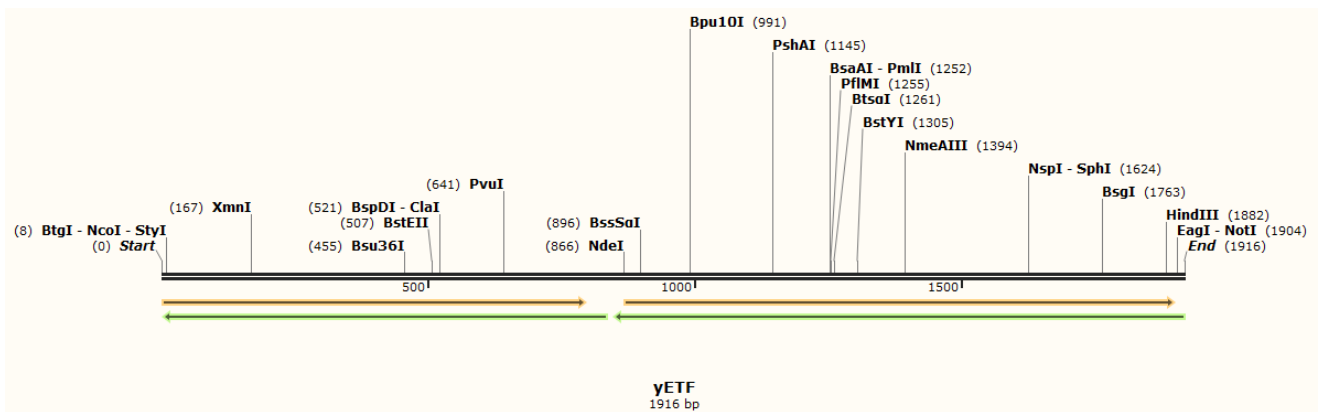
Figure 1. The gene map of yETF with the restriction sites.
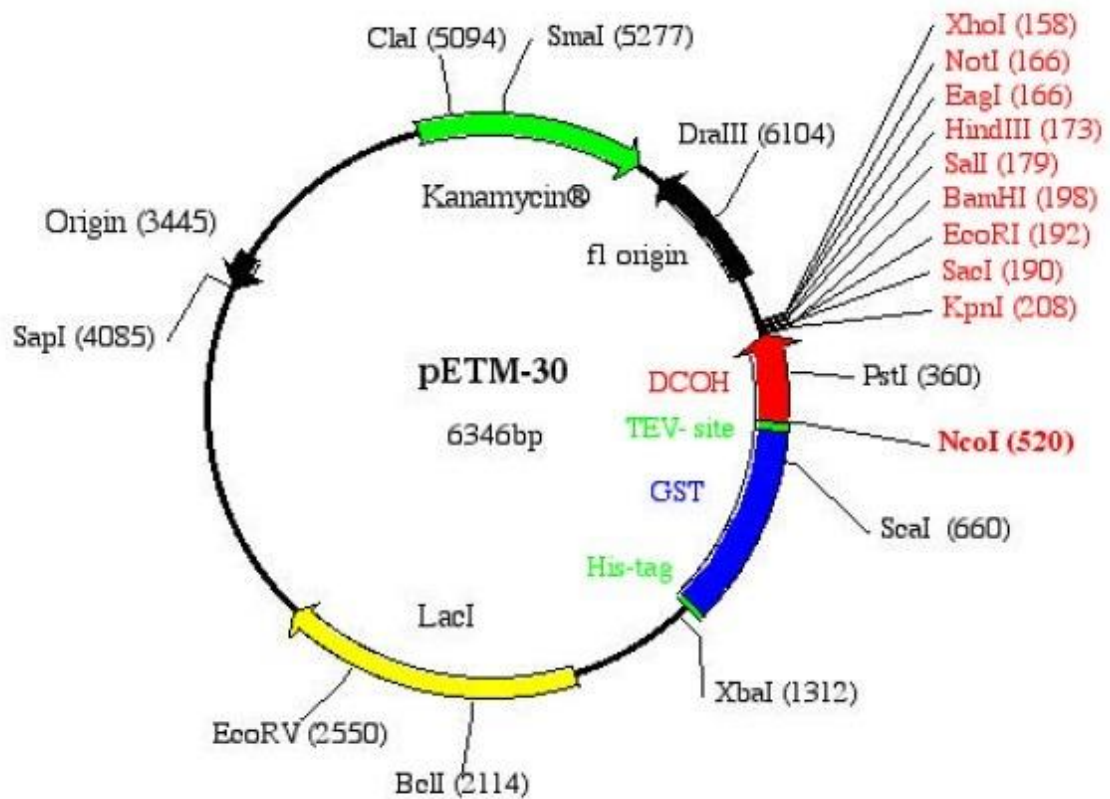
Figure 2. The map of pETM-11 vector showing the restriction sites with the kanamycin resistance gene.

Protein expression and purification

yETF was expressed in *E. coli* Rosetta expression strains that confer chloramphenicol resistance in shake flasks in an HT Multitron Standard shaking system (Infors AG, Basel, Switzerland). Main cultures were inoculated to an optical density at 600 nm (OD_{600}) of about 0.1, by adding an overnight culture to fresh LB medium containing 50 mg/ml Kanamycin and 20 mg/ml Chloramphenicol and incubated at 37 °C and 140 rpm until an optical density of 0.7 was reached. Then, production of yETF was induced by adding 200 µM IPTG, before incubating the cultures at 20 °C for 15 h to maximize protein yield. The cells were harvested by centrifugation at 5,000 *g* for 15 minutes and stored at -20 °C until further use. Protein purification was carried out at 4 °C. To purify the enzyme, the pellet was suspended in lysis buffer (50 mM phosphate/NaOH, 150 mM sodium chloride, 15 mM imidazole pH 7) and sonicated using a Labsonic U sonication probe (B. Braun Biotech, Berlin, Germany) for 10 min. The lysate was centrifuged at 38500 *g* for 60 min and the supernatant was filtered through a filter paper. The clear supernatant was loaded onto a Ni-NTA sepharose fast flow column (GE Healthcare) prewashed with lysis buffer. The column was washed with 10 column volumes of washing buffer (100 mM phosphate/NaOH, 150 mM NaCl,15 mM imidazole pH 7), before the enzyme was eluted with elution buffer (100 mM phosphate/NaOH, 150 mM NaCl, 200 mM imidazole pH 7). The eluted protein was incubated at 30 °C to precipitate the separated subunits. The precipitated protein was removed by centrifugation and the resulting enzyme solution was dialyzed against 100 mM phosphate/NaOH, 150 mM NaCl pH 7 (storage buffer) overnight. Then, the protein was concentrated in an Amicon Ultra-15 centrifugal filter with a 30-kDa cut-off (Merck-Millipore, Darmstadt, Germany).

The protein sequence for both α and β subunit is as following:

Aim45: (alpha)

MFKSLAAVLPRASKAKFLQKNYASTLAFIESSKDGSVSRSSLSLLAAAQKLSNPITAVITGSKAEKTAEA
LKSSYSCSNLEKLVIFEDSKLDTCLPEQLTPLLVKLLKGGDYSHFVVSNSSVGKSVLPRVGALLDVQPVC
EVTVIKDPKTFIRPIYAGNIISTIECQAEKKLLIIRASAFPPIAEGSMDSVTIEKRTDIPPCDLNVTWVKTIL
TKSERPELTSAQNVVTGGRALKDKETFEKLLSPLADVLHAAIGATRASVDNGLCDNSLQIGQTGKVV
APNLYIAIGVSGAVQHLAGMKDSKVIVAINNDPDAPIFNVADYGLQGDLYKIVPELTEKLGKYK

Cir1: (beta)

MSAKQQLRILVPVKRVVDFQIKPRVNKTLTGIETSGIKFSINPFDDIAVEEAIRIKEKNKSLVESTHAVSI

GSAKAQDILRNCLAKGIDTCSLIDSVGKENIEPLAIAKILKAVVEKKGSNLVLMGKQAIDDDCNNTGQ

MLAGLLNWPQATNAAKVEFLDNGRVQVTREIDDGEEVIEASLPMVITTDLRLNTPRYVGLPKLMKA

KKKPIEKLDIAKDFPEINIEPQLKIVSMEEPKTKSPGVKLNSVDELIEKLKEVKAI

yETF parameters

Table 1. The Expasy protparam software shows the following parameters for yETF:

Number of amino acides	605
Molecular weight:	65543.3
Theoratical pI	8.75
Total number of negatively charged residues	72
The estimated half-life	30 hours (mammalian reticulocytes, in vitro). >20 hours (yeast, in vivo). >10 hours (Escherichia coli)
The instability index (II)	35.24 (stable)

UV-Vis absorption spectroscopy and calculation of the extinction coefficient

A Specord 210 spectrophotometer (Analytik Jena, Jena, Germany) was used for UV-Vis absorption spectroscopy. Concentrations of purified enzyme samples were determined according to the absorption of bound FAD at 450 nm. The molar extinction coefficient of FsqB was determined as described in reference (1).

Protein thermal stability

The thermal stability of yETF was assessed by recording the change in fluorescence due to the release of the FAD cofactor as an intrinsic probe to monitor protein stability and folding in a ThermoFAD assay (2). The measurements were carried out in triplicate with

an FX Connect real-time PCR system (Bio-Rad). The starting temperature was 20 °C for 5 minutes, then it was increased at a rate of 0.5 °C/min to 95 °C. The CFX Manager 3.0 software was used to determine the optimal pH (in the range between 6.5 and 8.5) for wild type yETF.

Anaerobic photoreduction and reoxidation

Photoreduction of FsqB was done according to the procedure reported by Massey and Hemmerich (3). About 40 µM of yETf in 100 mM phosphate/NaOH, pH 7, 1 mM EDTA, 1 µM 5-deaza-FMN and 2 µM methyl viologen were rendered anaerobic by 2-h incubation in an anoxic, nitrogen-filled glove box (Belle Technology, Weymouth, UK). The anoxic samples were transferred to quartz cuvettes and sealed. Photoirradiation was carried out with a 10 W LED flood light (Luminea, Buggingen, Germany), while cooling the cuvette to 15 °C. Spectra were recorded between 300 and 800 nm until no further changes were observed. For reoxidation of the enzyme, the cuvettes were opened to expose the sample to air and again absorption spectra were recorded between 300 and 800 nm until no further changes were observed.

References

1. Macheroux, P. (1999) UV-Visible Spectroscopy as a Tool to Study Flavoproteins. in *Flavoprotein Protocols. Methods in Molecular Biology*, pp. 1–7, 10.1385/1-59259-266-X:1

2. Forneris, F., Orru, R., Bonivento, D., Chiarelli, L. R., and Mattevi, A. (2009) ThermoFAD, a Thermofluor??-adapted flavin ad hoc detection system for protein folding and ligand binding. *FEBS J.* **276**, 2833–2840

3. Massey, V., and Hemmerich, P. (1978) Photoreduction of Flavoproteins and Other Biological Compounds Catalyzed by Deazaflavins. *Biochemistry*. **17**, 9–17

Chapter 4: Results

Production and transformation of yETF plasmid to an expression strain

yETF was ligated into the pETM-11 vector and correct insertion of the gene was checked by digestion with *NcoI* and *NotI*. The correct sequence of the gene was confirmed by plasmid sequencing.
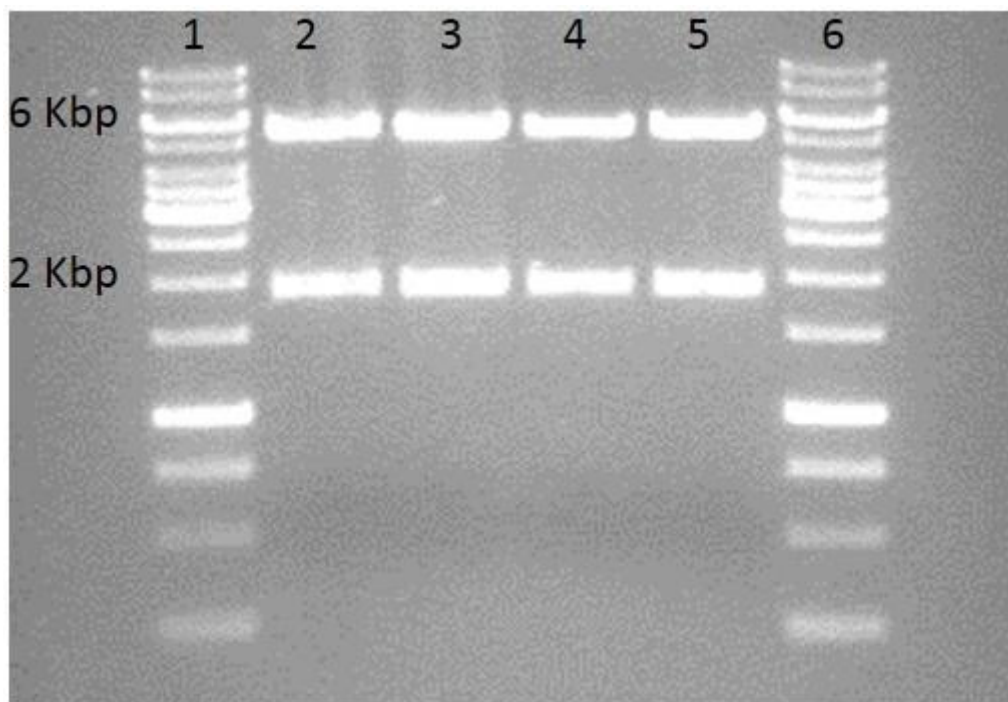
Figure 1. DNA agarose gel (1%) for digested yETF containing plasmid. Lane 1; 1 kb gene ruler. Lane 2 to 5 digested samples. Lane 6; 1 kb ruler. The first band which is about 6 kb is the pETM-11 vector and the second band which is about 1.9 kb is the gene with sticky ends.

yETF containing plasmid was transformed to different *E. coli* expression strains in order to detect the best expressing strain by performing small scale induction (Figure 2). The small scale induction was done under two different pH conditions: 7 and 8.5.

Figure 2. Small scale induction of yETF containing plasmid. 3 different colonies were taken from every expression strain. The molecular weight of the α and β subunits are 36.8 and 39.6 kDa respectively.

<u>Panel A.</u> Lane 1; pre-stained-protein ruler. Lane 2; none induced sample 1 in *E. coli* Rosetta strain (pH 8.5). Lane 3; induced sample 1 in *E. coli* Rosetta strain. Lane 4 (pH7). Lane 4; induced sample 1 in *E. coli* Rosetta strain (pH 8.5). Lane 5; none induced sample 2 in *E. coli* Rosetta strain (pH 8.5). Lane 6; induced sample 2 in *E. coli* Rosetta strain (pH 7); lane 7; induced sample 2 in *E. coli* Rosetta strain (pH 8.5). Lane 8; none induced sample 3 in *E. coli* Rosetta strain (pH 8.5). Lane 9; induced sample 3 in *E. coli* Rosetta strain (pH 7). Lane 10; induced sample 3 in *E. coli* Rosetta strain (pH 8.5). Lane 11; none induced sample 1 in *E. coli* Rosette DE3 strain (pH 8.5). Lane 12; induced sample 1 in *E. coli* Rosetta DE3 strain (pH 7). Lane 13; induced sample 1 in *E. coli* Rosetta DE3 strain (pH 8.5). Lane 14; none induced sample 2 in *E. coli* Rosetta DE3 strain (pH 8.5). Lane 15; induced sample 2 in *E. coli* Rosetta DE3 strain (pH 7).

<u>Panel B.</u> Lane 1; induced sample 2 in E. coli Rosetta DE3 strain (pH 8.5). Lane 2; none induced sample 3 in *E. coli* Rosetta DE3 strain. Lane 3; induced sample 3 in *E. coli* Rosetta strain (pH 7). Lane 4; induced sample 3 in *E. coli* Rosetta strain (pH 8.5). Lane 5; pre-stained protein ruler. Lane 6; none induced sample 1 in *E. coli* RP strain (pH 8.5). Lane 7; induced sample 1 in *E. coli* RP strain (pH 7). Lane 8; induced sample 1 in *E. coli* RP strain (pH 8). Lane 9; none induced sample 2 in *E. coli* RP strain (pH 8.5). Lane 10; induced sample 2 in *E. coli* RP strain (pH 7). Lane 11; induced sample 2 in *E. coli* RP strain (pH 8.5). Lane 12; none induced sample 3 in *E. coli* RP strain (pH 8.5). Lane 13; induced sample 3 in *E. coli* RP strain (pH 7). Lane 14; induced sample 3 in *E. coli* RP strain (pH 8.5).

<u>Panel C.</u> Lane 1; lane 2; lane 3; negative controls. Lane 4; pre-stained protein ruler. Lane 5; none induced sample 1 in *E. co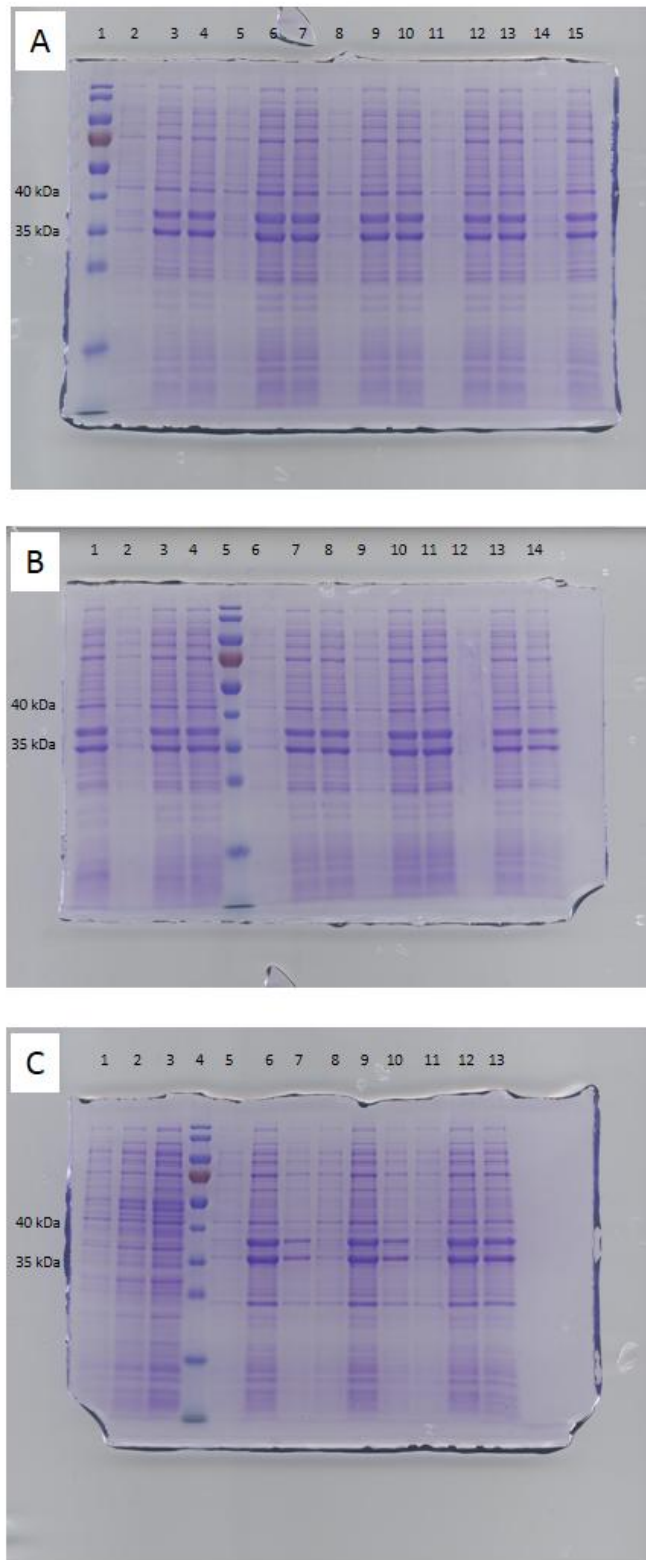li* RIL strain (pH 8.5). Lane 6; induced sample 1 in *E. coli* RIL strain (pH 7). Lane 7; induced sample 1 in *E. coli* (pH 8.5). Lane 8; none induced sample 2 in *E. coli* RIL strain (pH 8.5). Lane 9; induced sample 2 in *E. coli* RIL strain (pH 7). Lane 10; induced sample 2 in *E. coli* RIL strain (pH 8.5). Lane 11; none induced sample 3 in *E. coli* RIL strain (pH 8.5). Lane 12; induced sample 3 in *E. coli* RIL strain (pH 8.5). Lane 13; induced sample 3 in *E. coli* RIL strain (pH 8.5).

The optimal pH for yETF for purification and stability

E. coli Rosetta expression strain was chosen for the protein expression at large scale. The yield of expression was high. However, the protein was not stable since it consists of two subunits, which tend to precipitate easily. Therefore, the protein was purified under different pH conditions from pH 6.5 to 8.5 and the melting point of purified protein was determined under different pH and buffer conditions (table 1 and table 2).

Table 1: Melting point of yETF in different pH. The used buffer is 50 mM Hepes; 150 mM NaCl buffer.

pH	Melting point [°C]
8.5	44.5
8	46
7.5	47.5
7	50.5
6.5	51

Table 2: Melting point of yETF enzyme in different buffers and pH conditions.

Buffer	Melting point [°C]
50 mM TRIS/HCl pH 6	53.5
50 mM TRIS/HCl pH 7	52.5
50 mM TRIS/HCl pH 8	49
50 mM HEPES/NaOH pH 5	56
50 mM HEPES/NaOH pH 7	54.5
50 mM phosphate pH 6	54
50 mM phosphate + 150 mM NaCl pH 7	52.5
50 mM phosphate + 150 mM NaCl pH 7 + 10% glycerol	51
50 mM MOPS pH 7.5	53.5

Expression and purification of yETF and spectral properties

FsqB was expressed in *E. coli* Rosetta at large scale and purified by mean of Ni-NTA affinity chromatography. 50 mM phosphate/NaOH + 150 mM NaCl (pH 7) was chosen to purify yETF. The purified protein was run on SDS page to confirm the identity (Figure 3). The UV-Vis absorption spectrum of FsqB possesses the typical features of an FAD containing protein with absorption maxima at 438 and 378 nm, (Figure 4). The bathochromic shift of the long wavelength absorption maximum by about 10 nm compared to free FAD is most likely due to the non-covalent binding of FAD to yETF.
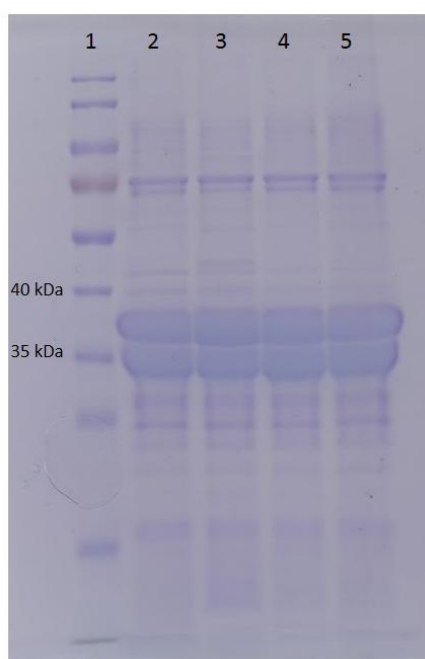
Figure 3. SDS page (12.5%) showing purified yETF after large scale expression. Lane 1; is pre-stained protein ruler. Lane 2-5; purified protein from different elution fractions. The protein was purified in 50 mM HEPES/NaOH pH 7.
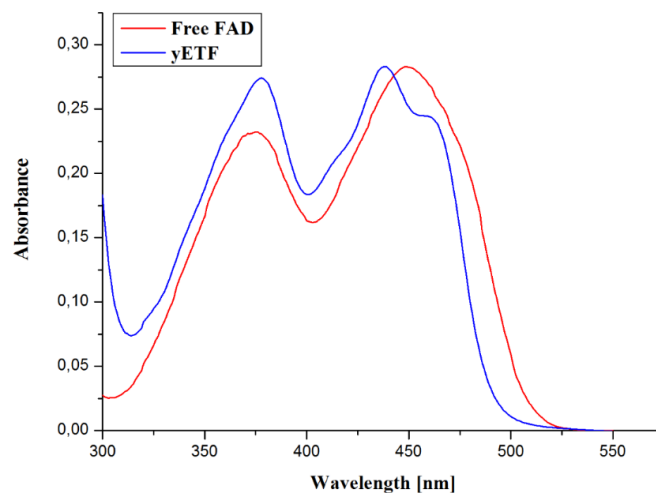
Figure 4. UV-Vis absorption spectrum of yETF (solid blue line) in comparison with free FAD (solid red line). The absorption spectrum of yETf was recorded in sodium phosphate buffer, pH 7.

Definition of the extinction coefficient

The extinction coefficient of the FAD bound to yETf was calculated to be 13000 M^{-1} cm^{-1} (Figure 5). The extinction coefficient of free FAD was used to define the flavin linked to yETF (1).
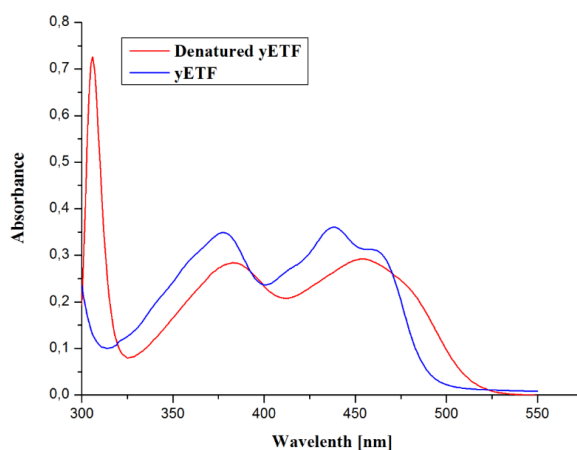
Figure 5. UV-VIS absorption spectrum of yETF before denaturation (blue line) and after denaturation (red line). This experiment was applied to define the extinction coeffiecient of yETF in relevance to the extinction coefficient of FAD.

Photoreduction of yETF

Photoreduction of yETF led to the formation of a flavin semiquinone for short time with an absorption maximum at 396 nm. Then the flavin was fully reduced to hydroquinone (Figure 6). The reduced flavin was reoxidized by molecular oxygen reaching completion after ca. 85 minutes (Figure 7).
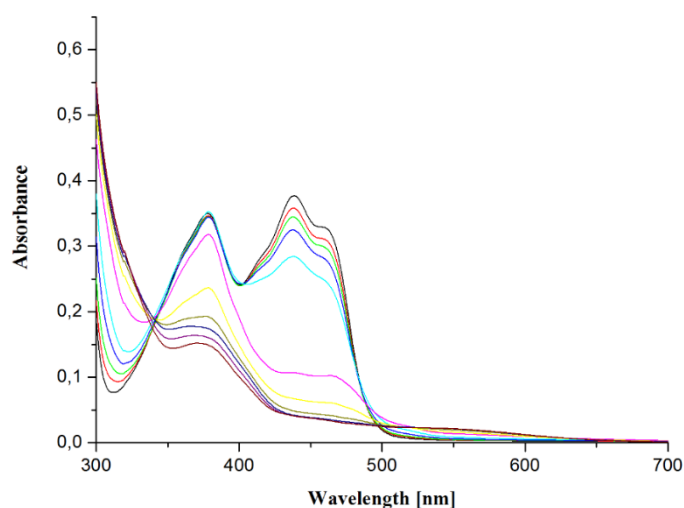
Figure 6. Shows the photoreduction of yETF as a function of light irradiation.
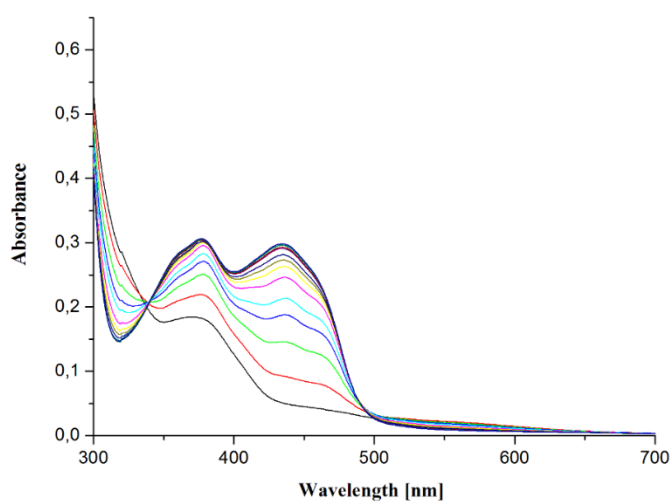
Figure 7. Shows the reoxidation of yETF by molecular oxygen.

yETF Homology structure

The yETF homology structure was created by using is a fully automated protein structure homology-modelling server: SWISS-MODEL. The protein structure of human ETF (hETF) was used as a template (PDB code 1EFV). The primary sequence alignment (Figure 8 between the yETF and hETF shows that both proteins have the same conservative residues that play a role in the mechanism and that hETF is a valid template to create the homology model of yETF (Figure 9 and 10). PyMOL software was used to visualize the PDB files and the created homology structure.


```
1EFV:hETF    --------------------MQSTLVIAE-HANDSLAPITLNTITAATRLGGEVSCLVA    38
yETF         MFKSLAAVLPRASKAKFLQKNYASTLAFIESSKDGSVSRSSLSLLAAAQKLSNPITAVIT   60
                                 ***.: *   :.*:: :*. ::** :*.. ::.::: 

1EFV:hETF    GTKCDKVAQDLC---KVAGIAKVLVAQHDVYKGLLPEELTPLILATQKQFNYTHICAGAS   95
yETF         GSKAEKTAEALKSSYSCSNLEKLVIFEDSKLDTCLPEQLTPLLVKLLKGGDYSHFVVSNS  120
             *:*.:*.*: *    . :.: *::: :.. .  ***:****:: * :*:*: .. * 

1EFV:hETF    AFGKNLLPRVAAKLEVAPISDIIAIKSPDTFVRTIYAGNALCTVKCDEKVKVFSVRGTSF  155
yETF         SVGKSVLPRVGALLDVQPVCEVTVIKDPKTFIRPIYAGNIISTIECQAEKKLLIIRASAF  180
             :.**.:****.* *:* *:.:: .**.*.**:* ***** :.*::*: : *:: :*.::* 

1EFV:hETF    DAAATSGG-SASSEKASSTSPVE-ISEWLDQKLTKSDRPELTGAKVVVSGGRGLKSGENF  213
yETF         PPIAEGSMDSVTIEKRTDIPPCDLNVTWVKTILTKSERPELTSAQNVVTGGRALKDKETF  240
              * .. *.: ** :. * :    *:. ****:*****.*: **:***.**. *.* 

1EFV:hETF    K-LLYDLADQLHAAVGASRAAVDAGFVPNDMQVGQTGKIVAPELYIAVGISGAIQHLAGM  272
yETF         EKLLSPLADVLHAAIGATRASVDNGLCDNSLQIGQTGKVVAPNLYIAIGVSGAVQHLAGM  300
             : ** *** ****:**:**:** *: *.:*:*****:***:****:*:***:****** 

1EFV:hETF    KDSKTIVAINKDPEAPIFQVADYGIVADLFKVVPEMTEILKKK----MAELRVLVAVKRV  328
yETF         KDSKVIVAINNDPDAPIFNVADYGLQGDLYKIVPELTEKLGKYKMSAKQQLRILVPVKRV  360
             ****.*****:**.****:*****: .**.*:***.** * *     :**.** **** 

1EFV:hETF    IDYAVKIRVKPDRTGVVTDGVKHSMNPFCEIAVEEAVRLKEK--KLVKEVIAVSCGPAQC  386
yETF         VDFQIKPRVNKTLTGIETSGIKFSINPFDDIAVEEAIRIKEKNKSLVESTHAVSIGSAKA  420
             :*: :* **:   **: *.*:*.*:*** :*****:*:*** .**... *** * *:. 

1EFV:hETF    QETIRTALAMGADRGIHVEVPPAEAERLGPLQVARVLAKLAEKEKVDLVLLGKQAIDDDC  446
yETF         QDILRNCLAKGIDTCSLI--DSVGKENIEPLAIAKILKAVVEKKGSNLVLMGKQAIDDDC  478
             *: :*..** * *   :    *.: ** :*::* :.**: .:***:*********** 

1EFV:hETF    NQTGQMTAGFLDWPQGTFASQVT-LEGDKLKVEREIDGGLETLRLKLPAVVTADLRLNEP  505
yETF         NNTGQMLAGLLNWPQATNAAKVEFLDNGRVQVTREIDDGEEVIEASLPMVITTDLRLNTP  538
             *:**** **:*:***.* *::*  *::.::* ****.* *.. .** *:*:***** * 

1EFV:hETF    RYATLPNIMKAKKKKIEVIKPG--DLGVDLTSKLSVISVEDPPQRTAGVKVETTEDLVAK  563
yETF         RYVGLPKLMKAKKKPIEKLDIAKDFPEINIEPQLKIVSMEEPKTKSPGVKLNSVDELIEK  598
             **. **::****** ** :. .   ::: :*.::*:*:* :: ***:::.::*: * 

1EFV:hETF    LKEIGRI  570
yETF         LKEVKAI  605
             ***: * 
```

Figure 8. Sequence alignment between hETF and yETF. The asterix symbol shows the conserved residues in these two proteins. The Clustal omega (1.2.4) software was used to perform this alignment.
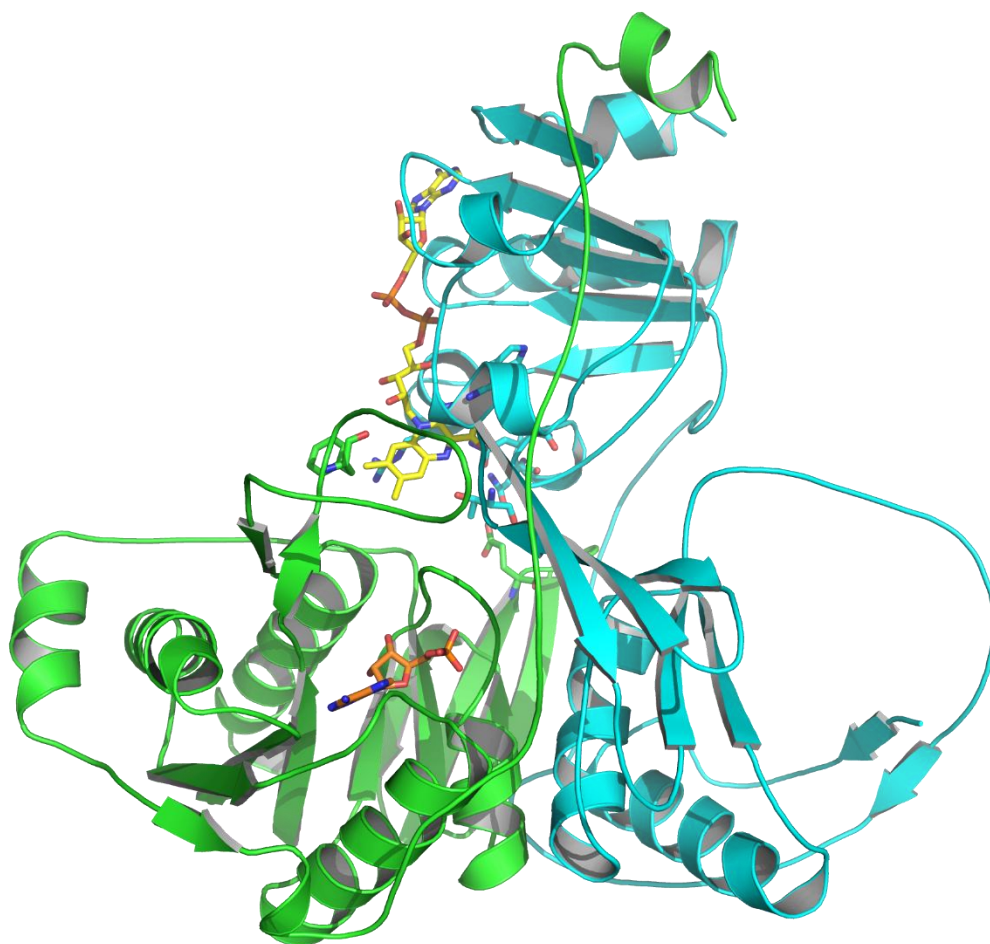
Figure 9. The Homology model of yETF based on the crystal structure of hETF (PDB code 1EFV). The α subunit is shown in cyan and β subunit is shown in green. FAD molecule is shown as yellow sticks. The AMP molecule is shown as orange sticks.
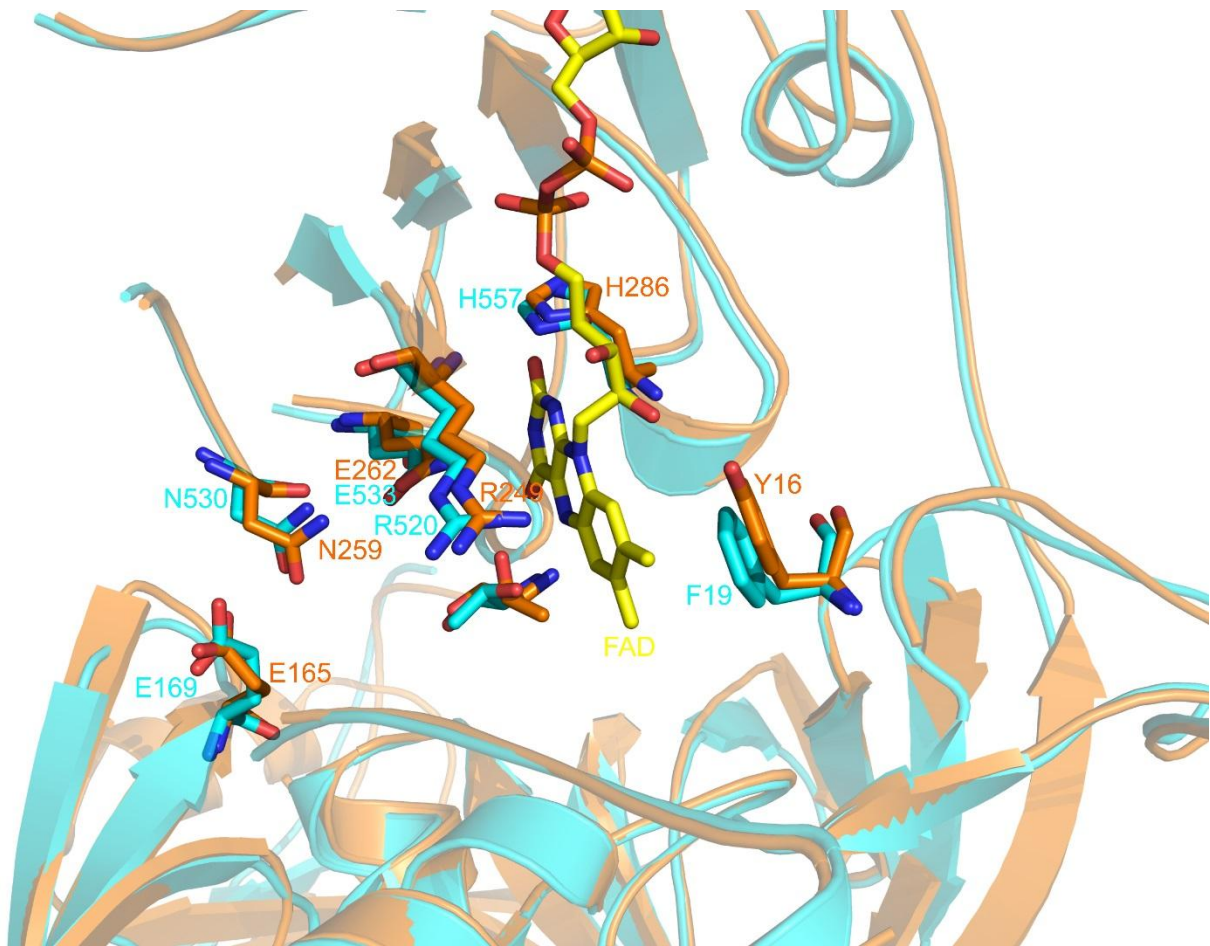
Figure 10. Superimposed active sites of yETF and hETF. hETF is shown in orange and yETF is shown in cyan. The figures show the most important residues that play a role in the mechanism of ETF.

Chapter 5: Discussion

The yETF containing plasmid was purified in two different pH conditions (7 and 8.5). At pH 8.5, the enzyme shows only low stability, which may be due to its isoelectric point at ≈ 8.5. The aim of this purification at two different pH values is to reveal if yETF possesses the 8-formyl-adduct of the flavin similar to hETF, where the adduct is formed at pH 8.5 and appears as a spectral peak at 415 nm(1). yETF does not show this adduct even after incubation of the protein for a long time (24 hours) at room temperature as described in the experimental work of Augustin et. *al* (2018) (1). 8-formyl FAD is usually formed to allow the ETF system in human to choose the appropriate electron donor. Until now, thirteen clients are recognized as electron donors for hETF (2, 3). To the best of our knowledge, there is only one electron source for yETF, which is DLD2. Thus, the formation of 8-formyl-FAD seems to be not beneficial in this ETF system, although it was observed in the fungal enzyme formate oxidase, but for another role (4). Melting point experiments show that yETF is more stable at a pH value around 7 (Table 1 in the results section). On the other side, the alignment of yETF protein sequence with hETF protein sequence shows high similarity that allows us to create a homology structure of yETF. By creating this homology structure we could compare the residues responsible for the open and closed conformation in both human and yeast enzymes. Except for βTyr 16 in hETF that is found to be βPhe 19 in yETF (Figure 10 in the results section), all the studied residues that form the active site are conserved in both enzymes. Ausgustin et. *al* (2018) suggested that the phenolate side chain of βTyr 16 in hETF plays the role of base in the process of oxidizing the 8 methyl group to 8 formyl in FAD (1). Since the formation of 8-formyl FAD is not required for yETF, it is rational that the yeast enzyme possesses phenylalanine instead of the tyrosine residue.

Whereas the photorduction of hETF leads to the clear formation of an anionic red semiquinone (1), the photoreduction of yETF leads to the formation of an anionic red semiquinone for a short time that appeared as slight increase in the absorbance at 396 nm and then the flavin is reduced to the hydroquinone. This observation proves that the mechanism of flavin reduction is not the same in both enzymes.

References

1.   Augustin, P., Toplak, M., Fuchs, K., Gerstmann, E. C., Prassl, R., Winkler, A., and Macheroux, P. (2018) Oxidation of the FAD cofactor to the 8-formyl-derivative in human electron-transferring flavoprotein. *J. Biol. Chem.* **293**, 2829–2840

2.   Toogood, H. S., Leys, D., and Scrutton, N. S. (2007) Dynamics driving function - New insights from electron transferring flavoproteins and partner complexes. *FEBS J.* **274**, 5481–5504

3.   Ghisla, S., and Thorpe, C. (2004) Acyl-CoA dehydrogenases: A mechanistic overview. *Eur. J. Biochem.* **271**, 494–508

4.   Robbins, J. M., Souffrant, M. G., Hamelberg, D., Gadda, G., and Bommarius, A. S. (2017) Enzyme-Mediated Conversion of Flavin Adenine Dinucleotide (FAD) to 8-Formyl FAD in Formate Oxidase Results in a Modified Cofactor with Enhanced Catalytic Properties. *Biochemistry*. **56**, 3800–3807

List of abbreviations

BBE: berberine bridge enzyme

FsqB: amine oxidase of fumisoquin biosynthesis

MTOX: N-methyl-tryptophan oxidase

MSOX: (monomeric) sarcosine oxidase

NikD: amino acid oxidase involved in nikkomycin biosynthesis

THCS: tetrahydrocannabinol synthase.

hETF: Human Electron Transfer Flavoprotein

yETF: yeast Electron Transfer System

Curriculum Vitae

PERSONAL INFORMATION

Majd Lahham

✉ Petersgasse 12 - 8010 Graz - Austria

📞 📱 +4367761806951

@ majd.lahham@gmail.com

Sex Male | Date of birth 20/12/1978 | Nationality Syrian

WORK EXPERIENCE

September 2015 - Present

PhD researcher (Erasmus Mundus Scholarship: Avempace+)

Graz University of Technology (TU-Graz)

http://portal.tugraz.at/portal/page/portal/TU_Graz

- Main activities: Doctoral program in natural sciences, research in the field of protein expression, production, assay for drug development.

Sector: Biotechnology, biochemistry, and food chemistry

Jun 2012 - August 2015

Career centre director

International University for Science and Technology (IUST)

http://www.iust.edu.sy/project_careerCenter.aspx

- Main activities: Organizing free soft skills courses for students to increase their opportunities to find vacancies in labour market.

Sector Education

Jun 2012 - August 2015

Quality control director

International University for Science and Technology (IUST)

www.iust.edu.sy

- Main activities: working with TEMPUS project (European Union) to obtain accreditation for school of Dentistry.

Sector Education

Sep 2011 - August 2015

Biology and Microbiology lab instructor

International University for Science and Technology (IUST)

www.iust.edu.sy

- Main activities: Teaching undergraduates the practical part of biology and Microbiology.

Sector Education

Jul 2007 - Sep 2011

Monitoring and Evaluation officer, and Reporting officer

Department Of Ecumenical Relations And Development

- Main activities: Monitoring and evaluation officer and reporting officer for multi-sectors Iraqi refugee program (education, vocational training, community services projects, distribution of relief items, psychosocial support, and health awareness)

Sector Relief

Feb 2005 – Jun 2006

Biology and Microbiology lab instructor

Lebanese American University (LAU)

www.lau.edu.lb

- Main activities: Teaching undergraduates the practical part of biology and Microbiology.

Sector Education

| Sep 2002 – Sep 2003 | **Medical lab technician** |
| | Assad University Hospital |

www.auhd.edu.sy

- Main activities: Part time work in the context of postgraduate study.

Sector Education

EDUCATION AND TRAINING

| Dec 2009 | **Project Management Professional course (35 hours)** |
| | AMIDEAST (Lebanon) (certificate of attendance) |

| Sep 2004 - Sep 2007 | **Master of Science (Molecular Biology)** |
| | Lebanese American University (Beirut University College) Lebanon |

| Sep 2002 - Sep 2003 | **Diploma of Microbiology, Immunology, and Haematology** |
| | Damascus University (Syria) |

| Sep 1997 – Sep 2002 | **Bachelor of Pharmacy and Pharmaceutical Chemistry** |
| | Damascus University (Syria) |

PERSONAL SKILLS

Mother tongue(s) Arabic

Other language(s)

UNDERSTANDING		SPEAKING		WRITING
Listening	Reading	Spoken interaction	Spoken production	
English				
Very good	Very good	Very good	Very good	Very good
TOEFL Certificate (2013)				
German				
Intermediate	Intermediate	Intermediate	Intermediate	Intermediate

Communication skills Good communication skills gained through my experience as Reporting officer during my work for International Orthodox Christian Charities (IOCC)

Organisational / managerial skills Leadership through my work as monitoring and evaluation officer for IOCC and Career Centre director for IUST

Job-related skills Good experience in microbiology field through working as lab technician in university hospital and microbiology lab instructor in LAU and IUST.

Computer skills Good command of Microsoft Office™ tools

Voluntary work 2003: First aid course, and volunteer for one year at Syrian Arab Red Crescent
2011 - 2012: Volunteer at department of ecumenical relations and development (DERD) in the media department.

ADDITIONAL INFORMATION

International events
- Sep 17/ 2012 – Oct 17/ 2012: Peacemaker program organized by Presbyterian Church in the United States of America.

Quality control project
- Aug 4/ 2010 - Jan 14/ 2014: Accreditation – Pathway to Quality Assurance (TEMPUS PROJECT).

Career centre project
- Apr 4/ 2010 - Jan 14/ 2014: Skills and Career centres – Pathway to labour market (TEMPUS PROJECT).

POSTERS

- Characterization of putative fructosyl amino oxidase from Aspergillus fumigates. *Majd Lahham, Bastian Daniel, Karl Gruber,Tea Pavkov-Keller, Wolfgang Kroutil, Michael Fuchs and Peter Macheroux* (Oxizymes 2016).

- Biochemical characterization of a berberine bridge enzyme homologue from Aspergillus fumigates. *Majd Lahham, Bastian Daniel, Michael Fuchs, Tea Pavkov-Keller, Wolfgang Kroutil, Karl Gruber, and Peter Macheroux* (ÖGMBT 2016)

- Investigating the active site of an oxidase ring closure enzyme from Aspergillus fumigates. *Majd Lahham, Bastian Daniel, Michael Fuchs, Tea Pavkov-Keller, Wolfgang Kroutil, Karl Gruber, and Peter Macheroux* (17th DocDay - Graz University of Technology)

- Characterization of an oxidase ring closure enzyme from Aspergillus fumigates. *Majd Lahham, Bastian Daniel, Michael Fuchs, Tea Pavkov-Keller, Wolfgang Kroutil, Karl Gruber, and Peter Macheroux* (18th DocDay - Graz University of Technology)

PUBLICATIONS

- Lahham, M., Pavkov-Keller, T., Fuchs, M., Niederhauser, J., Chalhoub, G., Daniel, B., Kroutil, W., Gruber, K., Macheroux, P. (2018) Oxidative cyclization of *N*-methyl-dopa by a fungal flavoenzyme of the amine oxidase family J. Biol. Chem. published online September 7, 2018

- Daniel, B., Konrad, B., Toplak, M., Lahham, M., Messenlehner, J., Winkler, A., and Macheroux, P. (2017) The family of berberine bridge enzyme-like enzymes: A treasure-trove of oxidative reactions. Arch. Biochem. Biophys. 632, 88-103

REFERENCES

- Dipl.-Ing.Dr. Silvia Wallner
  Institute of biochemistry - Graz University of Technology
  Petersgasse 12/II
  8010 Graz / Austria
  +43991332340
  silvia.wallner@tugraz.at

- Prof. Dr. Costantin Daher
  Assistant dean of school of natural sciences - Lebanese American University
  Byblos- Lebanon
  +61-3-998985
  cdaher@lau.edu.lb